Distribution of deformation associated with relay and tip damage zones of normal faults - a case study from Kilve, UK

Siri Vaagan

Master thesis in

Petroleum Geoscience

Department of Earth Science

University of Bergen

June 2017

Abstract

The aim of this study is to investigate and characterize distribution of deformation and damage associated with relays and tips of normal faults at a range of scales. This is done through field based studies and digital analysis of aerial imagery of exposed wave-cut platforms along the Somerset coast, UK.

Damage zones have earlier been described geometrically and spatially, but a systematic quantification of deformation (i.e. displacement, strain etc.) is lacking. Damage at different scales (i.e. large faults, small faults and veins) is thus quantified to investigate the partitioning of deformation between different structures, and document damage zone complexity and spatial variation. The study provides new insight regarding brittle deformation at different scaled fault interactions, single faults and fault related veining, specifically focusing on distribution of deformation, partitioning of strain and spatial heterogeneity within relays and tip damage zones.

The results show that within studied fault networks, damage zones are widest and show highest vein intensity and vein strain in areas of fault interaction (i.e. relay zones, fault splays, cross-cutting or abutting relationships) and at fault tips. Mapping of relay structures shows a decrease in displacement of relay bounding faults as they overlap, which is compensated by the introduction of linkage damage structures that transfer displacement (~45 %), so that kinematic coherency is maintained. This illustrate that strain compatibility remains within relay zones, even though the partitioning of strain between different structures is changing through the zone.

Fault tip zones are characterized by a wide process zone in the outer tip, exchanged by a narrow damage zone where significant slip occurs. This shows that damage zone width decreases with increased displacement, indicating that deformation becomes more localized as the fault accumulates slip. This is supported by spatial heterogeneity analyses of deformation over both relay structures and fault tips, showing that deformation changes from distributed to localized moving away from the damage zones. This results in a decrease in structure complexity as deformation localizes onto the main faults.

These findings highlight the importance of documenting and quantifying small-scale structures of damage zones, because they are often under seismic resolution and represent structural complexities that might have implication on fluid flow and rock permeability.

Acknowledgments

First and foremost, I want to express my deepest gratitude to my supervisor Casey W. Nixon, and my co-supervisors David Sanderson and Rob Gawthorpe for your guidance, motivation and inspiration during the work with this thesis. Casey, I will thank you specifically for your extreme patience and all the great discussions we have had regarding this thesis, but also for all the other nice talks shared over a cool pint both in England and here in Norway. You have developed from being my supervisor to become a friend, and for that I am grateful. You also taught me ArcGIS from scratch, and for that I express my deepest thanks. Additionally, I would like to thank Ingvild Blækkan for being an excellent field assistant and source of knowledge and laughter during the second field season in Kilve. I also acknowledge financial support from The Norwegian Academy of Science and Letters who fund the VISTA Scholarship of Casey W. Nixon (Project No.: 6265), and the Department of Earth Science at the University of Bergen.

Another great thanks go to Casey and David for guiding me through the mine-field of academic writing, providing constructive reviews on my written work and feedback regarding specific sections of the thesis. A special thanks to Jamie (you lovely American!) who agreed to help me with proofreading, I really hope you did not regret it too much afterwards.

I owe a special thanks to my fellow geology students for all good memories created during the last 5 years. Here I would especially mention "Klubben" for the amazing times shared with you wonderful ladies, and Thomas for being the best study partner and field buddy ever! All the great people at "Midtrommet" also deserve gratitude, for support, laughter and companionship through the final year of writing.

Last but not least, I thank my dear family for loving and supporting me, and Thorstein for encouraging me and staying by my side even through the roughest times. Finally, all the amazing people at Kom og Dans Bergen is showered with thanks and hugs. Without you, this would actually not have been possible!

Siri Vaagan

Bergen 1st of June 2017

Table of content

1 Introduction

1.1 Rationale and background

Extensional strain in the upper crust is largely accommodated by opening and slip on fractures, producing joints, veins and faults. These structures represent brittle deformation over a wide range of scales, and with different geometrical and mechanical properties (Peacock and Sanderson 1994a; Putz-Perrier and Sanderson 2008b; Nixon et al. 2011, 2012). They rarely occur individually, and as networks develop (Zhang and Sanderson 1995, 1996; Sanderson and Zhang 1999; Sanderson and Nixon 2015), the different groups of structures will be found simultaneously in the same extensional setting (Peacock et al. 2016). Depending on the mechanical properties of the deformed crust and arrangement of structures, strain can be uniformly distributed or highly localized (Soliva and Schultz 2008; Putz-Perrier and Sanderson 2008a; Nixon et al. 2014b). This creates a very complex picture of strain distribution, where a network of structures at a range of scales must be taken into consideration when total contribution of deformation is addressed.

Normal fault networks contain a group of numerous fault segments that display a range of lengths, orientations and sizes (Knott et al. 1996; Peacock 2002; Nixon et al. 2014a). Interaction and development of triaxial strain systems (e.g. Reches 1978; Krantz 1988) between faults will create complex deformation due to localization of stress in certain zones (e.g. fault tips, relay structures, fault splays and fault abutments) (Fossen et al. 2005; Nixon et al. 2014a). As larger structures grow, strain compatibility is maintained by destruction of the neighboring wall rock (Long and Imber 2012), producing a damage zone (Cowie and Scholz 1992b; Caine et al. 1996; Kim et al. 2000; Kim et al. 2004). A damage zone is the volume of rock around a fault that show discrete brittle deformation due to growth and kinematic slip (Cowie and Scholz 1992a, 1992b, 1992c; Caine et al. 1996; Kim et al. 2000; Kim et al. 2004). This area accommodates displacement that contributes to the overall deformation of the rock, and must be considered while studying brittle deformation in a fault network. Damage zones of normal fault networks have been studied in detail over the last 20 years, where geometry, displacement distribution and formation of damage structures have been key aspects examined (e.g. Peacock and Sanderson 1991; McGrath and

Davison 1995; Knott et al. 1996; Kim et al. 2004; Faulkner et al. 2011; Choi et al. 2016). Yet, a quantification regarding distribution of deformation within a damage zone, and its relative contribution to the overall deformation of a normal fault network, is absent.

Faults within a network experience linkage both geometrically and/or kinematically, and transfer zones of displacement are established in zones where faults overlap. Relay structures (Larsen 1988; Peacock and Sanderson 1991; Walsh and Watterson 1991; Peacock and Sanderson 1994b; Peacock 2002) are found between overstepping normal faults, and represent areas of complex brittle deformation produced by interacting stress fields between the adjacent faults. Hence, relay structures are wonderful natural laboratories for examining deformation related to fault linkage.

Individually, normal faults and fractures have been studied in detail concerning spatial distribution of different attributes (e.g. orientation, displacement, length etc.) which can describe their geometry, kinematic behavior and scale ranges (e.g. Peacock and Sanderson 1991; Cowie and Scholz 1992c; Cartwright et al. 1995; Peacock and Sanderson 1996; Willemse 1997; Bonnet et al. 2001; Walsh et al. 2003; Peacock 2004; Kim and Sanderson 2005; Torabi and Berg 2011). Restricted resolution and small extent of geological data sets make it difficult to study structures at different scales. Most damage zone structures occur under seismic resolution, and would consequently be missed using seismic-based geological observations (Rotevatn and Fossen 2011). Field based studies where analogue out-crops are examined will then contribute to the lack of information, where scale ranges down to grain scale can be measured (Nixon et al. 2012; Sanderson and Nixon 2015). Due to resolution problems and restricted data sets, damage zones are often poorly represented when deformation of an area is studied, creating a knowledge gap on the contribution of small-scale structures to the overall deformation. Thus, this study attempts to quantify and characterize the distribution of deformation at different scales in these zones.

Damage zones might have a strong effect on fluid flow and permeability of the host rock, as they may contain numerous deformation structures of different scales, types and orientations (e.g. Caine et al. 1996; Shipton et al. 2002; Kim and Sanderson 2010). Intensified fracturing might increase the permeability of the rock, and damage zones may thus be important for exploration of different resources such as groundwater, hydrothermal ore minerals or hydrocarbons (e.g. Huyakorn et al. 1983; Curewitz and Karson 1997; Jiang et al. 1997; Sanderson and Zhang 1999; Gartrell et al. 2004; Fossen et al. 2005; Bense and Person 2006; Rotevatn et al. 2007). In the petroleum industry,

the knowledge on fault damage structures under seismic resolution has shown to be extremely valuable, as they are proven to act as both conduits and barriers to fluid flow (Rotevatn et al. 2007; Rotevatn and Fossen 2011; Fossen and Rotevatn 2016). Understanding the effects of these structures are therefore of high importance in choice of potential targets. An implication of this study is to strengthen the knowledge on distribution of deformation in damage zones based on outcrop observations, which might help avoid/minimize risk during hydrocarbon exploration and production due to lack of high resolution data sets. Another potential application is an addition to knowledge on former models of fault growth, as there are currently no studies that apply a quantitative characterization of damage zones along strike faults capturing the change in distribution of deformation.

1.2 Project aims and objectives

The aim of this study is to investigate and characterize the distribution of deformation in damage zones associated with normal faults cutting layered sedimentary rocks. The hope is to improve the understanding and importance of small-scale structures within fault damage zones, and to give a quantitative measure on deformation distribution within these zones.

To achieve this, a fieldwork study was conducted of outstanding outcrops at the Somerset coast, UK, where a population of normal faults and a well-defined stratigraphy provide an excellent framework for addressing fault relations and their associated damage zones. Combining this with analysis from aerial photographs of the same area in ArcGIS the distribution of deformation and damage associated with relays and tips of normal faults are assessed at a range of scales. Deformation distribution is investigated along strike fault zones to document spatial changes along single faults, and as adjacent fault segments overlap. By joining fault and vein data, deformation will be documented at different scales, in order to address the partitioning of overall brittle deformation provided by each structural group.

The specific objectives of this study are:

- Investigate spatial variations and the partitioning of deformation in damage zones at different scales.
- Characterize the network of structures within a damage zone associated with relay structures and fault tips.
- Analyze the relative contribution of strain from brittle structures of different scales, contributing to total extensional strain.

1.3 Thesis outline

Following this introductory chapter, there will be an overview of terminology and theory concerning normal fault networks and their associated damage zones in chapter 2, building a framework for the following chapters. Chapter 3 will introduce the regional geology of the study area, presenting the structural and stratigraphic framework of the Bristol Channel Basin, followed by the local deformation history of Kilve and Lilstock. Chapter 4 presents the methods used in field and ArcGIS to gather data, and further analysis done in ArcGIS and spreadsheets. The results from the data analyses will be presented in chapter 5 and 6, presenting results on the mesoscale relay examined at Kilve, and detailed fault tip studies done at Lilstock and East Quantocks Head. In chapter 7 the results will be interpreted and discussed in the light of relevant literature, followed by chapter 8 finishing off the thesis with conclusions and suggestions to further work.

2 Theoretical background

The purpose of this chapter is to introduce the general theoretical background of structural discontinuities found in extensional settings, i.e. fractures and faults (section 2.1) and explain the concepts of fault growth, propagation and linkage in normal fault networks (section 2.2). Further, relay structures and their relevance in fault linkage is highlighted (section 2.3), before a description of fault damage zones is presented (section 2.4). Additionally, a short introduction on some approaches used to quantify spatial distribution of deformation inside fault networks is given (section 2.5).

2.1 Brittle structures in extensional settings

Extension in the upper crust is mainly accommodated by brittle fractures that occur at a range of scales, such as joints, veins and faults (Peacock and Sanderson 1994a; Putz-Perrier and Sanderson 2008a, 2008b; Peacock et al. 2016). Fractures are sub-planar discontinuities along which material has broken resulting in a loss of cohesion at the surface (see definition in Peacock et al. 2016). This is seen as displacement and changes of mechanical properties over the fracture surface (Pollard and Segall 1987; Kim et al. 2004; Childs et al. 2009). Different types and geometries of fractures can form depending on the mechanical properties of, and stresses applied to the rock (e.g. Engelder 1987; Pollard and Aydin 1988; Sanderson 2016).

Various characteristics of fractures have made it natural to sub-divide them into smaller groups, and three main modes of fractures (Fig. 2.1) have been distinguished after the relative motion (i.e. mechanical property) across their surfaces (Engelder 1987). Tensile (mode I) fractures (Fig. 2.1a) has the relative motion perpendicular or at high angle to the fracture surface, resulting in opening of the fracture. This is fracture propagation by extension (Peacock et al. 2016). Shear (mode II and III) fractures (Fig. 2.1b-c) have a relative motion that is parallel to the fracture surface. They are distinguished by their tip displacement, where mode II fractures show sliding and mode III fractures show tearing (Engelder 1987; Pollard and Segall 1987; Peacock et al. 2016). In an extensional setting with regional horizontal stretching the most common fracture types are tensile fractures (mode I) (section 2.1.1) and normal faults (mixed-mode II/III) (section 2.1.2).

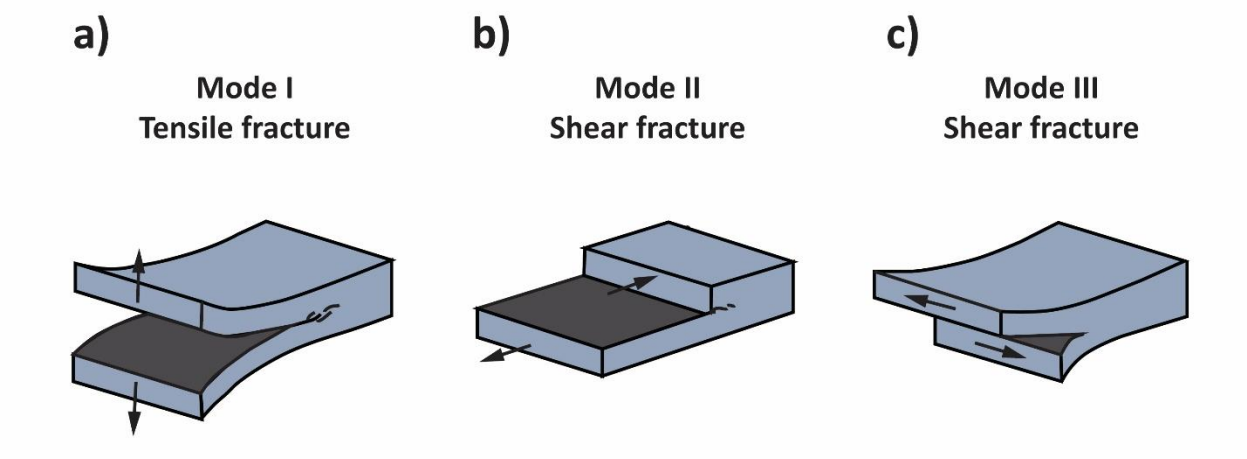

Figure 2.1 Brittle fracture modes based on relative motion across their surface. Mode I fractures have relative displacement perpendicular to the fracture plane (a). Mode II and mode III fractures have relative motion parallel to the fracture plane, where mode II fractures show sliding (b), and mode III fractures show tearing (c) as tip displacement. Modified after Hudson and Harrison (2000).

2.1.1 Tensile fractures – veins

Tensile (mode I) factures (Fig. 2.1a), also called extensional- or open-mode fractures consist of two opposing surfaces that produce an open void between them, displaying extension normal to the fracture wall (Peacock et al. 2016). Tensile fractures include joints, veins, fissures and dykes. Joints show no shear displacement (Pollard and Aydin 1988), while veins and fissures are extensional fractures that are filled with minerals (veins) and gas or fluids (fissures) (Engelder 1987; Peacock et al. 2016). Dykes are tabular magma intrusions in tensile fracture systems made by magma flow, or by infilling of pre-existing fractures (Wilshire and Kirby 1989). The *aperture* of a tensile fracture is defined as the maximum normal distance between the two separated surfaces, and mineralization of this open void (creating a vein) preserves the aperture of the former fracture (Engelder 1987; Peacock 2004). Tensile fractures may originate due to regional background stresses, creating a homogenous distribution over a large area, or they can be closely linked to the kinematic damage of other brittle structures (e.g. faults). Then fracture heterogeneity will be high and concentrated, as fractures are localized close to the main structure (Soliva and Schultz 2008; Putz-Perrier and Sanderson 2008a; Nixon et al. 2014b).

2.1.2 Normal faults and fault terminology

Faults are discrete discontinuous surfaces that show a visible shear displacement created by applied stress to a volume of rock (Segall and Pollard 1980). Thus, faults represent mixed-mode II/III fractures (Fig. 2.1b-c), or shear fractures. Displacement is the relative motion between two originally adjacent points on the surface of a fault (Peacock et al. 2016), and is accumulated on a fault plane during numerous slip events (Cowie and Scholz 1992b). When the applied stress exceeds the frictional strength of the fault plane, a stress-releasing slip event occurs. Afterwards, local strength recovery is again allowed, and stress builds up until next slip event takes place (Cowie and Shipton 1998). The fault zone (section 2.1.3) therefor consists of several segments that are individual slip planes oriented sub-parallel to each other (Segall and Pollard 1980; Willemse 1997; Walsh et al. 2003).

Normal faults (Fig. 2.2) are surfaces at which the *hanging wall* (*HW* – rock volume above the fault) is downthrown relative to the *footwall* (*FW* – rock volume below the fault) due to stretching of the host rock. The displacement on a normal fault plane can be either dip-slip or oblique-slip depending on whether the slip vector is parallel or not parallel to the maximum dip direction respectively. For pure dip-slip motion the separation between two originally adjacent points in the hanging wall and footwall is called the *displacement* or *dip separation* (*D*), while the horizontal and vertical component of this is the *heave* (*H*) and *throw* (*T*). The *stratigraphic separation* (S_S) is the thickness of strata between two adjacent points juxtaposed across a fault, representing a vertical thickness. For detailed definitions see Peacock et al. (2000).

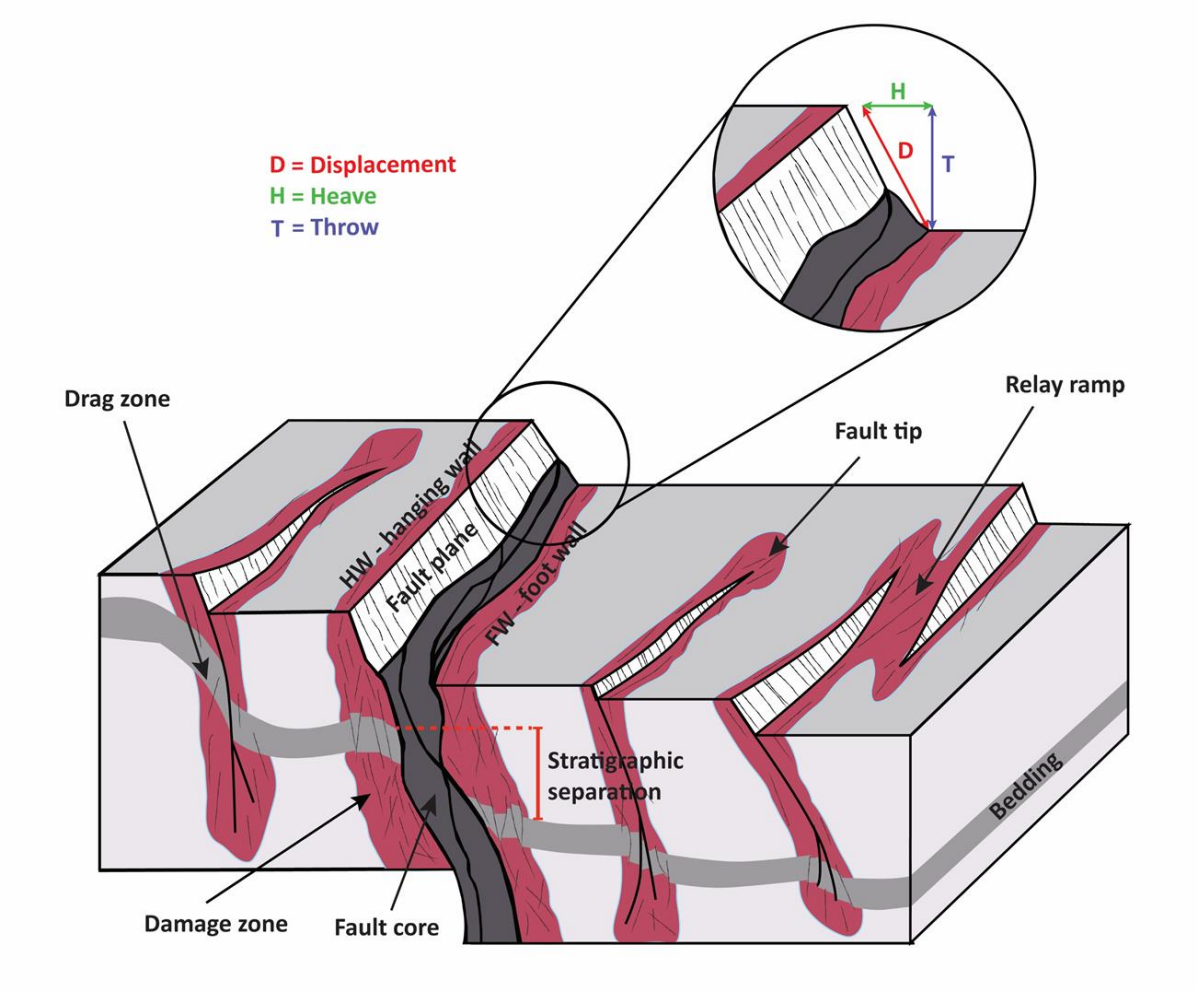

Figure 2.2: Block diagram illustrating features found in a normal fault network, where fault terminology used in this thesis is highlighted. Damage zone is marked in red, and shows small-scale fracturing. Modified after Torabi and Berg (2011).

2.1.3 Fault zone

The conventional way of describing a fault is as a discrete planar surface that accommodates slip (Walsh and Watterson 1987; Cowie and Scholz 1992a). This characterization becomes too simple when observing fault growth in both nature and laboratories where numerous slip surfaces are produced simultaneously as the closest volume of surrounding wall rock experiences deformation (Caine et al. 1996; Vermilye and Scholz 1998). This leads to a broader characterization of the system as a *fault zone*. The fault zone is comprised by a *fault core* and a *damage zone*, which sometimes can extend into a *drag zone* (Fig. 2.2). Outside the fault zone there is unaffected host rock, called protolith (Caine et al. 1996; Loveless et al. 2011).

The *fault core* is defined as the high-strain zone that accommodates most of the displacement (>95 %), and the fault core can include different structural, lithological and morphological elements, depending on the stress distribution and lithology of the host rock (Caine et al. 1996). In strong lithified rocks this includes slip surfaces, fault rocks (e.g. gouge, breccias and cataclasites), lenses of fault rock or host rock and fractures (e.g. Caine et al. 1996; Bastesen and Braathen 2010). In poorly lithified rocks, shale smear and deformation band shear zones dominate (e.g. Loveless et al. 2011).

The *damage zone* of a fault is the volume of rock around the fault core that accommodates less displacement (<5 %), shown as creation of different discrete structures (e.g. joints, veins, minor faults, deformation bands etc.), related to the formation and growth of faults (e.g. Sibson 1977; Cowie and Scholz 1992c; Chester et al. 1993; Caine et al. 1996; Childs et al. 2009). Damage zones are closely studied in this thesis, and will be further described in section 2.4.

The *drag zone* is an effect of fault growth and is seen as systematic variation of bedding dip adjacent to a fault (Reches and Eidelman 1995). Normal drag is commonly considered to form prior to faulting, often described as a fault propagation fold (e.g. Hesthammer and Fossen 1998; Rykkelid and Fossen 2002). Frictional drag observed during faulting is created as a consequence of strain hardening of the fault core during slip of the fault, increasing the friction along the fault plane (e.g. Rykkelid and Fossen 2002). These structures are generally not considered to be part of the (brittle) damage zone (Childs et al. 2009), but are both observed during this study, in connection to fault tips.

2.2 Fault growth, propagation and linkage

2.2.1 Fracture networks

Fracture network is an arrangement of two or more fractures that may, or may not interact kinematically and/or geometrically (see definition in Peacock et al. 2016). They display a range of scales, orientations, lengths and sizes, and can be described in terms of their intensity, frequency, spacing, size and topology (e.g. Wheeler and Dixon 1980; Aydin and Schultz 1990; Wu and Pollard 1995; Nixon et al. 2014b; Sanderson and Nixon 2015). Where more than two fracture sets are present in a network, a triaxial strain system develops (e.g. Reches 1978; Krantz 1988). The

complexity of fracture networks, and the valuable knowledge on network properties like connectivity and fluid flow have produced numerous studies on the topic (e.g. Zhang and Sanderson 1995, 1996; Sanderson and Zhang 1999; Leckenby et al. 2005; Kim and Sanderson 2010; Nixon et al. 2012; Sanderson and Nixon 2015; Morley and Nixon 2016). The fracture network that is studied in this thesis is a normal fault network, where the growth and evolution of it through fault propagation and linkage is in focus, subjects that have been acknowledged in earlier studies (e.g. Peacock and Sanderson 1991, 1994a; Cartwright et al. 1995; Childs et al. 1995; Childs et al. 1996a; Childs et al. 1996b; Knott et al. 1996; Peacock 2002; Walsh et al. 2003; Long and Imber 2012; Nixon et al. 2014a).

2.2.2 Growth of normal faults and normal fault systems

There are two end-member models describing the kinematic growth of normal fault systems; the 'isolated fault model' and the 'coherent fault model' (Fig.2.3). They describe two different approaches to mechanisms behind fault growth, and how overlap zones between unconnected fault segments may develop (Childs et al. 1995).

The 'isolated fault model' (e.g. Watterson 1986; Walsh and Watterson 1988; Cowie and Scholz 1992c; Cartwright et al. 1995; Childs et al. 1995; Huggins et al. 1995) propose that normal fault systems grow with increasing fault lengths by lateral propagation (i.e. fault tip propagation) of isolated and independent fault segments, that by coincidence happen to overlap at some point (Fig. 3.2). The fault segments are kinematically independent structures that only overlap by chance as they increase in size. As they grow to overlap an elastic strain field develops between the segments, and they are no longer kinematically independent. The birth of such fault segments must be random and overlap accidently, and the resulting fault zones are often fewer and larger (Cartwright et al. 1995; Childs et al. 1995). A systematic power-law relationship of the displacement and length for this model is proposed (Watterson 1986; Walsh and Watterson 1988 and references therein).

In the 'coherent fault model' (e.g. Peacock and Sanderson 1991; Cartwright et al. 1995; Walsh et al. 2002; Walsh et al. 2003) fault lengths are established quickly during rapid propagation, then followed by a period of accumulation of displacement, without fault length growth (Fig. 2.3). Fault tips are arrested due to interaction between segments in overlap zones (Walsh et al. 2002; Walsh et al. 2003). The coherent fault model also suggests that fault segments within a fault array initiate

and grow as kinematically linked components. Faults may show limited interaction in one level, but are part of a single geometrically- and kinematically coherent structure in three dimensions (Childs et al. 1995; Walsh et al. 2002; Walsh et al. 2003).

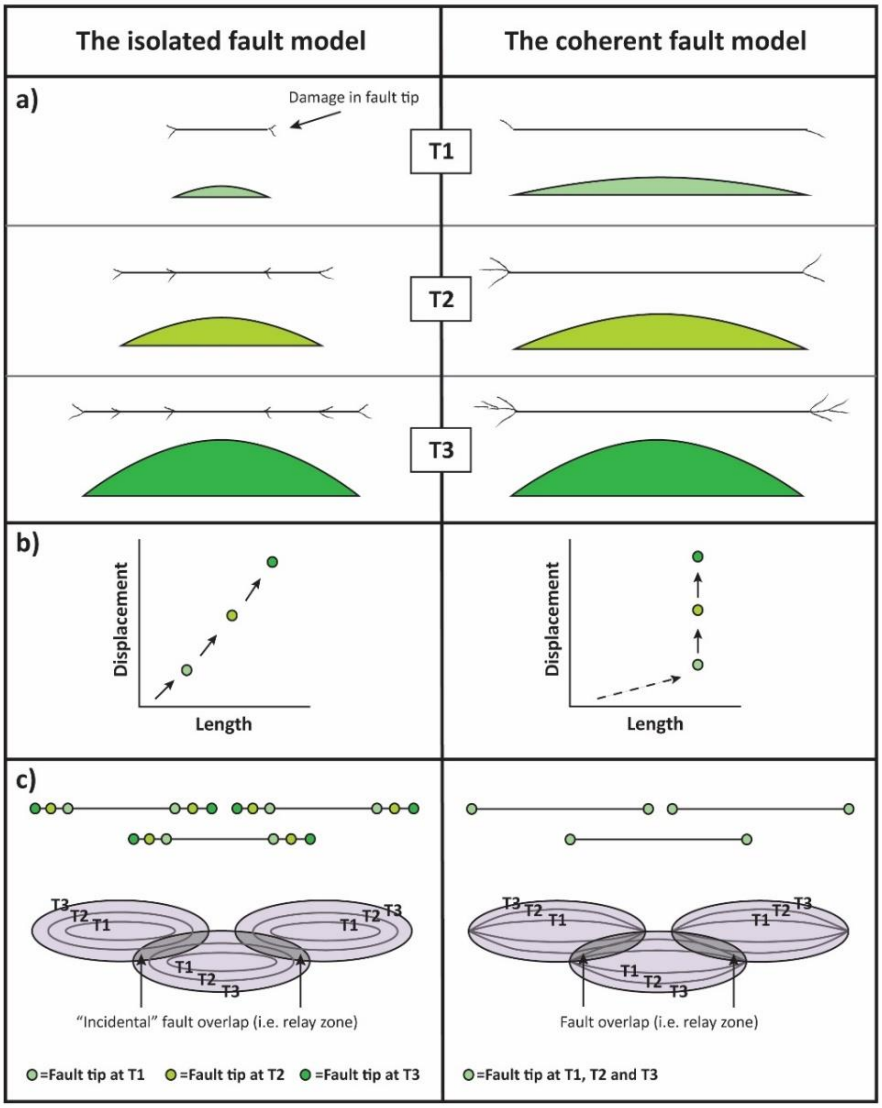

Figure 2.3: Illustration of the two fault growth models; the 'isolated fault model' to the left and the 'coherent fault model' to the right. a) Shows change in fault length, tip-zone and damage related structures in fault trace maps, together with models representing increase in displacement at three time steps (T1 - T3). b) Shows max length vs max displacement trends, where the isolated fault model shows a proportional increase in displacement and length, while the coherent fault model only increases in displacement. c) Present a normal fault system in map-view and strike-projection through three time steps (T1 - T3), where the geometrical and evolutionary features are highlighted for each step. Modified after Nicol et al. (2016) and Jackson et al. (2017).

2.2.3 Fault growth by segment linkage

Most faults consist of an array of discrete segments rather than a single, smooth and continuous slip surface (Peacock 1991; Peacock and Sanderson 1991, 1994a; Childs et al. 1995; Willemse 1997; Walsh et al. 2002; Walsh et al. 2003). Segmentation of normal faults on a wide range of scales has become a universal acknowledgment, and its influence on both growth and geometry of normal faults is highly approved (e.g. Peacock and Sanderson 1991; Walsh and Watterson 1991; Cartwright et al. 1995; Childs et al. 1995; Childs et al. 1996a; Peacock and Sanderson 1996; Walsh et al. 1999; Walsh et al. 2003). Fault zones commonly consist of linked en-échelon fault segments (e.g. Gamond 1987), where merging of these as the fault evolves straightens the active fault trace as well as changing the overall fault zone architecture (Childs et al. 1996a; Childs et al. 2009). Fault segmentation can happen in both map-view (laterally segmented) and cross-section (vertically segmented) which are end-members of the most abundant oblique segmentation. This produces a complex 3-D aspect of the fault (e.g. Walsh and Watterson 1987; Childs et al. 1996a). Linkage of branch lines, which is described as a line of intersection between a main fault and a secondary fault branch (Walsh et al. 1999; Imber et al. 2004), is a consequence of breaching of relay zones in normal fault networks (Childs et al. 1995; Walsh et al. 1999). The types of branch line linkage detected in relay zones during this study are *splay faults* and *abutting faults*.

A *splay fault* is one (or more) minor fault that joins a larger fault that it is related to, and the main fault *splays* if it is connected with a splay fault (Peacock et al. 2016). Fault tip-bifurcation is when the tip of a main fault splays into several fault strands, and this is the most common mechanism of creating splay faults (McGrath and Davison 1995; Nixon et al. 2014a). This is caused by build-up of tensile stress in the fault tip due to slip on the fault, together with heterogeneity in the mechanical properties of the host rock (Segall and Pollard 1983; Pollard and Segall 1987; Huggins et al. 1995; Martel and Boger 1998; Myers and Aydin 2004). Displacement on a splay fault increases towards the intersection line, while the main fault shows a drop of displacement in the line of intersection. This indicates that fault splays accommodate to a decrease in displacement on main faults (Nixon et al. 2014a; Perrin et al. 2016; Peacock et al. 2017).

An *abutting fault* is a fault that meets another fault in a branch line (sensu Peacock et al. 2016). In the definition, abutting faults can either be faults from different fault sets, or faults that have splayed from one another (Peacock et al. 2017). In this thesis, a distinction between splay fault and

abutting fault has been set to the amount of respective fault sets, where splaying faults are part of the same fault set, and abutting faults represent different fault sets. The fault tip of an abutting fault is pinned to the surface of the fault it intersects, and can only propagate away from its abutting tip (Nixon et al. 2014a). In the intersection line of abutments, displacement transfer from the abutting fault to the earlier fault occurs, resulting in increase of displacement where they share fault block (Maerten 2000; Nixon et al. 2014a).

2.3 Relay structures

A relay zone is a zone of geometric or kinematic linkage between sub-parallel faults that dip in the same direction, where displacement is transferred between the offset segments (Larsen 1988; Peacock and Sanderson 1991). This often leads to reorientation of the rock mass between the overstepping faults due to tilting and rotation, producing a *relay ramp* (e.g. Peacock and Sanderson 1991; Walsh and Watterson 1991; Peacock and Sanderson 1994a; Peacock 2002) (Fig 2.2). Relay structures are common in extensional settings, where they form between normal fault segments that step in map-view (e.g. Peacock and Sanderson 1991, 1994a; Peacock 2002; Fossen and Rotevatn 2016). The geometry of the relay structure can be determined by the displacement gradients of the fault segments, where the area of overlap will be marked as a minimum in displacement (Peacock and Sanderson 1991, 1994a). Displacement is accommodated between the two offset segments through the relay ramp, as the kinematic continuity between the footwall and hanging wall is maintained (Larsen 1988; Peacock and Sanderson 1991). Complex brittle deformation (i.e. faults and fractures) can occur to accommodate the rotation of the ramp, and to link the overstepping segments (Griffiths 1980). Displacement is thereby transferred over the relay ramp through brittle deformation and kinematic rotation (Peacock and Sanderson 1991, 1994a).

Peacock and Sanderson (1991) suggests a four-stage model of relay structure development, based on deformation and displacement characteristics of studied normal fault zones (Fig. 2.4). At stage 1 the fault segments are not overlapping and there is no interaction between segments. Fault segments have grown to overlap in stage 2, creating interaction between the segments without any physical linkage. At stage 3 the segments are overlapping and interacting, and secondary faults and fractures start to develop on the relay ramp, destroying it. The offset segments are in stage 4 connected by a continuous fault breaching the relay ramp. The previous fault tips are now relic,

creating a displacement minimum in the linkage zone. Stage 2 are often referred to as an intact relay or *soft linkage* relay (i.e. mechanic and geometric continuity between two adjacent fault segments that are not physically linked), and stage 4 as a breached relay or *hard linkage* relay (i.e. a physical link between adjacent fault segments creating a single continuous fault trace) (Walsh and Watterson 1991; Trudgill and Cartwright 1994; Willemse 1997; Childs et al. 2009). It is important to consider scale when determining soft or hard linkage, as an apparent soft linked structure may be hard linked when observed in more detail (Walsh and Watterson 1991).

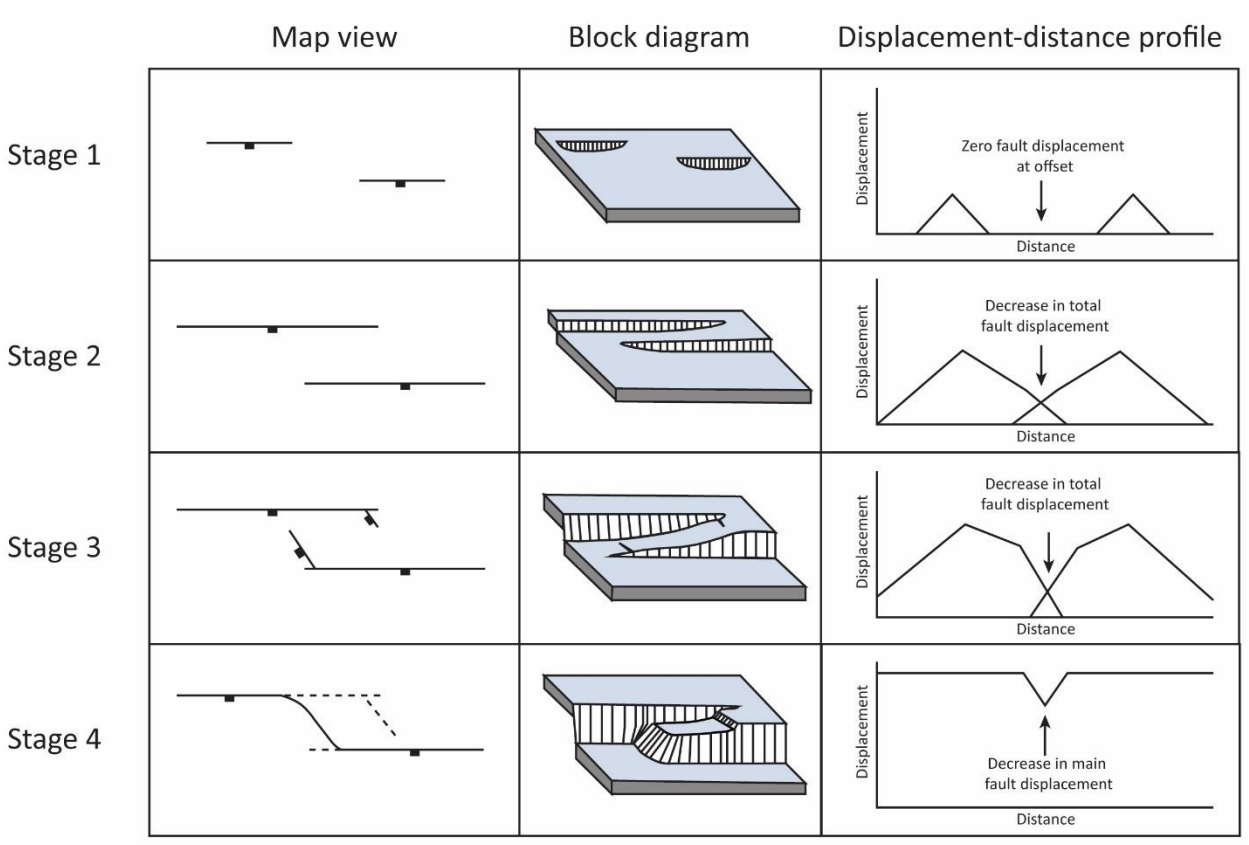

Figure 2.4: Four stage model of relay zone development (modified after Peacock and Sanderson 1991), presented in map-view, block diagram and displacement-distance (d-x) profile. Stage 1; offset underlapping faults. Stage 2; fault overlap, displacement transfer as rotation of relay ramp. Stage 3; overlapping faults continue to grow, and brittle structures start to form on the ramp, destroying it. Stage 4; fault segments are connected by a continuous fault cutting the former ramp, creating a breached relay structure.

The geometry and evolution of relay zones differs in the two models of fault growth for normal fault systems (Section 2.2.2.). In the isolated fault model the geometry of the relay ramp changes gradually as the length of fault overlap increases and displacement accumulates. Progressive rotation of the relay ramp exceeds until the strain compatibility can no longer be maintained, and the ramp breaches (Long and Imber 2012; Hemelsdaël and Ford 2016). For the coherent fault model the relay zones are established quickly, evolving purely by rotation of the relay ramp without lengthening before the breach happens (Hemelsdaël and Ford 2016).

Relay ramps can work as zones where connectivity and fluid flow may be maintained. This is caused by soft linkage across faults which would otherwise be sealing (Rotevatn et al. 2009), but it is also documented that damage zones associated with a relay ramp can represent potential baffles to intra-ramp fluid flow (Rotevatn et al. 2007). Building more knowledge on fault linkage and relay structures is therefore important for defining effective reservoir management strategies (Rykkelid and Fossen 2002).

2.4 Damage zones

A damage zone (Fig. 2.2) is the volume of deformed rock around a fault surface that results from the nucleation, growth, propagation, interaction and build-up of slip along faults (Cowie and Scholz 1992b; Caine et al. 1996; Peacock et al. 2000; Kim et al. 2004). Typically, the intensity of damage related structures decreases moving away from the fault core (e.g. Chester and Logan 1986; Shipton et al. 2006; Gudmundsson et al. 2010), and the boundary of the damage zone is therefore located where the intensity is reduced to a background or minimum value (e.g. Beach et al. 1999; Gudmundsson et al. 2010). A scaling relationship that shows a generally broad correlation between fault damage zone width and displacement has been encountered, but scatter in the distributions occur, and different parameters such as; lithology, diageneses, depth of faulting, tectonic environment and type of deformation mechanism, have been suggested to cause this (see Choi et al. 2016 for main references). The width of fault damage zones is not necessarily symmetrical on each side of the fault trace, and the damage zone width of a normal fault is generally widest in the extensional field of the hanging wall near the upper tip of the fault (Knott et al. 1996; Berg and Skar 2005). Since a single damage zone can consist of numerous deformation structures of different scales, types and orientations, and extend significantly outside the fault core,

it can provide control on permeability and fluid flow in the crust (e.g. Caine et al. 1996; Sanderson and Zhang 1999; Shipton et al. 2002; Kim and Sanderson 2010). The damage zone is thus a significant component of a fracture network, which should be considered in the search of hydrocarbon reservoirs (Aydin 2000; Rotevatn and Fossen 2011).

A general field based classification for damage zones is postulated by Kim et al. (2004), which is based on the location of damage in respect to the overall fault geometry (Fig. 2.5). It is used to describe variation in damage structures along a fault trace, and coincides with the classification of *along-fault damage zone*s (sensu Choi et al. 2016). Kim et al. (2004) defines three endmembers: (1) fault tip damage zone (section 2.4.1); (2) linkage damage zone (section 2.4.2); (3) wall damage zone (section 2.4.3).

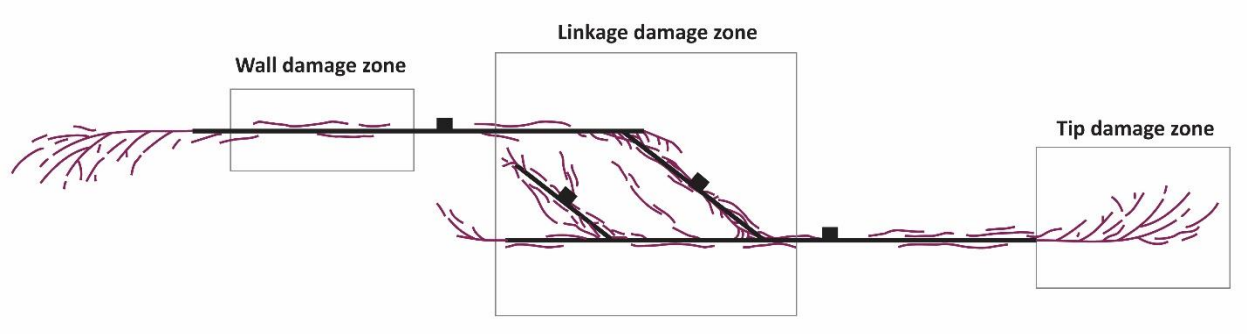

Figure 2.5: Map-view presentation of overlapping normal fault segments highlighting damage zone terminology suggested by Kim et al. (2004), used in this thesis. Tip damage zones are found in fault tips, linkage damage zones in areas where adjacent fault segments overlap and wall damage zones trailing along/parallel to a fault trace, where fault tips and linkage zones are absent.

2.4.1 Fault tip damage zone

The fault tip damage zone (Fig. 2.5), is a zone of increased fracturing in the tip of a fault, produced in the *process zone* (sensu Scholz et al. 1993) where stress concentrations by fault propagation creates micro-crack damage, resulting in fault growth and creation of a tip damage zone (Cowie and Scholz 1992a, 1992c; Vermilye and Scholz 1998). The geometry of the fault tip damage zone is often wedge shaped, and in plan-view a fault tip can be observed parallel (strike-slip sense) or perpendicular (dip-slip sense) to the main slip sense, as mode II or mode III, respectively (Kim et al. 2004) (Fig. 2.6). Fault tips can thus be classified as dominated by mode II (sliding), mode III (tearing) or mixed mode II/III fracturing in 3-D. Mode II and mode III tip damage zones are end-

members, and the majority would rather be mixed mode (Childs et al. 1995; Walsh et al. 2003; Choi et al. 2016). Mode II tip damage zones are usually asymmetrical and are typically characterized by wing cracks, horsetail fractures, antithetic faults and synthetic faults. Mode III tip damage zones are often more symmetrical, and commonly include antithetic and synthetic faults (McGrath and Davison 1995; Kim et al. 2004). Evidence of plastic deformation in tip damage zones are also found, where both frictional drag and fault propagation folds are observed (McGrath and Davison 1995; Hesthammer and Fossen 1998).

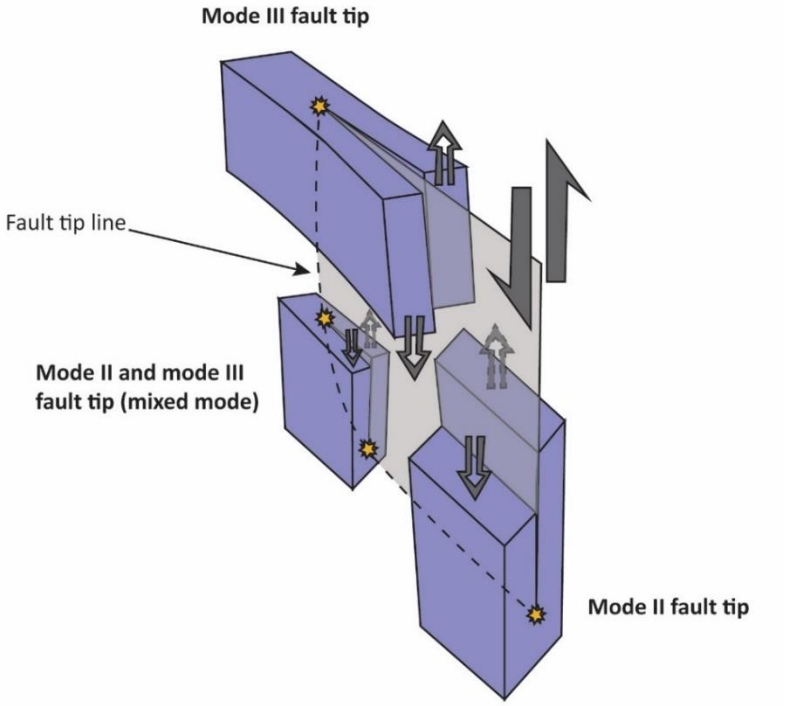

Figure 2.6: Schematic model of fault tip modes (modified after Kim et al. 2004) based on the slip sense of the fault at the observed fault tip. The model shows a part of a normal fault plane with the location of mode II (sliding), mode III (tearing) and mixed mode (combination of mode II and mode III) fault tips. The star symbols indicate exposed tip points.

2.4.2 Linkage damage zone

The linkage damage zone as defined by Kim et al. (2004) includes the zone of deformed rock caused by the interaction and linkage of fault segments that can create a wide range of fracture patterns depending on the nature of interaction. Peacock et al. (2017) defines this zone as an *interaction damage zone* which is a more general term. Linkage damage zone (Fig. 2.5) is thus a

very broad classification, as it includes damage zones associated with different types of interactions, including; cross-cutting faults, mutual interactions, single-tip interactions and double-tip interactions (Fossen et al. 2005).

Cross-cutting faults (i.e. faults of different ages that intersect) create a damage zone with overprint relation, where the youngest damage zone overprints the older. Mutual interactions (i.e. conjugate faults active under the same stress field) develop a significantly wider damage zone than the cross-cutting faults, due to repetitively mutual movement during strain accumulation (Watterson et al. 1998; Fossen et al. 2005).

Relay ramps may be considered as linkage damage zones (Kim et al. 2004), single- or double-tip interaction damage zones (Fossen et al. 2005) or mode III linkage damage zones (Choi et al. 2016). In a breached relay, single-tip interaction will occur where the breaching fault intersects with the relay bounding faults. Soft linked relays work as double-tip interactions, where the linkage area experiences both brittle damage and ductile deformation (Peacock and Sanderson 1994a; Fossen et al. 2005). The width of the damage zone includes the whole linkage area, which creates an abnormally wide damage zone (Fossen et al. 2005; Rotevatn et al. 2007). Combined with greater damage zone width, the fracture networks documented for breached relays also include increased fracture density (i.e. number of fractures / m) and varied fracture orientations (e.g. Bastesen and Rotevatn 2012). It is therefore expected that linkage areas have a wider damage zone, more complex fracture orientations and higher fracture intensity, compared with isolated faults (e.g. Peacock and Sanderson 1994a; Fossen et al. 2005).

2.4.3 Wall damage zone

Wall damage zone (Fig. 2.5) is the zone of deformed wall rock trailing along/parallel to the fault trace, produced by the propagation and kinematic slip of the fault (Kim et al. 2004). This zone is found in between tip damage zones for single isolated fault segments, and outside areas of linkage for segmented fault arrays (Kim et al. 2004; Fossen et al. 2005), although wall damage may still be related to both fault tips and linkage zones that do not intersect the exposed surface (Kim et al. 2003). The wall damage zone is generally quite narrow compared to the tip- and linkage damage zone, and structures are mainly oriented normal to extension direction (e.g. Peacock and Sanderson 1994a; Fossen et al. 2005).

2.5 Spatial distribution of deformation in normal fault networks

The four previous sections have introduced types of brittle structures typically found in extensional settings, how they grow and evolve into fault networks that show segmentation and linkage, and how the damage zone of a fault network changes after the geometry of participating fault interactions. What has not been highlighted is how these deformation structures contribute to the total accommodation of strain, and how they are distributed in a chosen normal fault network. Different approaches to quantify and illustrate distribution of deformation has been developed, and the two approaches used in this thesis will now be briefly described.

Spatial heterogeneity of strain is a measure of the overall distribution of strain in a fault network, based on the contribution from all involved segments (e.g. Putz-Perrier and Sanderson 2008a, 2008b; Nixon et al. 2014b). A method for quantifying the spatial heterogeneity is presented by Putz-Perrier and Sanderson (2008a) which consider both the size and displacement of the sampled structures. This method will be closer described in section 4.3.3. Using heterogeneity analysis a spatial measure of fault distribution is given, where a distinction between distributed and localized faulting can be achieved (e.g. Nixon et al. 2014b) (Fig. 2.7) . Distributed faulting is characterized by an array of numerous small faults, all contributing to the overall strain, shown as low heterogeneity of the network. Whereas localized faulting is characterized by few individual large faults that accommodate the majority of strain, shown as high heterogeneity (Soliva and Schultz 2008; Nixon et al. 2014b).

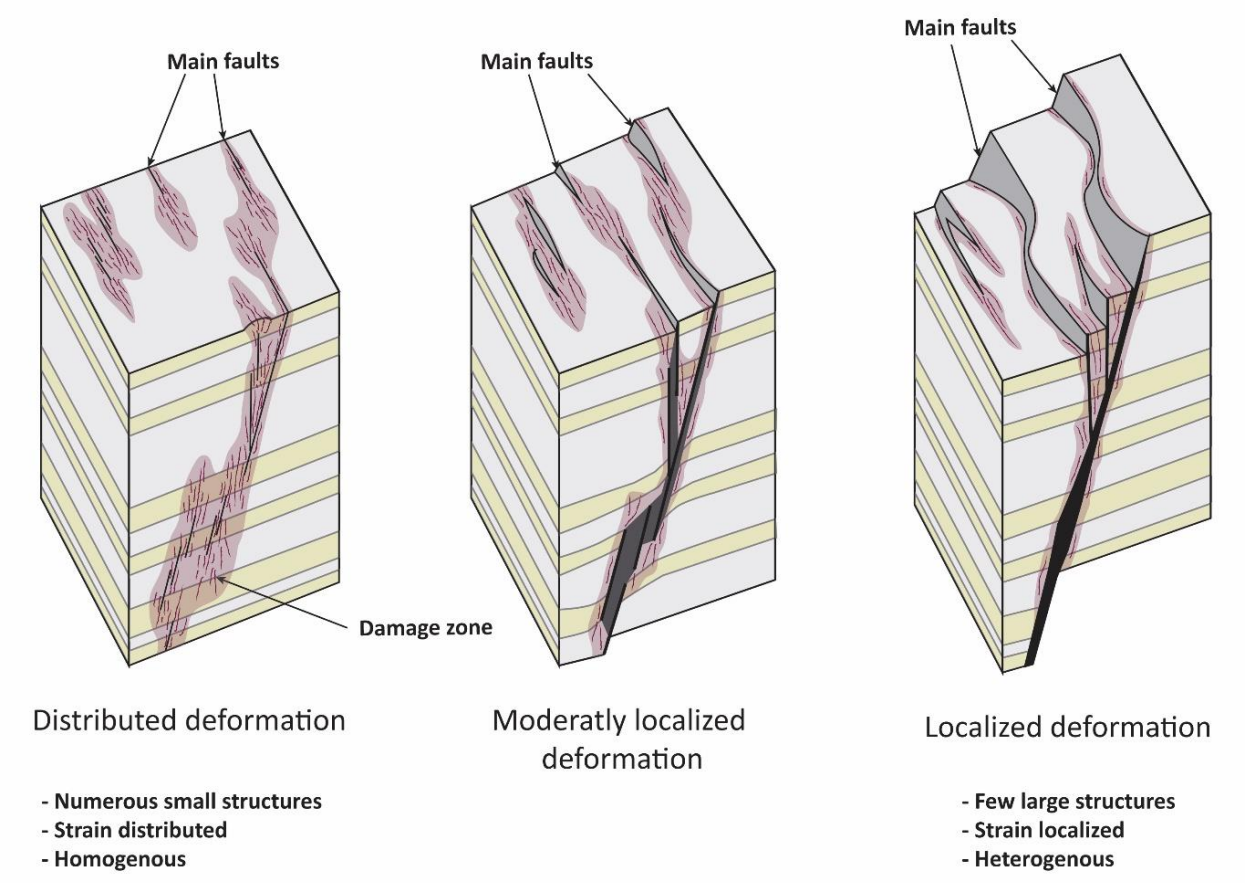

Figure 2.7: Characteristics in spatial distribution of deformation presented in 3-D block diagrams showing main differences between distributed and localized deformation.

Mapping displacement in normal fault networks is another approach to investigate the distribution of deformation, and is often done using a *displacement-distance (d-x) analysis* (Williams and Chapman 1983) illustrating how displacement varies along a geological structure (Peacock et al. 2000) (see section 4.3.2 for more details). This approach has been adapted to fault network analysis as well as for isolated faults, and some topics that are highlighted are: discovery and analysis of linkage and segmentation between faults (e.g. Peacock and Sanderson 1991; Childs et al. 1995; Huggins et al. 1995; Peacock and Sanderson 1996; Willemse 1997; Walsh et al. 2003; Long and Imber 2011; Nixon et al. 2014a), investigation of localized and distributed faulting (e.g. Soliva and Schultz 2008; Nixon et al. 2014b) and investigation of fault tip damage zones (e.g. McGrath and Davison 1995). For isolated faults a bell curved convex-up profile with maximum displacement in the centre of the fault trace is expected (Walsh and Watterson 1989), while for fault systems with overlapping fault segments, displacement minima's are expected in area of fault

segment overlap, due to local reduction in shear stress where slip is moved to adjacent segments (e.g. Peacock and Sanderson 1991; Willemse 1997; Walsh et al. 2003). Profiles representing cumulative total of a fault system comprising of several distinct segments will show shape similarities to the profile of an isolated fault if the segments behave as one kinematically coherent structure (Walsh et al. 2003). Studying the shape of (d-x) profiles can thus be used to identify fault overlap zones and segmentation (Peacock and Sanderson 1991; Soliva et al. 2008).

3 Geological setting

Kilve and Lilstock are located on the Somerset coast on the southern margin of the Bristol Channel Basin (BCB), which is part of the larger south Celtic Sea (Van Hoorn 1987; Brooks et al. 1988; Peacock and Sanderson 1999) (Fig. 3.1a). In this chapter the structure and evolution of the Bristol Channel Basin will be presented (section 3.1), before the extensional deformation at Kilve and Lilstock will be introduced (section 3.2). Finally, the stratigraphic framework of the area is emphasized (section 3.3).

3.1 Structure and evolution of the Bristol Channel Basin

The narrow and elongated Bristol Channel Basin is structurally divided into two sub-basins, the Main Bristol Channel Basin (MBCB) and the East Bristol Channel Basin (EBCB), based on structural trends and basin fill. The MBCB, in the west, is oriented ENE-WSW, whereas the smaller EBCB, located to the east, is orientated E-W (Kamerling 1979) (Fig. 3.1a). Between these two basins is an intermediate area, which incorporates structural and stratigraphic features of the sub-basins on either side. This sub-division seems to result from major NW-SE trending basement faults (e.g. Sticklepath Fault and Cothelstone Fault) that intersect the Bristol Channel area (Kamerling 1979; Glen et al. 2005). These were originally dextral wrench faults during the Variscan orogeny in Devonian and Carboniferous (Kamerling 1979), that were reactivated during the Alpine orogeny (Cretaceous and Paleogene). In the center of the basin an en-échelon S-dipping normal fault zone termed Central Bristol Channel Fault Zone (CBCFZ) is located, which influenced the sedimentation in the BCB (Peacock and Sanderson 1999).

The BCB sits on a basement of Carboniferous limestones and Devonian sandstones and slates, deformed during the N-S contraction of the Variscan orogeny (Dart et al. 1995; Nemcok et al. 1995) and formed primarily during the Jurassic to Early Cretaceous (Kamerling 1979; Chadwick 1986; Van Hoorn 1987). Large faults cutting parts of, or the entire BCB, show a strong control on the structural framework of the basin, and three main faults are directly involved in the controlling mechanisms of the Somerset coast. The Cothelstone Fault mentioned earlier, is a dextral NE-SW trending basement fault that cut across the whole BCB, intersecting the coastline of Somerset in

the Watchet area (Fig. 3.1b). On each side of this fault, two E-W trending N-dipping normal faults with large throws are detected. The North Quantocks Fault (NQF) explains the boundary between Devonian and Carboniferous rocks of the Quantock Hills and the Mesozoic rocks of the BCB seen at Somerset (Peacock and Sanderson 1999). It is located along the northern edge of the Quantock Hills, shows at least 1 km throw, and dies out around Watchet. Along the northern edge of the Exmoor Hills, the evidence of another fault termed the North Exmoor Fault (NEF) is found. NQF and NEF may originally have been a single fault displaced by the Cothelstone fault, or alternatively they have initiated as separate faults with a relay ramp between them (illustrated as grey area in Figure 3.1b), where a link in the sub-surface is likely (Peacock and Sanderson 1999).

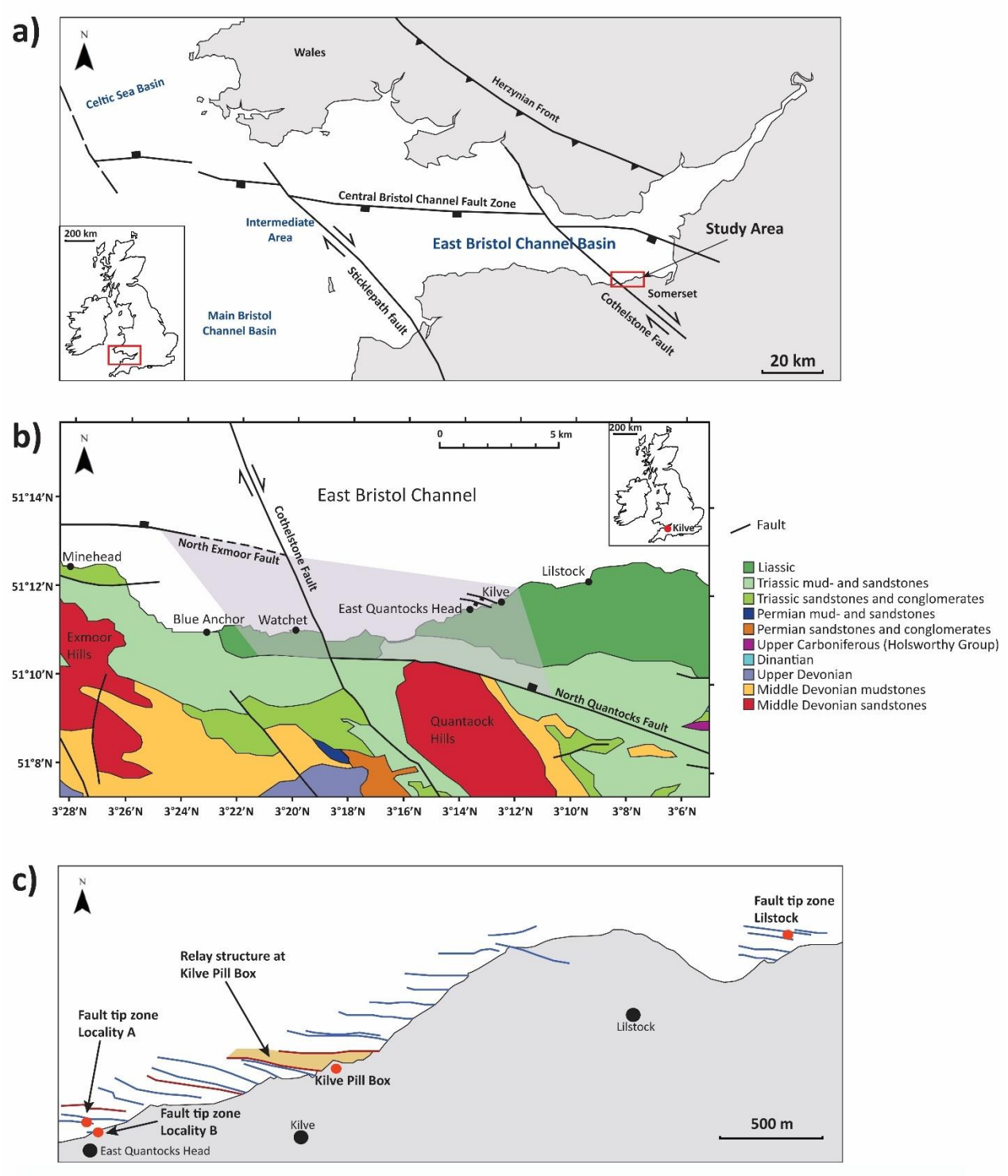

Figure 3.1: a) Geological map over the Bristol Channel Basin and surroundings, showing the main structural features. Modified after Kamerling 1979, Dart et al. 1995 and Skar et al. 2016. Study area is located on the southern margin of the East Bristol Channel Basin, marked with red box on the map over UK. b) Geological map over part of the Somerset coast, including lithology grouped after depositional age. Modified after Peacock et al 2017, who had it reproduced

with permission of the British Geological Survey ©NERC. All rights Reserved. The Cothelstone Fault, North Quantocks Fault (NQF) and North Exmoor Fault (NEF) are marked, and the grey area represents a possible relay between NQF and NEF. c) Map over the study area, where localities are marked with red dots. The relay ramp at Kilve Pill Box is shaded. Large normal faults, representing main structural features of the area between East Quantocks Head and Lilstock, are in red (south-dipping faults) and blue (north-dipping faults), showing even spacing and similar orientations (approximately E-W).

The structural evolution of the BCB is well constrained and involves basin formation during the Mesozoic and reactivation and post-basinal deformation during the Paleogene. During the structural evolution the regional stress orientation affecting the basin varied significantly resulting in a range of different structures. The evolution of these stresses and timing of the structures are summarized below.

Late Permian to Early Triassic

A regional fault controlled subsidence started the structural evolution of the BCB, causing N-S extension and reactivation of the Variscan thrust zone in Late Permian - Early Triassic (Kamerling 1979; Van Hoorn 1987; Brooks et al. 1988). This tectonic setting lasted until the Late Jurassic, and the deformation structures of the area were dominated by E-W 095° striking normal faults with associated calcite veining and gentle folds (e.g. Nemcok et al. 1995; Peacock and Sanderson 1999). The NQF and NEF was formed during this deformation stage (Peacock and Sanderson 1999).

Late Jurassic and Cretaceous

In the Late Jurassic the area experienced some epeirogenetic movements, which resulted in uplift of the basin. The tectonic deformation was not great, and regressive sedimentation and erosion of the basin margins dominated, giving the basin the elongated and narrow shape seen today (Kamerling 1979; Van Hoorn 1987). It is suggested that in the Early Cretaceous σ^1 was oriented ~NW-SE, as evidence of sinistral shear followed by dextral reactivation of some 095° striking normal faults are found (Peacock and Sanderson 1999).

Paleogene

In Paleogene, the regional main compressive stresses experienced a reversal. Before this, σ^1 was oriented ~E-W, making an extension oriented N-S in the basin. Due to the deformation creating the Alpine Mountain Belt further south and southeast in Europe, the main compressive stresses shifted to N-S, producing N-S contraction and mild basin inversion of the BCB (Kamerling 1979;

Van Hoorn 1987; Dart et al. 1995; Peacock and Sanderson 1999). An array of structural features was produced, including: reverse reactivation of former 095°striking normal faults, N-S striking calcite veins, E-W striking thrusts and tightening of E-W striking folds and earlier roll-overs related to wall rock deformation around normal faults (e.g. Peacock and Sanderson 1992, 1995; Rawnsley et al. 1998; Kelly et al. 1999; Peacock and Sanderson 1999). Strike-slip faults conjugate about N-S with displacements of up to hundreds of meters also cut the reverse reactivated normal faults (Dart et al. 1995).

Observed joints post-date faulting because they are not displaced by, cross-cut or abut against faults in the area, and thus represents a more recent deformation stage (Engelder and Peacock 2001; Peacock 2004). They may represent post-Alpine relaxation of stresses related to regional erosion and uplift (Rawnsley et al. 1998; Peacock 2004).

3.2 Extensional deformation at Kilve and Lilstock

Based on the structural framework presented in the former section, structures found on the Somerset coast demonstrate both Mesozoic basin evolution and Paleogene (Alpine) basin inversion. This study focuses on extensional structures (i.e. faults and veins) found at Kilve and Lilstock, so a detailed description of such structures found in the area is needed. Mesoscale 095° striking normal faults dipping both to north and south is observed along the entire coast line of the study area (Fig. 3.1c), and they represent deformation during the Mesozoic N-S extension (e.g. Nemcok et al. 1995; Peacock and Sanderson 1999). The S-dipping faults are nearly vertical (80°), while N-dipping faults show dips around 33 - 48° (e.g. Peacock and Sanderson 1991; McGrath and Davison 1995; Skar et al. 2016). The N-dipping faults of the fault population show approximately similar separations (10 – 30 m) and planar geometries. They also have regular spacing of ~100 m, and bedding is tilted ~20°S within the fault blocks, indicating a domino effect rotation (Dart et al. 1995). These larger N-dipping faults may thus represent a regional system of domino faulting.

The fault population in Somerset is described by Peacock and Sanderson (1991) as a series of interacting and linked segments, although in map-view they appear planar. The faults are geometrically linked by abutting faults, cross-cutting relationships and fault splays, and kinematically linked through relay structures (Peacock et al. 2017). The largest displaced faults

exposed in the area (tens to hundreds of meters separation) dip to the south (Fig. 3.1c), and relay ramps created between these faults show populations of smaller antithetic N-dipping faults. These faults transfer displacement between the overstepping segments (Peacock and Sanderson 1999). The field location at Kilve is located in such a relay (Fig.1.3c). Paleogene N-S compression is mostly represented by strike-slip faults conjugate about N-S, but some reverse-reactivated normal faults also occur (e.g. Peacock and Sanderson 1995; Rawnsley et al. 1998; Kelly et al. 1999). These structures are not of focus in this study, and normal faults used are not reactivated.

More complex deformation structures are observed at Lilstock than at Kilve. This complexity is described by Peacock and Sanderson (1999), which explain it by the possible formation of a large-scale relay between the NQF and NEF (Fig.3.1b). Kilve would be located inside this major ramp, and the geometry of the relay structure would work as a stress shadow, refracting regional stresses. Lilstock would be located outside the ramp, and experience the occasional flip of σ^1 and σ^2, explaining sinistral movement on some faults at Lilstock, not observed at Kilve. This can also explain the origin of the large-scale S-dipping faults observed at Kilve, which would be located within the relay ramp, working as transfer faults of displacement between NQF and NEF (Peacock and Sanderson 1999). This, combined with the observed N-dipping transfer faults within relays of the large-scale S-dipping faults, illustrates a scaling relationship between relays representing at least three orders of magnitude.

Small-scale deformation structures representing damage of the larger faults are characterized by antithetic or synthetic secondary faults, and extensional fractures (e.g. McGrath and Davison 1995; Skar et al. 2016). In this study, the focus is on the mineral filled extensional fractures found in limestone bedding. The fractures are sub-vertical and are characterized by extensive calcite cementation, creating calcite veins (Peacock and Sanderson 1991, 1992; McGrath and Davison 1995). The veins typically occur at fault tips and sub-parallel to fault traces, highly localized close to the normal faults (Peacock and Sanderson 1991; Putz-Perrier and Sanderson 2008a). As faults die out laterally, they are exchanged by veins striking parallel to their orientation continuing the fault trace, and Peacock and Sanderson (1992) suggest that faults initiated as veins (or later mineralized open fractures). Veins in the area are thus associated with the formation and growth of faults. In the dip-direction vein lengths are constrained by the thickness of limestone beds, demonstrating that they are generally stratabound. In the strike direction vein lengths can extend freely, and lengths up to 20 m are observed by Skar et al. (2016). The veining at Kilve has earlier

been studied both in meso- (e.g. Peacock and Sanderson 1991; McGrath and Davison 1995; Roberts et al. 1999; Skar et al. 2016) and microscale (e.g. McGrath and Davison 1995).

3.3 Stratigraphic framework

The BCB is a narrow and elongated sedimentary trough that is filled with Triassic marls and Jurassic marine sediments represented by limestones and shales (Palmer 1972; Whittaker 1983; Van Hoorn 1987). The EBCB shows an almost completely preserved Jurassic sedimentary section of about 2000 m in the deepest part of the basin, which is said to be underlain by up to 270 m of Triassic sediments (Lloyd et al. 1973). The sedimentary section exposed on the inter-tidal platform that stretches from Kilve to Lilstock has been closely studied and mapped out, and a detailed stratigraphic log has been drawn of a 120 m thick sequence based on the work of Palmer (1972) and Whittaker (1983) (Fig. 3.2).

This sets the stratigraphic framework of the study area, as the structures examined at Kilve and Lilstock cut through Early Jurassic (Liassic) interbedded limestones and shales. The limestone beds are well cemented and represented by laterally persistent beds (>200 m), and some lenticulate beds. The lenticular bedding might have formed due to secondary diagenetic calcite precipitation (McGrath and Davison 1995). The limestone beds work as useful maker beds that can be traced and correlated across the whole study area. The shales make up ~75 % of the total sequence (McGrath and Davison 1995). A division of the stratigraphic succession into different groups based on the lithological differences found within it has been done by Palmer (1972). The Blue Lias is the part of the sequence that shows the highest limestone bed intensity represented by bed thicknesses varying from 10 - 60 cm. It also contains all the key marker beds used in this study. Above and below the Blue Lias there are shale dominated units, the Kilve Shales above, and the St Audrie's Shales below (Fig 3.2).

Due to fault block rotation, there is an observed rotation of bedding in the Kilve area. The former horizontal bedding is now tilted to the SE, with an average dip value of 16°. Due to this bed rotation and erosion, limestone bedding planes are exposed. The size of the exposed area depends on the above-laying stratigraphy, the tilt of bedding and the amount of erosion, but mostly a shelf of ~1 m width is visible, giving great exposure of brittle structures cutting the surface.

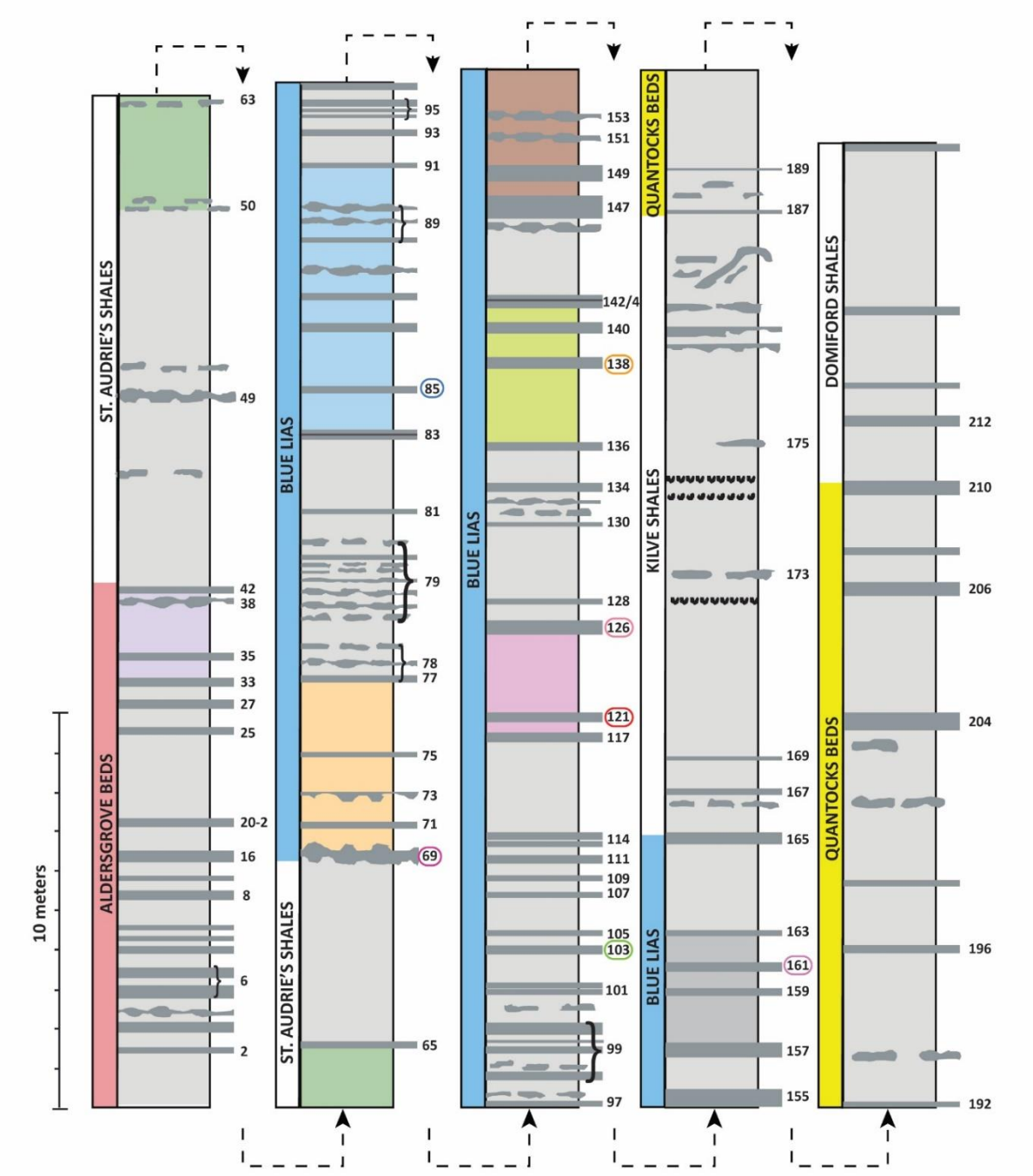

Figure 3.2: Stratigraphy of the studied section, modified after Palmer (1972) and Whittaker and Green (1983). Carbonate beds are presented in dark grey and are labelled with their bed numbers. Key marker beds have colored circles around their bed number (same color as used for bed interpretation in ArcGIS, which will be used in chapter 5). Shales are presented in light grey. Distinctive bed-sequences used to highlight the stratigraphy in cross-sections (Fig 5.2) are marked with the same color code.

4 Methodology

Using a combination of field observations and analysis from digital aerial photography in ArcGIS the distribution of deformation and damage associated with relays and tips of normal faults was assessed at a range of scales.

Different examples of relays and tip zones (locations marked in Figure 3.1c) of varying length scales (one meter to hundreds of meters) were examined in field by documenting damage related small faults and veins. Veins measured in mm and major faults measured in hundreds of meters give an examined structural scale range of three orders of magnitude. Small-scale deformation (veins and small faults) were documented during field work, while the large-scale deformation was studied using ArcGIS. ArcGIS was also used for further analysis and processing of data gathered in field. The work flow from field and map interpretation, to data processing and analysis in ArcGIS and spreadsheets is visualized in a simple flow chart (Fig. 4.1). This chapter thus provides an overview of the methods used for data collection done during field work (section 4.1), and interpretation of aerial photographs, together with processing and analysis of field observations using ArcGIS (section 4.2). Additionally, methods used for further fault-, vein- and strain analysis, covering spatial distribution of faulting, veins, displacements and strain is presented (section 4.3), before a final section highlights some of the limitations and sources of errors related to the study (section 4.4).

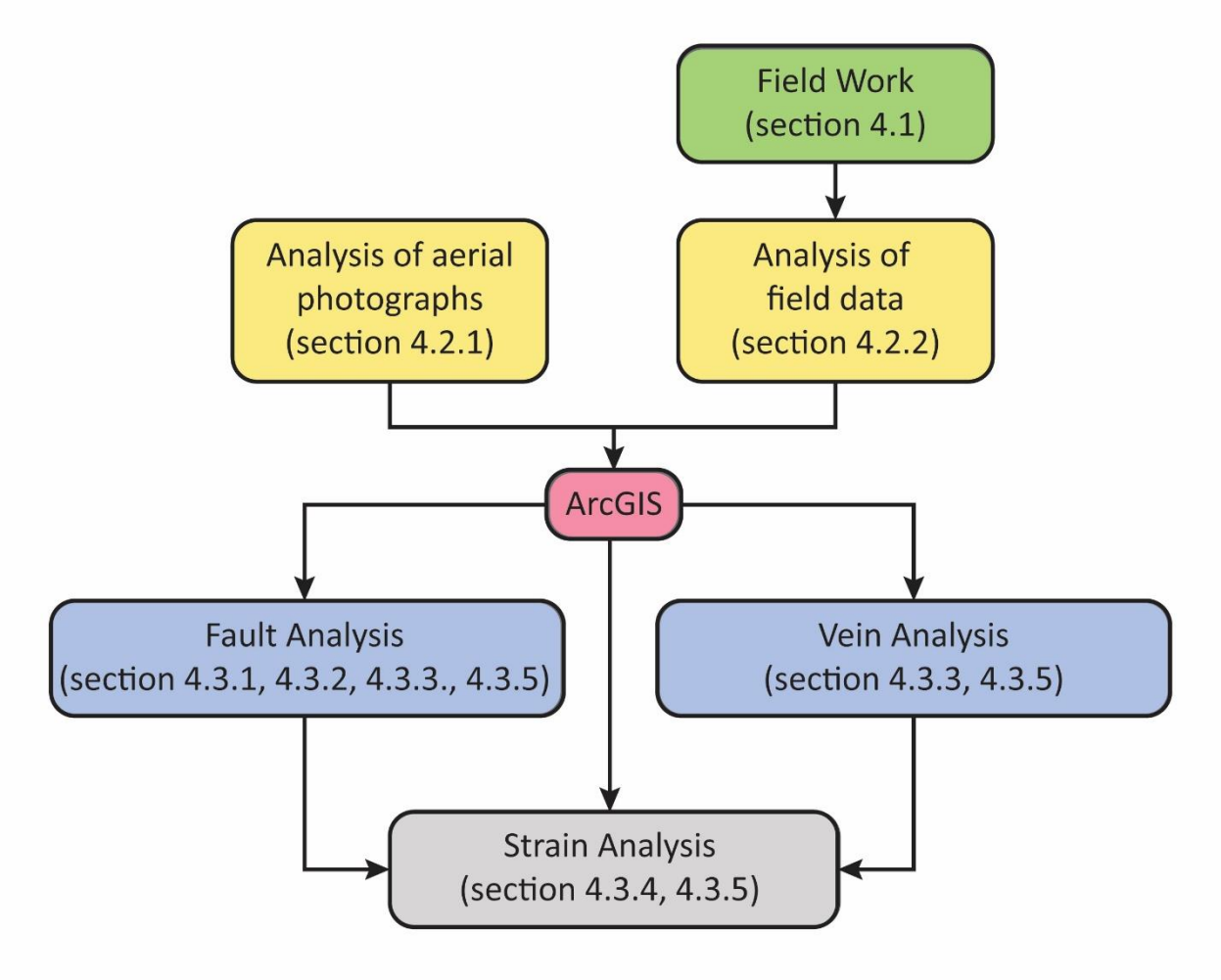

Figure 4.1: Work flow chart of thesis; field work lead to further interpretation and data processing in ArcGIS, to extraction of data for further fault-, vein- and strain analysis.

4.1 Field methods

Two field seasons to Kilve were carried out during autumn 2016, from 31st of September to 11th of October, and 2nd to 13th of November. Field work focused on the mapping and collection of vein data and 3-D structural measurements (i.e. dip and dip direction of faults, bedding and slickensides) associated with the normal faults within the mesoscale relay structure on the wave-cut platform at Kilve Pill Box (Fig. 3.1c). Furthermore, outcrop scale damage zones at fault tips at Lilstock and East Quantocks Head (Fig. 3.1c) were documented and mapped to gather data on displacements and distribution of deformation within these zones.

4.1.1 Documentation of outcrop scale examples

At the study area at Kilve Beach (Fig. 3.1c) a normal fault network created in the relay ramp of two overlapping S-dipping faults was mapped in detail. This was done using printed maps of the wave-cut platform from ArcGIS and measuring tools. Mapping of faults in field was concentrated on the more complex areas, since non-complex areas could be interpreted in ArcGIS directly (section 4.2.1). Detailed mapping of faults and bedding in such areas was done on printed maps from ArcGIS, guided by the high resolution (≤0.2 m) stratigraphic log drawn of the sequence exposed (Fig. 3.2). In this way ground truth data collected directly at location could be combined with further mapping in ArcGIS to decrease resolution errors, and increase details of the resulting fault map. By matching up marker beds on each side of fault traces, fault separations could also be found directly in field (same method as used in ArcGIS, see further description in section 4.2.1). Measurements of fault orientations were spread out over the whole main study area, to capture the diversity. Vein data was collected with the sampling strategy presented in section 4.1.2.

Detailed outcrop scale studies of tip zones at Lilstock and East Quantocks Head (Fig. 3.1c) was performed to give a broader data set covering both linkage damage- and tip damage zones. The fault tips were mapped by taking displacement measurements and documenting vein distributions along strike, using the same sampling strategy used at Kilve (section 4.1.2). 3-D structural measurements of faults and bedding were sampled, together with photographs documenting vein geometries and tip related deformation of bedding.

4.1.2 Vein data collection

Calcite veins associated with faulting of the area was identified as mm scale planar lines oriented sub-parallel to, and near fault traces. In the mesoscale relay structure at Kilve, vein sampling was designed to systematically capture any spatial variation throughout the relay zone. Veins were sampled in the hanging wall and footwall of faults along seven key limestone marker beds (69, 85, 103, 121, 126, 138, 161) (Fig. 3.2). These key marker beds have similar thicknesses (~15 - 25 cm) and cover the width of the relay zone producing approximately N-S oriented scan lines providing a spread of measurements both across and along-strike of the relay zone. They are also isolated, not interfered by other limestone beds. Multiple 1 m transects were taken along each marker bed spaced ~5 - 10 m focused on capturing FW and HW of every fault and fault tip crossing the marker

bed. Transects were taken perpendicular to the trend of veining starting at fault core or with largest vein in the middle when a fault trace was absent (Fig. 4.2). Visible veins with apertures >1 mm were measured, while veins with apertures <1 mm were counted, and bed dip, dip direction and thickness measured. For transects near faults the distance from the fault core to the last visible vein moving normal away from the fault plane was measured, mapping out the damage zone width of the fault.

The same sampling strategy was used to capture the vein distribution in the damage zone for the fault tip studies, but here the whole damage zone width represents the length of the sampling transect, and all veins inside this length were documented.

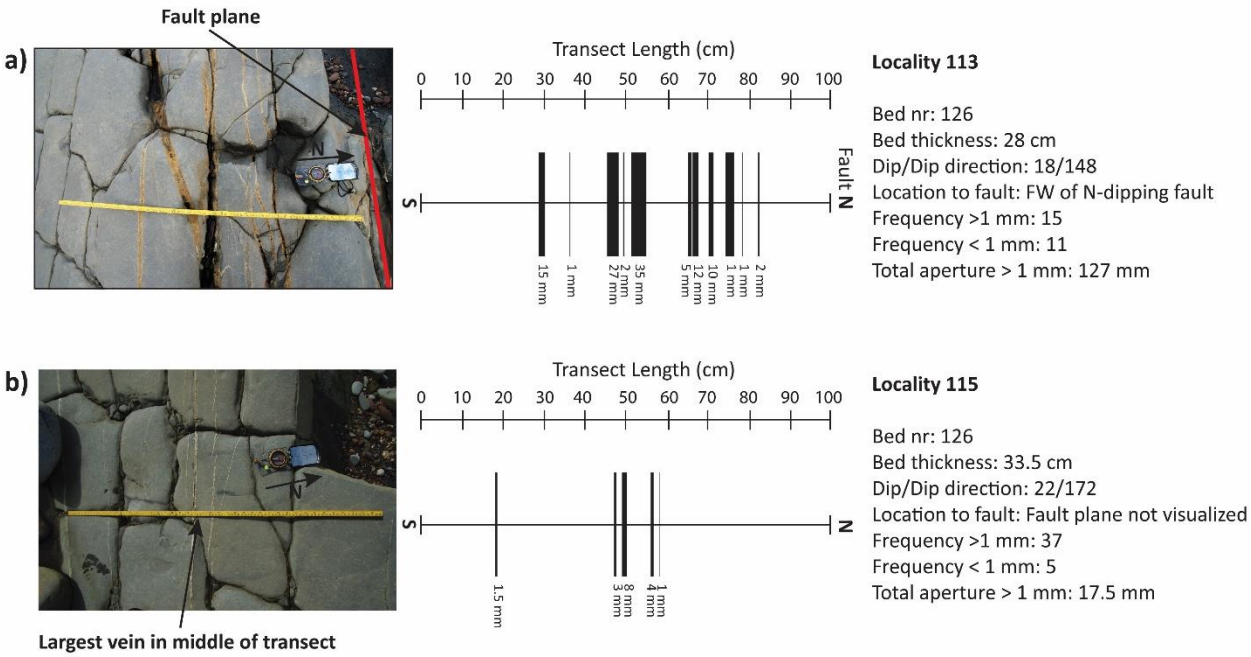

Figure 4.2: Vein sampling strategy as preformed in field. a) Picture of a vein transect at the FW block of a N-dipping fault (locality 113), where the transect stops at the fault core. b) Picture of a vein transect where the fault plane is not visualized (locality 115), where the thickest vein is placed in the middle of the transect. The transects were drawn as the illustrations show, and measured parameters are listed to the right of each transect.

4.1.3 Parameters calculated from vein data

The vein data collected in field (i.e. aperture and vein frequency) was used to calculate different parameters used in the distribution analyses done later in the project.

i. Vein intensity

Vein intensity is defined in this study as the frequency of veins >1 mm per unit length, here represented by the transect lengths:

Intensity = frequency of measured veins / transect length

ii. **Vein strain (% extension)**

Vein strain is defined in this study as the percentage amount of opening (i.e. aperture) produced by veins >1 mm of the original transect length:

% extension = (total aperture / (transect length – total aperture))

iii. **Damage zone**

The width of the damage zone is defined as the normal distance away from a fault trace, in both directions, to where the last visible vein is observed. This length was measured directly in field, and the vein intensity and strain of the FW and HW side of the faults were extrapolated from those calculated from frequencies and apertures sampled in the 1 m transects.

4.2 Analysis in ArcGIS

ArcGIS is a geographic information system (GIS), and was used both for interpretation and mapping of faults and bedding using digital aerial photographs of the study area, and for integration and further analysis of field data. During data processing in ArcGIS, key attributes (e.g. displacement, stratigraphic separation, heave, vein aperture, vein frequency, vein intensity, strain etc.) were used to produce attribute based maps where visualization of measurements eased further analyses of data.

4.2.1 Fault mapping by aerial photographs

A detailed fault and marker bed map of the mesoscale relay at Kilve was interpreted and analyzed in ArcGIS. The relay ramp outcrops across the width (~150 m) of an extensively exposed wave-cut platform. Faults and marker beds were interpreted and digitized from digital aerial photographs, acquired during low tide in 2008 and made available courtesy of the Channel Coast Observatory. The pixel resolution of the photographs is 0.1 m and they are orthorectified. Additional UAV photography with a pixel resolution of 0.03 m was acquired and used for better examination of the fault tip zone at Lilstock.

Marker beds from the well-documented log of the local stratigraphy (Fig. 3.2), were identified and correlated across faults, creating laterally offset stratigraphic sequences. The stratigraphic juxtaposition (cut-off) of a marker bed represents the stratigraphic separation at that location along the fault (e.g. Sanderson 2016). Measured lateral stratigraphic distances between different marker bed cut-offs on either side of a fault can be proportionally converted into vertical stratigraphic distances using the local stratigraphic log. Thus the stratigraphic separation of marker bed cut-offs can be determined at various points along each fault trace (Fig. 4.3a) (see appendix I – workflow 2 for more details). To determine average separation values along the faults, fault traces were divided into segments separated by the stratigraphic separation cut-off points. By calculating an average value of the points enclosing a segment, an average value of stratigraphic separation of that segment is assigned. Stratigraphic separations were also measured directly in the cliff section for some faults (Fig. 4.3b).

If the orientation of the bedding and fault plane are known together with the *stratigraphic separation* (S_S) then the geometrical relationships can be used to determine any other separation parameter, including *displacement* (*D*), *throw* (*T*) and *heave* (H) following:

$$D = S_S / \sin\theta$$

$$H = D \times \cos\Phi = (S_S \times \cos\Phi) / \sin\theta)$$

$$T = D \times \sin\Phi = (S_S \times \sin\Phi) / \sin\theta)$$

Where θ and Φ represent the bed dip and fault dip, respectively.

To use these calculations, all dip values must be corrected to represent dip in the orientation of the slip vector. In this study the slip vector is approximately N-S, so measured dips of both faults and beds were corrected and re-calculated in the N-S direction (see Appendix 2).

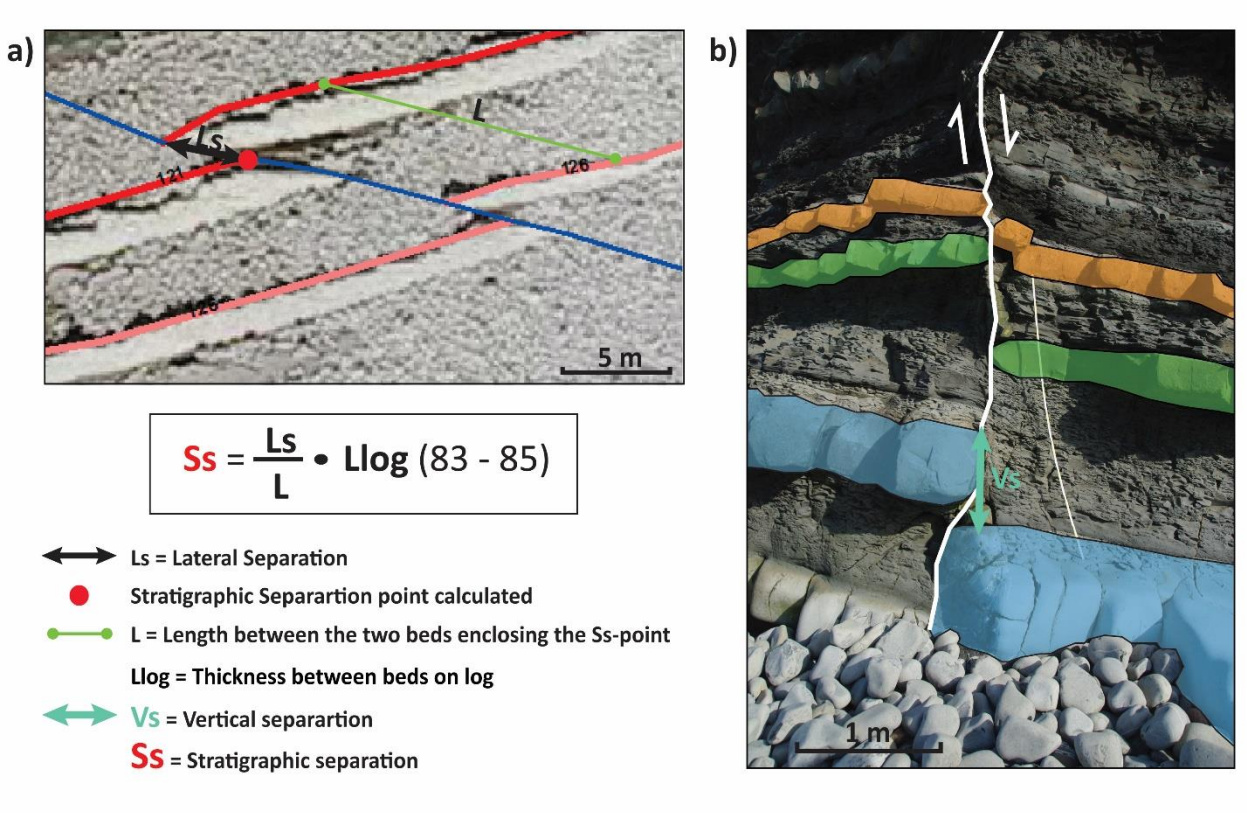

Figure 4.3: a) An example of calculating stratigraphic separation from measuring lateral separation on aerial photograph in ArcGIS. In this case, the formula in the black box is used (for more examples see Appendix I – workflow 2). Llog represents the thickness between beds found on the stratigraphic log representing the local sequence (Fig.3.2). b) Example of direct measurement of vertical separation done in cliff-section in field.

4.2.2 Contour plots of vein data

Vein data collected in field was added to the ArcGIS map as point data for further vein analysis. All measurements taken were added to each point, so that maps based on different attributes (e.g. intensity and strain) could be constructed. The damage zone distribution was interpreted and plotted using the measurements of damage zone widths, and combining this with vein attributes, contour maps of vein intensity (m^{-1}) and strain (% extension) were created (see Appendix I – workflow 4). To get the required amount of point data, linear extrapolation along fault strikes was needed. After increasing the amount of point data, it was interpolated using an interpolation tool

(natural neighbor) that finds the closest subset of input samples to a query point, and applies area based weights to them to interpolate a value (Watson 1999). This tool was chosen because it only uses a subset of samples surrounding a query point, so that interpolated highs are guaranteed to be within the range of the samples used, and artificial peaks and ridges will not be constructed.

4.3 Quantitative fault and vein analysis

Combining field observations with further processing done in ArcGIS, more detailed fault-, vein- and strain analyses could be produced. Field data and exported data from ArcGIS was gathered in spreadsheets, producing a wide platform of information to use in quantitative calculations (e.g. structural statistics, displacement-distance profiles, spatial heterogeneity plots, scatter plots etc.).

4.3.1 Fault orientations

3-D structural data were collected from the relay structure at Kilve, including bedding and fault orientations, as well as slickenside measurements. Stereographic equal-area projections of dips and dip directions for both faults and beds were made to determine a general orientation of fault planes and bedding. Projecting slickensides in a stereo plot with the fault orientations gave information on the slip vector. General trends within the faults of the study could be detected from these projections.

Length-weighted rose diagrams of fault orientations were created by calculating the total trace length within varying orientation bins, where each bin represents 10°. These plots are mainly used to examine variation in orientation and frequency of the faults observed, making it possible to divide them into major groups based on these variations. The length-weighted rose diagrams together with the stereographic projections were further used to apply dip corrections for faults and bedding needed for later extension analysis (see Appendix 2).

4.3.2 Displacement-distance (d-x) profiles

Traditional displacement-distance (d-x) profiles (Williams and Chapman 1983) of faults were used to investigate and illustrate the spatial variations in displacement and stratigraphic separation along strike fault zones.

The stratigraphic separations calculated from the marker bed cut-offs in ArcGIS were exported to spreadsheets and used for displaying stratigraphic separation-distance profiles of faults within the relay structure at Kilve, and displacements measured in field were plotted for the fault tip zones. The distance (x) represents the length of the fault trace, or the projection of trace lengths along a chosen direction for fault systems. For all locations examined in this study, the E-W direction approximates the strike-direction of fault lengths. By plotting adjacent fault segments separately in the same (d-x) profile the contribution of each segment can be studied, and a cumulative total can be constructed to see the overall shape of the profile (e.g. Peacock and Sanderson 1991).

4.3.3 Assessing spatial heterogeneity of faults and veins

Quantifying the spatial heterogeneity of both fault and vein distribution inside a network, the individual contribution of each structural group to the overall strain can be investigated (Putz-Perrier and Sanderson 2008a, 2008b; Nixon et al. 2014b). Using this method, sampling was done at transects oriented normal to fault strike. Along an E-W trending scan line following the strike of the relay bounding faults at Kilve, N-S oriented transect lines were taken with even spacing (25 m), where stratigraphic separation and frequency of faults cutting the transect was documented. For the tip zone at Lilstock two N-S oriented transects covering the studied relay ramp between en-échelon faults were placed outside and inside the relay, and both fault heaves, vein apertures and frequencies were sampled, so that extensions could be calculated. For the tip zone at locality B numerous transects (N-S oriented) were chosen at different locations within limestone beds along the fault trace, where vein apertures and frequencies were sampled.

Plotting parameters such as frequency, stratigraphic separation, aperture and extension as a cumulative distribution it can be compared with a uniform distribution, and a measure of spatial heterogeneity (i.e. localization of deformation and strain) can be determined (Putz-Perrier and Sanderson 2008a).

A non-parametric quantity $V = |D^+| + |D^-|$, where D^+ and D^- represents the maximum deviation above and below the cumulative uniform distribution, is calculated. This value represents the spatial heterogeneity (Fig. 4.4). This value is then normalized by dividing by the cumulative total to be able to compare data from different line samples (e.g. for frequency: $V_f = (|D_f{}^+| + |D_f{}^-|)/n$, where n = number of faults). The values of V varies from 0 to 1, where heterogeneity increases towards 1 (i.e. V_f measures the degree of localization of faulting on a scale from 0 – uniformly distributed fault spacing, to 1 – all deformation on one fault). For a detailed description of the methodology and the use of it, see Putz-Perrier and Sanderson (2008a, 2008b) and Nixon et al. (2014b).

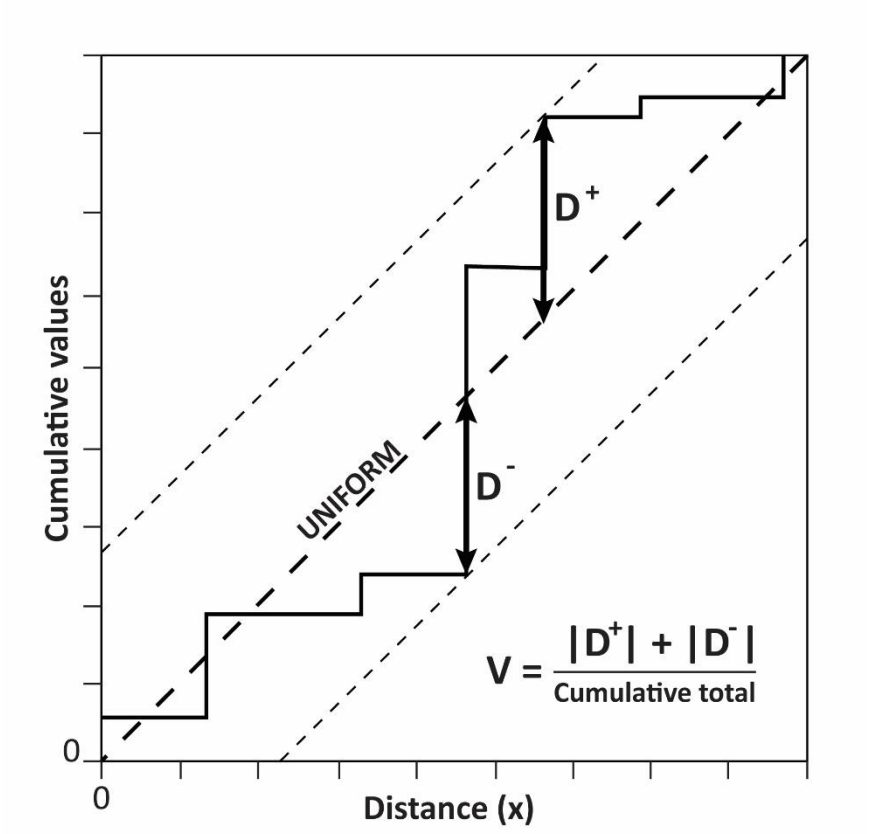

Figure 4.4: Cumulative curve over distance. (D^+) and (D^-) are the maximum positive and negative deviations of the cumulative graph (solid line) from the uniform distribution (thick dashed line), used to calculate the non-parametric quantity V using the listed formula.

4.3.4 Strain analysis

In this study, extension is measured as the bed parallel increase in length of a marker bed compared to its original size. By summing bed-parallel components of fault separations (heaves) and vein thicknesses (apertures) on a flat laying bed, the extensional strain accommodated by these structures can be quantified. By collecting fault data along the same seven key marker beds as the vein sampling was done for the relay structure at Kilve, the entire scale range of structures was captured (i.e. relay bounding faults, damage related faults and veins). Adding these together, a representation of total extensional strain for each scan line could be presented. The marker beds are also oriented at a high angle to the regional fault trend, easing the correction of fault dip into the N-S slip vector direction (see Appendix II). A correction for bed rotation was also needed to ensure calculation of flat lying extensions (see Appendix II), and N-S lengths of the marker beds were calculated using the strike of the beds.

Vein strain was calculated using the vein apertures of detected veins >1 mm in the 1 m transects taken along the marker beds (section 4.1.2). The measurements were extrapolated to include the whole width of the damage zone as transect length. When the total aperture of veining and the transect length is known, the vein strain can be calculated as followed:

Vein strain = total aperture / (transect length - total aperture)

Fault heaves represents the horizontal extension of the fault separations, and was calculated using the formulas presented in section 1.2.1.

Knowing the observed length of the beds (L_f) in the N-S direction, original bed lengths (L_0) are found by subtracting the apertures and heaves from L_f, and *Total % extension* is calculated following:

Total % extension $= ((L_f - L_0) / L_0) * 100$

4.3.5 Scatter plot analysis

An easy way of arranging numerous data sets to show relationships between different parameters, is to use scatter plots. In this study, spatial parameters were compared (e.g. HW vs FW) and relationships between certain parameters were tested (e.g. strain and vein intensity vs damage zone widths). Certain effects on veining (e.g. bed thickness, location in HW, location in FW) were tested, and affects on damage zone development (e.g. strain and vein intensity vs displacement) were examined. Using a logarithmic scale helps examine data that is clustered around the origin, so plotting data on normal scale axis and logarithmic scale axis was tested for all plots, choosing the best suitable for each data set.

4.4 Limitations – sources of error

4.4.1 Stratigraphic separation calculations

Measurements of lateral stratigraphic separation were done both in ArcGIS, and by direct measurements in field. Comparison of these two approaches show a clear agreement and separations on large faults found in ArcGIS are considered to have errors of +/- 0.5 m, while direct measurements of small-scale faults in field have an accuracy of +/-10 mm. Since the map in ArcGIS function as a 2-D surface being interpreted, topography of the map may affect the bed cut-offs with the faults, but given the shallow topography of the beds observed in field, this is thought to be minimal. Interpretations of marker beds might also have an error of accuracy affecting the stratigraphic separation calculations.

4.4.2 Vein sampling

The vein sampling at Kilve, Lilstock and East Quantocks Head has a measuring accuracy down to ≥1 mm, but there are several sampling errors to be considered while gathering the vein measurements in the limestone marker beds:

- The limestone surface might be eroded and therefore represent vein apertures located closer to the center of the bed. Since measurements are done on top of the limestone bed surfaces, this might give an anomalous large value, due to possible lens shape of veins in the vertical section.

- At fault tips, monoclonal structures are created, which may create a local compression in the HW and local stretching in the FW. This might give the veins in the HW a wedge shape thinning to the top surface, while the veins in the FW show a wedge shape thickening towards the top surface of the bed, which may give sampling anomalies.
- Erosion and destruction in the fault zones might give an intensity and aperture of veining not really representing the area.
- The further out on the wave-cut platform, more mud and sea weed are covering the marker beds. This makes sampling more difficult, and veins might have been overlooked. Veins < 1 mm are most likely to be affected by this.

4.4.3 Correction of bed rotation and fault/bed dips

Regarding bed rotation, there is observed a slight difference in bed dip throughout the fault blocks of the relay at Kilve. The bed dip used in further calculations is an average, calculated from all measured dips, not taking local differences into consideration. The differences are caused by fault block rotation and folding close to faults due to kinematic effects. Fault measurements are not as numerous as bed dip measurements, and will probably give a higher uncertainty to the average values calculated. As measured dips are in agreement with past studies done in the same area (45 - 75°, McGrath and Davison 1995; 33 - 42°, Skar et al. 2016) the uncertainty seems minimal.

5 Results – Kilve Pill Relay

This chapter focuses on the distribution of deformation and damage associated with a mesoscale relay structure, representing a linkage damage zone, located to the west of the Kilve Pill Box. It has been closely documented in terms of structural features and their contribution to strain. First, the general structure of the Kilve Pill Relay zone is presented through a structural overview, and description of observed fault arrangements (section 5.1). This leads on to a description and quantification of the spatial distribution of faulting and displacement within the relay zone (section 5.2), and characterization of veining and damage zones around faults (section 5.3). The chapter closes with a quantification of total extensional strain and the partitioning of strain between different scale structures (section 5.4).

5.1 General structure of the relay zone

5.1.1 Structural overview of the Kilve Pill Relay

The fault zone studied at Kilve encompasses normal faults of different scales oriented approximately E-W, downthrown both to the south and north. These will be referred to as S-dipping and N-dipping, respectively. A series of large-scale faults are distributed from north to south in the study area, and represents main structural features (Figure 5.1a). These are observed in the whole section from Kilve to Lilstock (Fig. 3.1c), where six of them are marked on Figure 5.1a; two S-dipping faults (FS1 and FS2) which are the largest faults in the system (up to 79 m stratigraphic separation), and four N-dipping faults (D1 – D4) with separations ranging from ~10 – 30 m. These N-dipping faults are evenly spaced approximately 100 m apart. There is no evidence of inversion of any of the faults described in this section. An extensive part of the local stratigraphy is represented, as seen where FS2 terminates in the cliff, where the Blue Lias is separated from the Quantocks Beds across the fault. Thus much of the Lower Jurassic stratigraphy is involved in this fault zone (Fig. 3.2).

The main structural element of this study is a mesoscale relay ramp (Fig. 5.1a) bounded by the two major S-dipping faults (FS1 and FS2) steeply dipping to the south (~80°) and striking ~N275°E

with evidence of pure dip-slip motion (Fig. 5.1b, Table 5.1). FS1 bounds the relay to the south and decreases in displacement to the east where it splays into several strands with low displacements before terminating at the cliff. The full extent of the fault to the west has not been documented due to no available exposure of the wave-cut platform. FS2 bounds the relay to the north, where the fault tip to the west can be observed. The relay zone between these two faults is ~170 m in length (E-W) and ~110 m wide (N-S), producing an extensive ramp of 18700 m².

Inside the relay structure are 39 N-dipping faults or fault strands that vary in length (5 - 500 m) and have stratigraphic separations up to 27 m. The faults have dips varying from 33 - 48° striking approximately N105°E and N096°E (Fig. 5.1b, Table 5.1). ENE-WSW trending faults show oblique-slip on their fault planes with a slickenside rake of up to 64° from the horizontal, while the E-W trending faults show dip-slip motion like the relay bounding S-dipping faults. The slip of the faults indicates N-S extension. Based on the differences in fault geometries described above, the faults are divided into three main groups after their dip and slip motion: 1) S-dipping faults; 2) N-dipping faults with dip-slip motion; 3) N-dipping faults with oblique-slip motion (Fig. 5.1b, Table 5.1).

Most S-dipping fault segments are associated with the fault zone of the two relay bounding faults. The N-dipping faults with dip-slip motion are located both inside and outside the relay zone between FS1 and FS2 to the NE, while the N-dipping faults with oblique-slip are located mainly inside the overlap zone (Fig. 5.1a). Fault D3 and D4 represent the largest N-dipping faults within the relay structure with oblique-slip, and these are throughgoing, extending out of the overlap zone to the west. Fault interactions and linkage between the smaller N-dipping faults is extensive inside the relay zone, but no clear breach between the bounding segments is detected. The relay structure can thus be described as a stage 3 relay in the classification of Peacock and Sanderson (1991) (Fig.2.4).

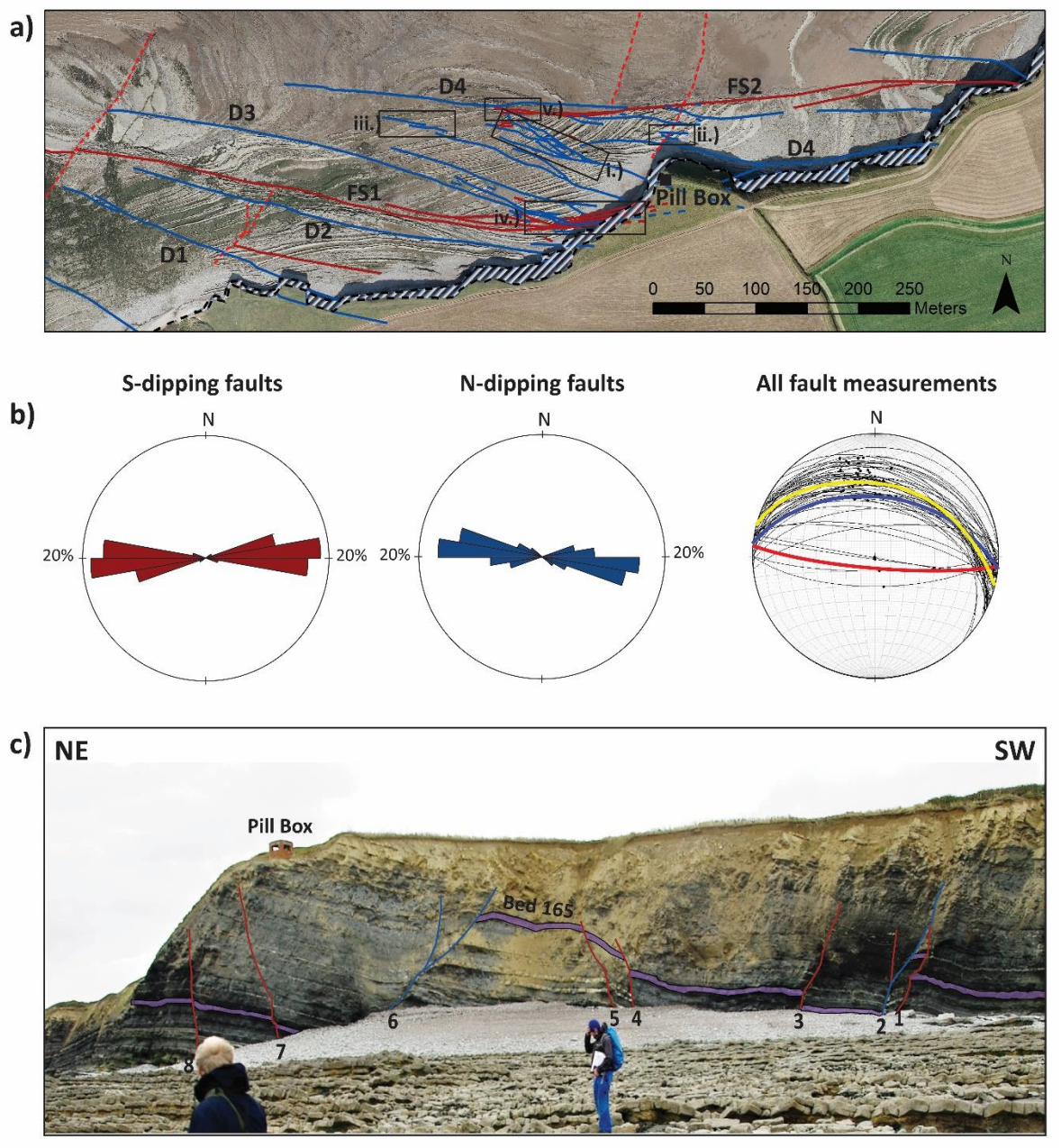

Figure 5.1: a) Map of the study area at Kilve Beach. S-dipping faults are marked in red, and N-dipping faults in blue. Main structural features have been given names (i.e. relay bounding faults FS1 and FS2, and domino faults D1 – D4). Strike slip faults are shown as dashed red lines, and the cliff section as dashed grey polygon. Black boxes (i. – v.) highlight general features of interest within the fault network. b) 3-D structural fault measurements shown in length-weighted rose diagrams (1 bin = 10°) showing general fault trend of S-dipping and N-dipping faults, together with a stereographic equal-area-projection of all fault measurements, with group-averages shown in colored great circles (S-dipping = red, dip-slip N-dipping = blue, oblique-slip N-dipping = yellow). c) Picture taken of the cliff section (NE-SW). Eight faults are observed, S-dipping faults in red and N-dipping faults in blue. Bed 165 (purple) is highlighted to illustrate the fault movements. Note that fault 1 and 3 looks overturned due to the perspective of the photography.

Table 5.1: 3-D structural measurements of the three fault groups at Kilve.

	Average Dip/Dip direction - Fault plane	Average Plunge/Azimuth - Slickensides	Dip of fault plane in N-S direction
S-dipping faults	82/185	80/186	80
N-dipping faults with dip slip motion	50/006	48/004	48
N-dipping faults with oblique slip motion	41/015	34/349	33

The cliffs of Kilve Beach provide an oblique section of the observed fault network. The vertical geometry of eight faults are observed in a 75 m long cliff section stretching from where FS1 terminates the cliff to the south, to the Pill Box in north (Fig. 5.1c). Six S-dipping faults and two N-dipping faults are observed, and all except one (fault 5) are matched up with fault traces on the wave-cut platform. All faults show a planar geometry, except fault 6 that has a synthetic splay in the hanging wall. On the wave-cut platform this fault array shows a complex network displaying both fault splays and abutting interactions in the NW of the relay zone (Fig. 5.1a – i.). Note that fault 1 and 3 seen SW in the section (Fig.5.1c) looks overturned, caused by the oblique perspective of the photography, since the faults are nearly vertical. Fault 1 (FS1) is also cut by fault 2 (D3), and this cross-cutting relationship demonstrates that FS1 formed earlier than D3 (Fig. 5.1a. – iv.).

Three N-S oriented transects (T8, T12 and T17) of 150 m length, covering the width of the overlap zone between FS1 and FS2 is illustrated in Figure 5.2a. T8 is located to the west (British National grid: 31 4507/14 4637), 185 m from where overlap occurs, while T12 is located further east (British National Grid: 31 4607/14 4587), only 85 m from the start of the overlap zone. T17 is located 40 m inside the overlap zone from the west (British National Grid: 31 4731/14 4557). This gives a description of changes in fault intensity moving from outside to inside the relay zone. The fault intensity increases by 75 % moving from T6 to T17 over an area of 225 m. Figure 5.2b illustrates three cross-sections based on transect T6, T12 and T17. At T6 the spacing of faults is even and quite extensive (~50 - 75 m) and is only represented by main structural features (i.e. FS1, D2, D3 and D4). A general dip of bedding of 10 - 20°S (Fig. 5.2c) is seen within the fault blocks. The observations in T12 are of similar character, only with higher fault intensity and fault spacing alternating between 10 - 50 m as more faults are introduced. In T17 faults are closely spaced and N-dipping faults show interaction between each other and with the relay bounding faults within

the relay. The fault geometry at depth is interpretive, and fault interactions can either be as abutments or cross-cutting relations. Since a cross-cutting relationship is observed in the cliff between the S-dipping faults and the large N-dipping faults (D1 – D4) (Fig.5.1c), the same relationship is interpreted at depth (marked with black circle in T6, Fig. 5.2b). Fault abutment is observed in plan-view between smaller N-dipping faults and FS2 (Fig. 5.1a - i.), leading to this interpretation for FS2 at depth (marked with black circle in T17, Fig. 5.2b). N-dipping faults within the relay zone show a gentler dip than those located north and south of it, producing an observed maximum bed dip of 19°SE (Fig. 5.2c) in the center of the relay zone. The steeper bed dips correspond to a shallower fault dip, explained by increased fault rotation within the relay zone. The observed change from S-dipping bedding outside the relay to the north, south and west, to SE-dipping bedding inside the relay, indicate an oblique rotation, explained by relay ramp rotation caused by displacement transfer between the two relay bounding faults.

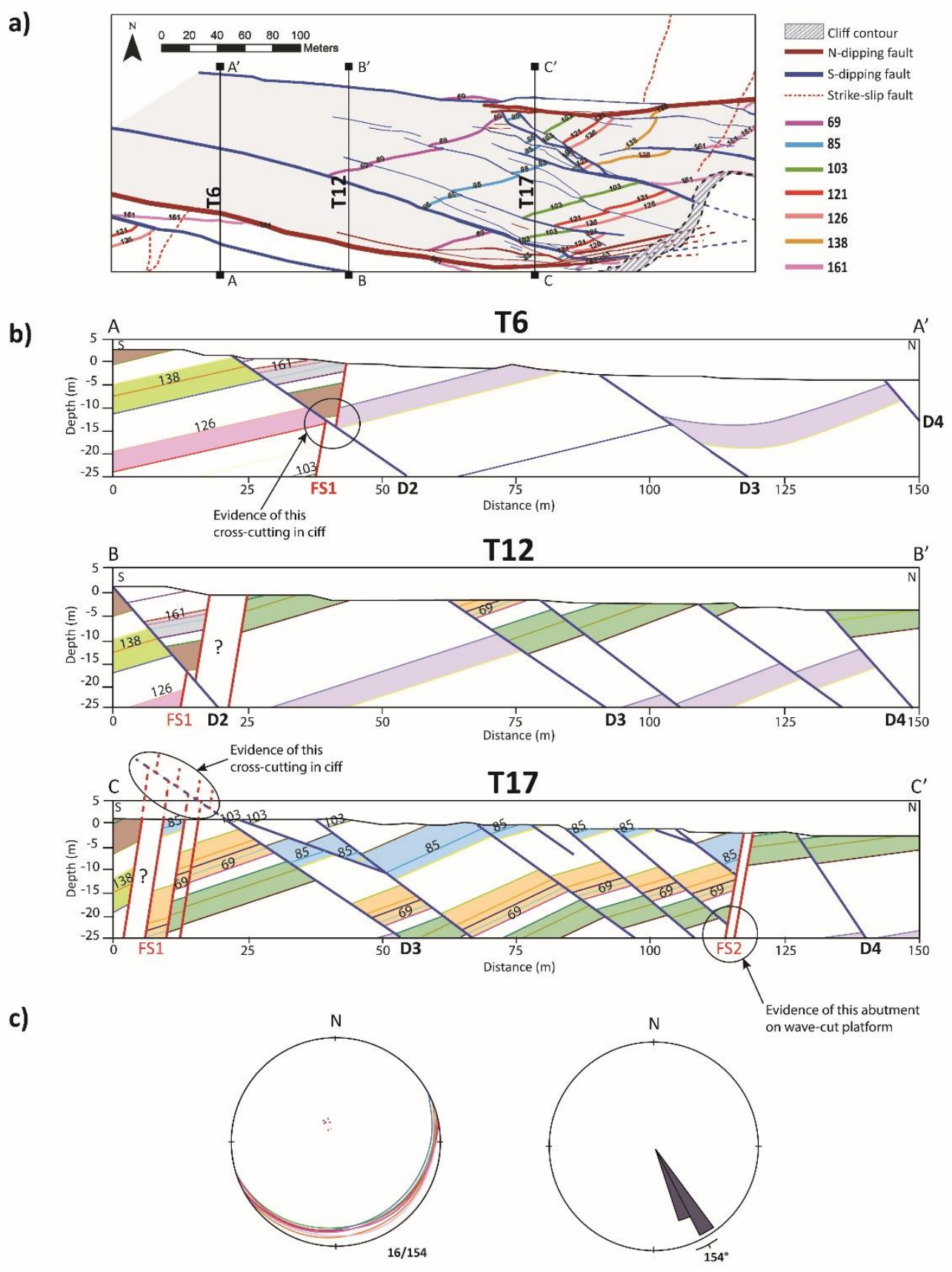
a)
N
0 20 40 60 80 100
Meters
A′
B′
C′
T6
T12
T17
A
B
C
Cliff contour
N-dipping fault
S-dipping fault
Strike-slip fault
69
85
103
121
126
138
161
b)
T6
A
A′
S
N
Depth (m)
Distance (m)
FS1
D2
D3
D4
Evidence of this
cross-cutting in ciff
T12
B
B′
?
T17
C
C′
Evidence of this abutment
on wave-cut platform
c)
16/154
154°

Figure 5.2: (previous page) a) Map of relay zone (greyed out) showing key marker beds used for this study (69, 85, 103, 121, 126, 138, 161), and three N-S oriented transects (T8, T12, T17). Transects mark the placement of the cross-sections in (b). Stratigraphy and fault geometry is shown covering a depth of 25 m. Thick red and blue lines mark faults, while thin sub-horizontal lines mark limestone beds. Key marker beds are numbered, and color coded as in stratigraphic log (Fig. 3.2). Colored grouping of beds is used to highlight fault movement and fault block rotation, and the same grouping is also illustrated in the stratigraphic log. c) Stereographic equal-area-projection of average key marker bed measurements, with same color code as in (a), also presented in a rose diagram (1 bin = 10°) highlighting average dip direction.

5.1.2 Fault arrangement and interactions

The plan-view and cross-sectional geometries of the faults within the relay zone illustrate the presence of different fault arrangements and interactions within the fault network. In particular, we can identify isolated faults, splaying faults, abutting fault terminations and cross-cutting relations (Fig. 5.1a). Faults can also be involved in more than one interaction (e.g. a splaying fault may also abut another fault etc.)

Isolated

Individual faults that do not connect to any other fault in plan-view (Fig. 5.1a – ii.), are termed isolated. These are few and usually short in length, probably due to the fact that longer faults are more likely to interact with other faults. Sometimes isolated faults appear as en-échelon arrays at the tip of a larger fault (Fig. 5.1a – iii).

Splaying

Faults with splay characteristics, where one fault branches into several fault strands in plan-view, are mainly located inside the overlap zone of the relay structure. Such splays are synthetic as is seen for the main relay bounding faults and the N-dipping faults. The splay faults are often associated with the tips of larger faults, for example, the four-branched splay of the eastern tip of FS1 (Fig. 5.1a – iv.).

Abutting

When one fault terminates another in a fault network, an abutting relationship is observed. In the relay zone at Kilve, N-dipping faults often terminate and show an abutting relationship with the

main S-dipping faults (Fig. 5.1a – v.). This example shows an antithetic relationship, indicating that the formation of the N-dipping fault and FS2 is related to each other.

Cross-cutting

Faults showing cross-cutting relationships are observed between the S-dipping relay bounding faults and larger N-dipping faults, and a good example is seen in the eastern splay of FS1, where D3 cuts through and offsets the S-dipping splay branches. This is seen both in plan-view and cross-section in the cliff (Fig. 5.1a and c).

Based on the observed fault geometries, and the structural relations between them, a hypothesis regarding their relative formation and interaction to each other can be drawn (Fig. 5.3). The larger N-dipping faults (D1 – D4) show an even distribution and size-similarity, together with a general tilt of bedding within their fault blocks. They are thus interpreted to be part of a regional domino fault system. Their cross-cutting relationship to the relay bounding S-dipping faults also indicate that they formed slightly after FS1 and FS2, which strengthens the domino fault theory. This separates them from the smaller N-dipping faults, which are mainly located within the overlap zone of the relay, and show abutting relations to FS1 and FS2, making them antithetic to each other. This indicates a close relationship, and the smaller N-dipping faults are interpreted as damage related faulting produced by the overlap of FS1 and FS2. Choosing to identify the domino faults and isolate them from the remining N-dipping faults, a separation between damage related faulting and main faults have been encountered. For further damage analysis, the domino faults (D1 – D4) are thus excluded, to capture only damage related faulting within the relay zone.

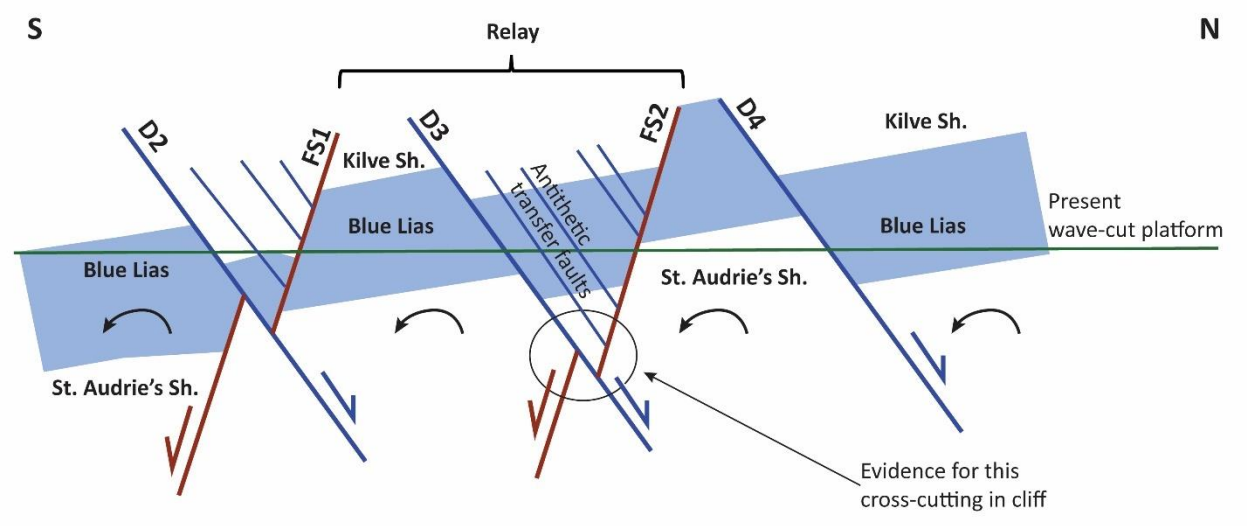

Figure 5.3: Schematic cross-sectional model from south to north that shows possible relationships between the three interpreted structural groups observed at Kilve Beach; S-dipping relay bounding faults (FS1 and FS2), domino faults (D1 – D4) and damage related faults. Both the domino faults and the damage related faults show an antithetic relationship with the relay bounding faults, where domino faults show cross-cutting, and the damage related faults show abutting. A representative line of the present wave-cut platform is marked in green, representing our plan-view map. The position of stratigraphic units is marked, to highlight fault movement together with arrows on faults.

5.2 Spatial distribution of faulting and displacement

5.2.1 Stratigraphic separation map and profile

Stratigraphic separations (S_S) were calculated along all faults displacing limestone marker beds, in total 349 measurements were made across the fault network. From these points, a map of stratigraphic separation (Fig. 5.4a) and a S_S-distance profile (Fig. 5.4b) was made to investigate the spatial distribution of fault separation along the relay (see section 4.2.1 and Appendix I).

The map of stratigraphic separation (Fig. 5.4a) indicates that the relay bounding S-dipping faults (FS1 and FS2) have high stratigraphic separations (~20 - 80 m) along their entire fault traces, but FS2 tips out to the west, and FS1 also shows a decrease of separation as it splays into strands close to the cliff in east. The average stratigraphic separation on each damage related fault is lower than for the main faults (~0.5 - 40 m). Stratigraphic separations vary along the length of fault traces, but r/d_{max} profiles (where r = distance between maximum displacement point and the fault tip, and d_{max} = maximum displacement) (sensu Peacock and Sanderson 1996) are not constructed because

significant censoring due to cliff-line and low water would be expected. But a general trend is seen where larger separations are detected along longer faults, compared to smaller separations along shorter faults. Isolated faults appear to have smaller separations, and splays and abutments have maximum displacements at intersections with other faults.

S_S-distance profiles (Fig. 5.4b) were made to investigate the change in stratigraphic separation along strike of the studied faults, and to understand the contribution from the main faults and damage faults to overall deformation. The profiles of relay bounding faults includes the main S-dipping faults as well as their splay branches, and N-dipping faults inside the relay represents the damage related faults (domino faults are excluded). FS1 and FS2 are plotted individually, both creating (d-x) profiles where separations increase from the observed fault tips. Note that the (d-x) profiles do not show complete fault lengths, as the faults are not examined in their full extent due to lack of exposed wave-cut platform to the west and the arrival of the cliff to the east. FS2 has a maximum stratigraphic separation of 69 m while FS1 increases up to 79 m. Corresponding to the overlap zone on the map (Fig. 5.4a), both faults show a rapid decrease in separation from 45 to 0 m over a distance of approximately 150 m. The gradient of the profiles for both faults changes when overlapping, the gradient is $du/dx \approx 0.1$ in the area outside of the overlap zone, whereas inside the overlap zone the gradient steepens to $du/dx \approx 0.3$ (Fig. 5.4b).

The profile representing damage faults (Fig.5.4b) shows a convex-up geometry, with an extensive increase in stratigraphic separation located within the overlap zone (maximum value of 42 m), decreasing moving away from it both to the west and east. The change in gradient moving into the overlap zone is approximately the same as seen for FS1 and FS2, but positive rather than negative.

The cumulative profile (Fig. 5.4b) shows total summed values of stratigraphic separations ranging from approximately 50 - 90 m but indicates an overall coherency along the relay zone averaging ~70 m. The profile is controlled by the major bounding faults outside of the relay as they contribute the majority of total stratigraphic separation. Whereas inside the overlap zone damage related structures show an extensive contribution of ~45 % of the observed total. The shape of the cumulative profile also shows the same convex-up geometry as the profile representing damage, producing a bell shape with maximum values in the middle of the overlap zone. Just outside the overlap zone, the cumulative profile and the profile of damage faults show a rapid decrease that is inconsistent with the overall shape of the profiles. On the eastern side this can partly be caused by

the arrival of the cliff, which produces undersampling in this region, but the main cause might be the presence of small-scale structures related to increased faulting (i.e. veining and small-scale faulting in fault tip zones, splays and fault interactions) that also contribute to the overall deformation, but is not sampled.

The shape and the gradients of the profiles of FS1 and FS2 show a similar pattern to the (d-x) profile representing evolutionary stage 3 of relay zone development (Peacock and Sanderson 1991) (Fig. 2.4), with steeply decreasing gradients within the overlap zone. This supports the suggestion, based on geometrical relations between damage structures and main faults made earlier, that this relay structure represents a partly breached relay. The general bell shape of the cumulative profile (Fig. 5.4b) indicates that strain coherency is maintained by adding strain produced by the main faults and strain produced by damage related faults together. The rapid increase of the damage fault profile entering the overlap zone illustrate a significant increase in strain and that their total contribution to strain is noteworthy. The increases in strain are caused by the formation of damage related faults, and their function to transfer displacement between the bounding faults of the relay.

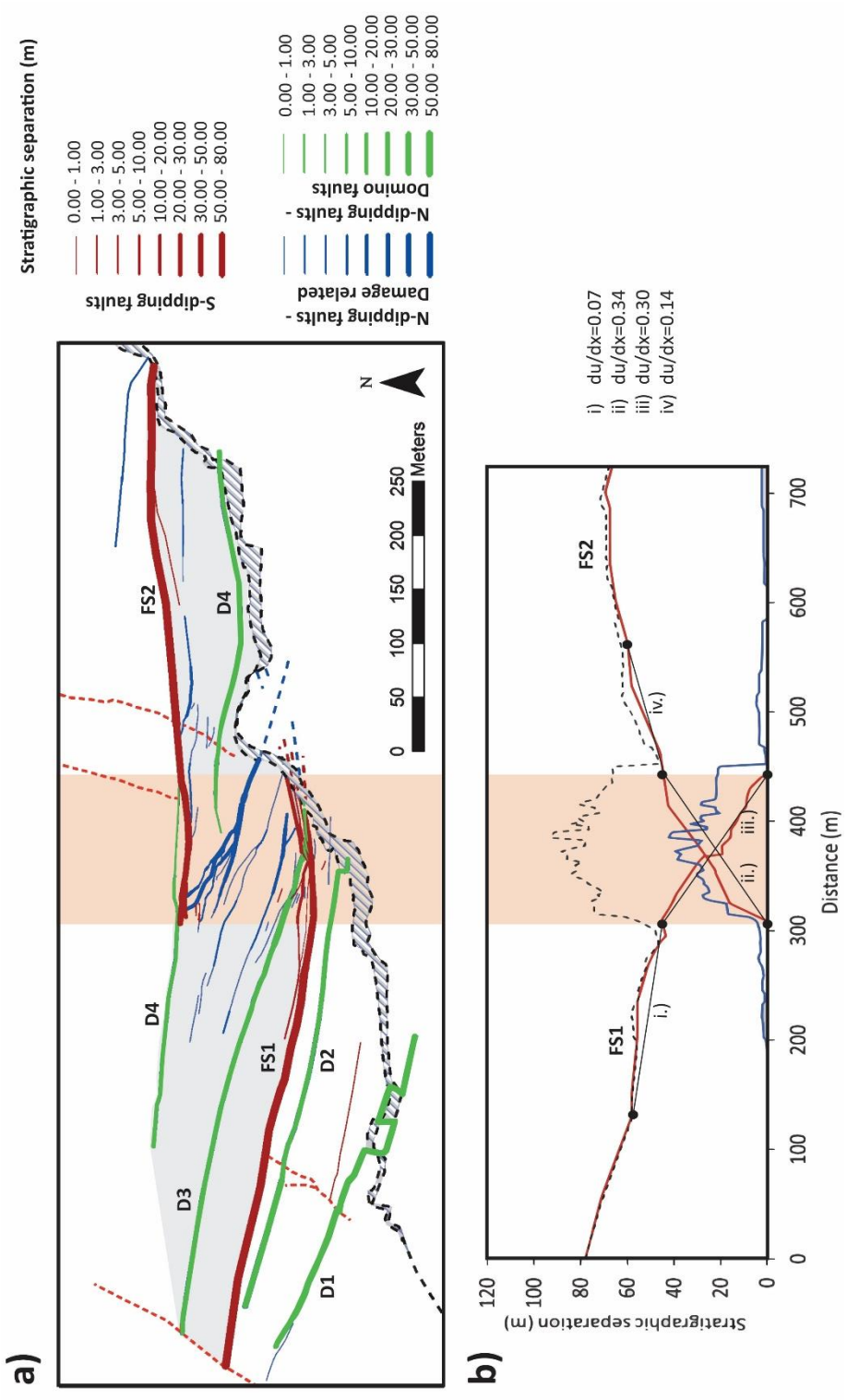

Figure 5.4: Map of the Kilve Pill Relay (greyed out) where fault thicknesses represent stratigraphic separations (m). Main structural features are named, where FS1 and FS2 are red and domino faults are green. b) Stratigraphic separation – distance profile along strike faults of the relay structure. Note that the contribution of domino faults is excluded, to make it represent only relay bounding faults vs damage related faults. FS1 and FS2 are plotted separately (red curves) and damage related faulting are gathered in one profile (blue curve). The cumulative total of stratigraphic separations is represented as a dashed black line. Line gradients of the curve of FS1 (i. and ii.) and FS2 (iii. and iv.) are marked on the curve and values listed, to show the change in gradient from inside to outside the area of fault overlap (shaded orange). The gradients increase from ~0.1 outside of the overlap area, to ~0.3 inside the overlap area.

5.2.2 Spatial heterogeneity of the fault network

In this section the spatial heterogeneity of faulting and stratigraphic separation throughout the relay zone is investigated, from outside to inside the overlap zone. A simple and effective way to present this is by using plots showing cumulative displacement against transect distance across strike of the relay zone (Fig. 4.4). From normalized plots, non-parametric quantities of stratigraphic separation (Vs_s) and fault frequency (V_f) were found, but the data is presented in non-normalized plots so as to compare the gradient of the cumulative curves between transects. Vs_s measures the degree of localization of the fault separation (and hence strain) on a scale from 0 - uniformly distributed strain, to 1 – all strain on one fault, and V_f measures the degree of localization of faulting on a scale from 0 – uniformly distributed fault spacing, to 1 – all deformation on one fault.

Based on the same 150 m long N-S oriented transects presented in section 5.1.1 (T6, T12 and T17, Fig. 5.5a), three spatial heterogeneity transect-plots are presented in Figure 5.5b, while Figure 5.5c shows along strike plots of Vs_s and V_f of all 17 transects (T4 - T20, Fig. 5.5a). Values of D^+, D^-, Vs_s and V_f for all transects are presented in Table 5.2. In this analysis all faults are recorded, also the domino faults. They are included because they are present in all transects, and are the only contributors part from the relay bounding faults moving outside of the relay to the west.

Table 5.2: Values of spatial heterogeneity calculated along the Kilve Pill Relay.

	D+ Stratigraphic separation	D- Stratigraphic separation	D+ Fault frequency	D- Fault frequency	Vs_s	V_f
T4	0.49	-0.31	0.27	-0.31	0.80	0.59
T5	0.52	-0.27	0.31	-0.27	0.79	0.57
T6	0.55	-0.22	0.33	-0.22	0.77	0.55
T7	0.57	-0.20	0.36	-0.20	0.77	0.56
T8	0.54	-0.15	0.21	-0.21	0.69	0.42
T9	0.55	-0.10	0.25	-0.20	0.66	0.45
T10	0.58	-0.06	0.29	-0.18	0.64	0.48
T11	0.60	-0.03	0.33	-0.16	0.63	0.50
T12	0.59	-0.001	0.25	-0.04	0.59	0.29
T13	0.55	-0.09	0.19	-0.09	0.65	0.29

T14	0.56	-0.07	0.23	-0.07	0.64	0.31
T15	0.60	-0.05	0.35	-0.05	0.65	0.40
T16	0.38	-0.10	0.17	-0.15	0.49	0.32
T17	0.29	-0.12	0.18	-0.04	0.41	0.23
T18	0.21	-0.11	0.28	-0.04	0.33	0.32
T19	0.22	-0.19	0.20	-0.06	0.41	0.30
T20	0.20	-0.34	0.18	-0.11	0.54	0.29

Comparing the plots and V-values (Fig. 5.5b) moving from outside (T8) to inside (T17) the relay ramp, the heterogeneity generally decreases into the relay. The heterogeneity measures of Vs_s representing all faults decreases from 0.69 – 0.41 and V_f decreases from 0.42 – 0.23 moving into the overlap zone. Heterogeneity measures for Vs_s and V_f were also calculated for faults only within the relay for the three transect plots (T8, T12 and T17). These values are generally lower than for the values representing all faults, but show the same decreasing trend moving into the relay from 0.65 – 0.34 and 0.64 – 0.25 respectively. This decrease in spatial heterogeneity explains that away from the relay the deformation is focused on the main faults (i.e. relay bounding faults and domino faults), but as you enter the relay the deformation becomes more distributed across the whole zone. The gradients representing the heterogeneity of stratigraphic separation of faults within the relay in the cumulative plots (Fig. 5.5b) also show steepening whereas the width of the relay stays fairly constant. This shows that even as the size of the relay is constant, faults contribute more to the total stratigraphic separation moving into the relay, indicating increased faulting within the relay zone.

The values of Vs_s and V_f against fault-strike distance (Fig. 5.5c) strengthen the observed tendency from the transect-plots. There is a general linear decrease in both Vs_s and V_f values from west to east, ranging from 0.80 – 0.33 and 0.59 – 0. 23 respectively. This give a change from moderately localized faulting to moderately distributed faulting moving from outside to inside the overlap zone of the relay. The grouping of the values (shaded areas in Fig. 5.5c) highlights sets of new faults being progressively introduced to the network as you move from west to east along strike of the relay zone, producing a number of step like jumps in the plot.

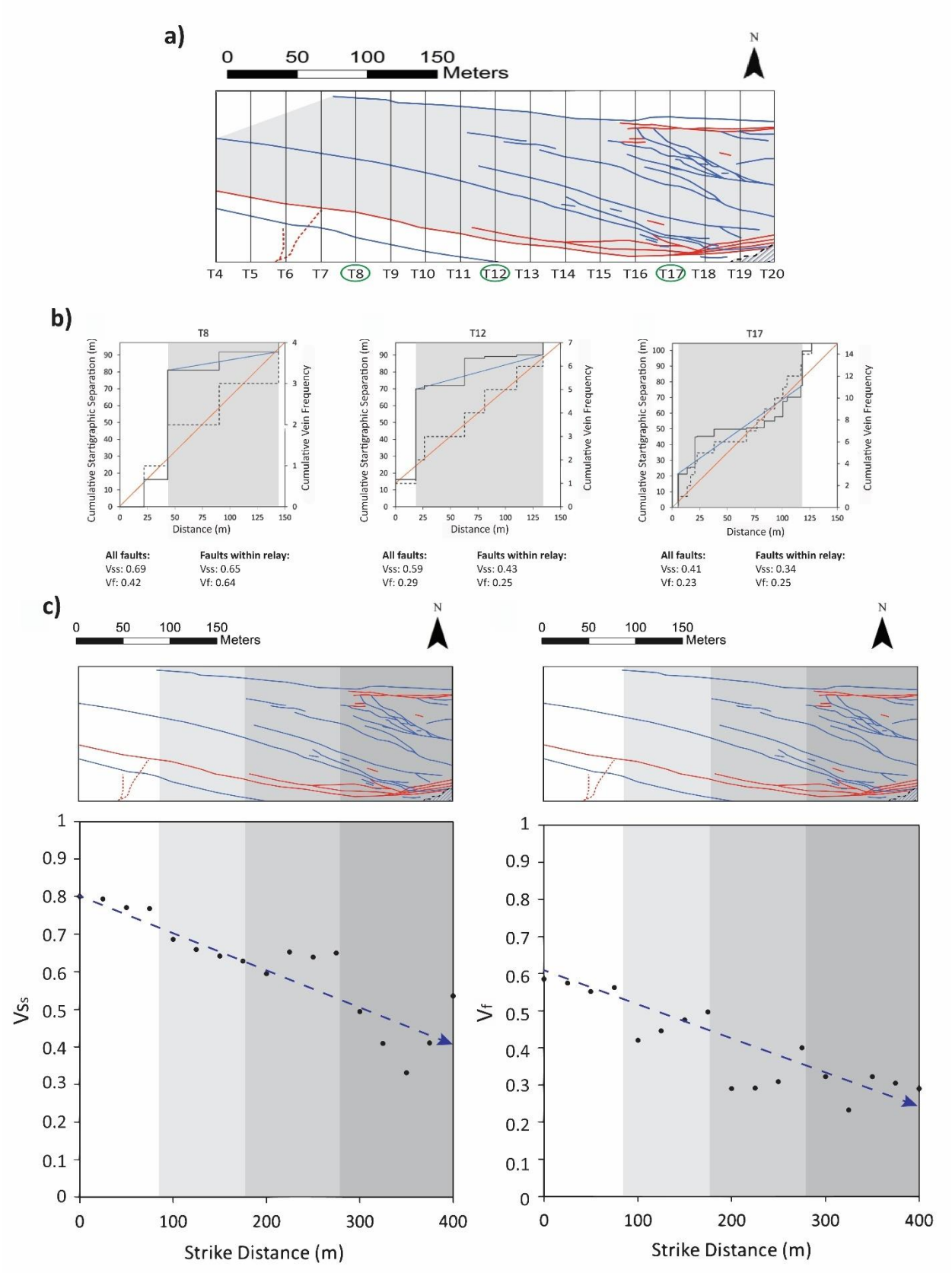
a)
0 50 100 150
Meters
N
T4 T5 T6 T7 T8 T9 T10 T11 T12 T13 T14 T15 T16 T17 T18 T19 T20
b)
T8
T12
T17
Cumulative Startigraphic Separation (m)
Cumulative Vein Frequency
Distance (m)
All faults:
Vss: 0.69
Vf: 0.42
Faults within relay:
Vss: 0.65
Vf: 0.64
All faults:
Vss: 0.59
Vf: 0.29
Faults within relay:
Vss: 0.43
Vf: 0.25
All faults:
Vss: 0.41
Vf: 0.23
Faults within relay:
Vss: 0.34
Vf: 0.25
c)
0 50 100 150
Meters
N
Vss
Vf
Strike Distance (m)

Figure 5.5: (previous page) Map presentation of 17 N-S oriented, 150 m long transects (T4 – T20) with 25 m spacing covering the whole width of the relay ramp (shaded grey). Along each transect fault frequency and stratigraphic separations were measured for heterogeneity analyses. S-dipping faults are in red, while N-dipping faults are in blue. Note the increase of faulting moving from outside (west) to inside (east) the relay structure. Transect T8, T12 and T17 are marked with green circles. b) Non-normalized cumulative plots representing T8, T12 and T17, where Vs_s is the heterogeneity measurements of stratigraphic separation (solid black line) and V_f is the heterogeneity measurements of vein frequency (dashed black line). The gradients representing damage related faults are indicated as blue solid lines for Vs_s and orange solid lines for V_f. Grey fields indicate the width of the relay. c) Along strike variation of heterogeneity measures of Vs_s and V_f are combined with the fault map. A general decrease from west to east in both Vs_s and V_f values are indicated with blue dashed arrows. Step like jumps associated with the introduction of new faults are indicated with increasing grey scale shading.

5.3 Characterization of damage zones around faults

Damage zones of faults also contribute to the total amount of strain of an area. In this study, the damage zones are represented by calcite veining associated with almost all of the faults, and hence will contribute to the deformation. In this section characterization of veining is addressed and the spatial distribution of veins throughout the entire fault network is presented.

5.3.1 Vein geometries and characteristics

Veins used in this study are localized around fault planes, oriented sub-parallel to these (see transect picture, Fig 4.2a). This means that veining in the area is trending E-W and is normal to the N-S extension direction. Thus, veins formed during the same stress field as the normal faults. Based on this, veins are interpreted to be part of fault damage zones. Background veining is observed, but only in certain beds and with apertures <1 mm, and as Putz-Perrier and Sanderson (2008a) suggest that most observed veining is in damage zones, it is assumed a negligible background strain (<< 1 %). The veins are calcite filled sub-vertical tensile fractures, in agreement with past studies (e.g. McGrath and Davison 1995; Putz-Perrier and Sanderson 2008a; Skar et al. 2016). In plan-view veins are observed on bedding plane surfaces of marker beds throughout the relay zone. The spread of vein aperture measurements is large, from the smallest 1 mm veins to a maximum of 320 mm, where apertures generally decrease away from fault planes. Two measures of vein frequency were done for each 1 m transect, one for veins >1 mm where the maximum frequency is 18 veins, and one for veins <1 mm, where the maximum frequency is 374. The

contribution of veins <1 mm was thought to be insignificant to vein strain, and calculations show that 90 % of vein strain is contributed by veins >1 mm. Smaller veins are thus excluded from further calculations without affecting the results significantly. Veins are observed in cross-section as sub-vertical, sometimes showing a slight lens shape thinning towards upper and lower bed surface, and sometimes with stabile thickness through the whole bed section. Veins in fault tip zones show a wedge shape thinning towards the bed top surface in HWs and thickening towards the bed top surface in FWs (Fig. 5.6a), where bedding get a monocline fold structure due to fault propagation related folding (e.g. Gawthorpe et al. 1997). This is due to higher degree of extension in the outside of fold hinges (Fig. 5.6b), and indicates that veins and the monocline developed simultaneously.

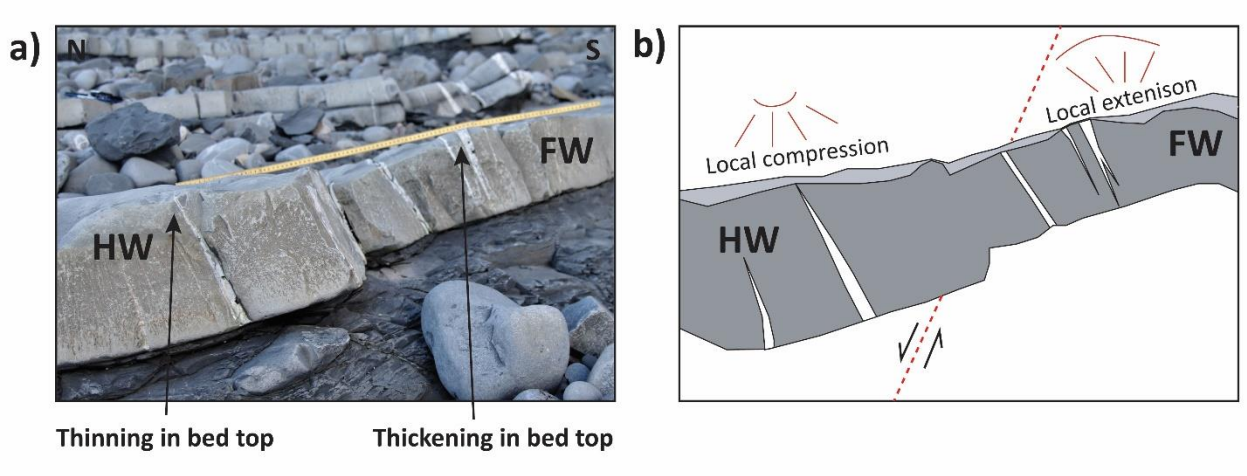

Figure 5.6: a) Picture showing a cross-section of bed 99 at East Quantocks Head (locality B in fig. 6.7a) showing the geometry of the limestone bed and associated veining in a fault tip zone. A slight monocline structure of bedding is observed, with a low in the HW fault block and a high in the FW fault bock. Veins have wedge shapes, with thinning toward the bed top surface in HW fault block and thickening to the bed top surface in FW fault block. b) Illustration of picture in a) where the wedge-shaped geometries of veining are explained by local compression in the HW monocline hinge, and local extension in the FW monocline hinge.

5.3.2 Spatial distribution of vein intensity and strain

The extent of veining around each fault represents the width of the fault damage zone with the total defined as the normal distance across the fault to the last visible veins in the HW and FW blocks (Fig. 5.7). This is a threshold similar to that defined by Skar et al. (2016) for fractures. Figure 5.7 schematically plots veining normal away from a fault core and illustrates how veins >1

mm and <1 mm can be distributed within the damage zone, and how the limits of the damage zone are set. The distribution of damage zones within the relay structure was interpreted based on the measured damage zone widths in field, so that damage zone contour maps (Fig. 5.8) could be constructed (see section 4.2.2 and appendix I for more details).

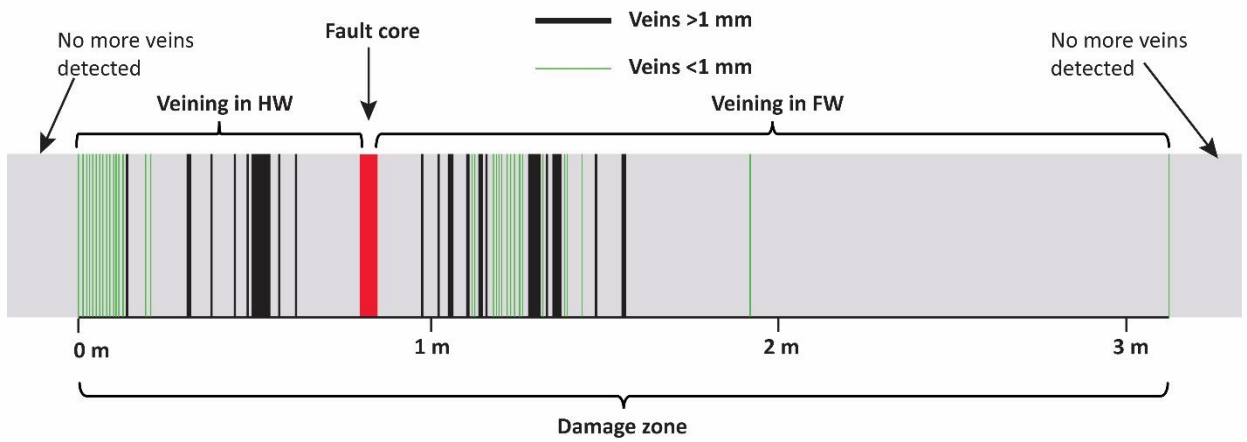

Figure 5.7: Schematic model of a damage zone, where the outer boundary of the zone is defined at the last visible vein detected in the HW and FW moving normal away from the fault core. Both veins >1 mm and <1 mm are represented.

The observed damage zone widths (Fig. 5.8a) are generally narrow, ranging from 0.06 m to 31 m, with the broadest damage zones found in areas of fault interaction. Still, these are not very wide damage zones considering the displacements observed on the faults. Together with veining, the fault damage zones also show structural elements as small splay faults, small antithetic faults, in addition to local folding associated with drag and monoclines at fault tips. The relay bounding faults FS1 and FS2 are also associated with a fault zone (Fig. 5.8a) of high strain, where the wall rock is transformed beyond recognition. The zone is approximately 10 m wide on its widest.

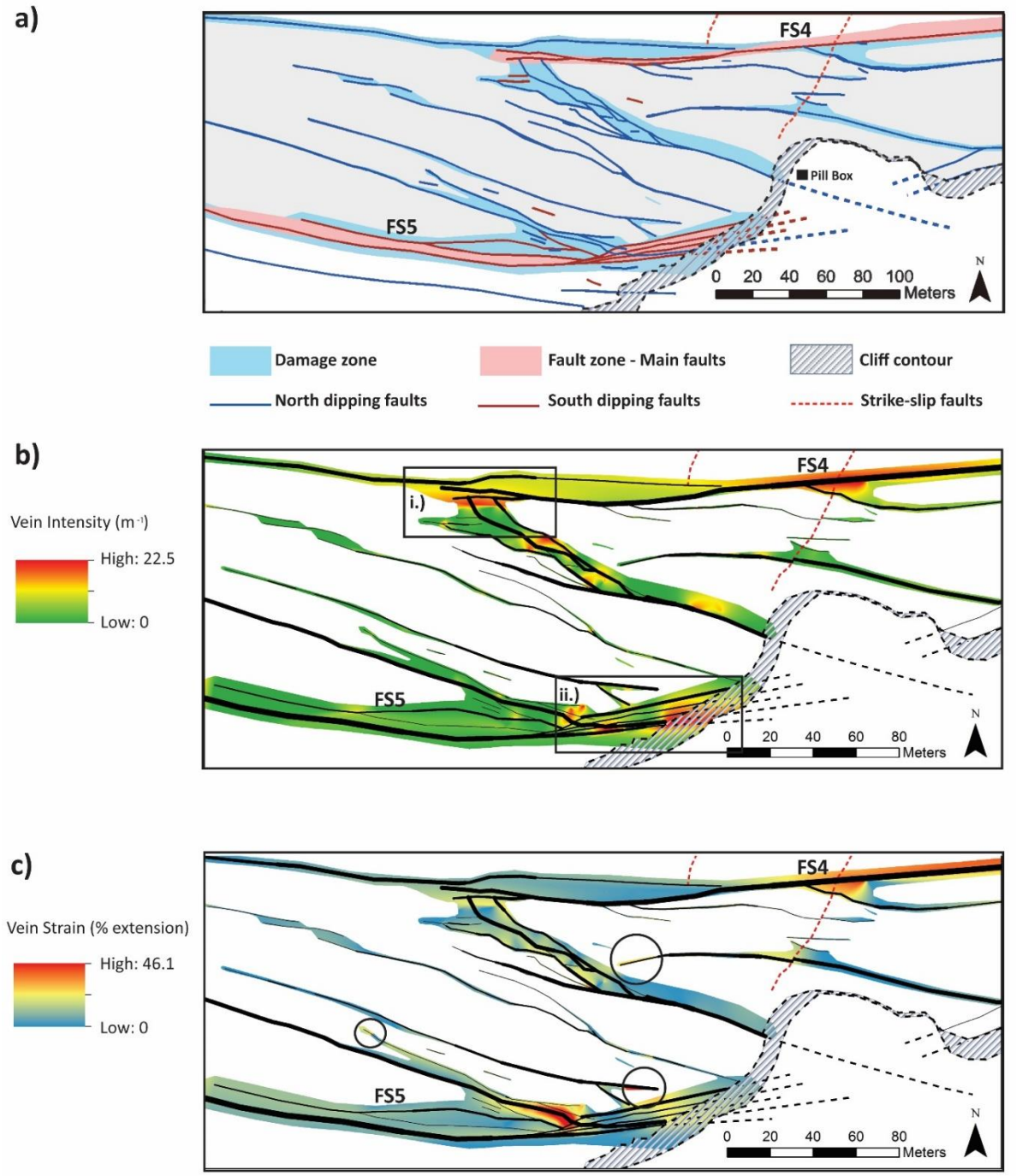

Figure 5.8: Contour maps made in ArcGIS over damage zone of the fault network within the relay structure at Kilve. a) The extent of the damage zone (blue), illustrate that damage zones are widest in areas of fault interaction (i.e. fault splays and abutting relations) and at fault tips. The fault zones of high strain related to the relay bounding faults (FS1 and FS2) are marked in red. b) Vein intensity (m^{-1}) map shows that high vein intensities correspond to areas of wide damage zones, represented by areas of fault interaction (i. – ii.). c) Vein strain (% extension) map follow the same pattern, with high values in areas of fault interaction and at fault tip zones (marked with black circles). Faults thickness within (b) and (c) illustrates stratigraphic separations (as presented in Figure 5.4).

The relationship between damage zone width, fault size and veining (i.e. intensity and % strain) is presented in scatter plot statistics in Figure 5.9. Plot a-, b-, c- and d- show % strain vs displacement, intensity vs displacement, intensity vs damage zone width and displacement vs damage zone width respectively. For plots a- to c- no statistically significant correlation can be drawn between veining and kinematic slip of the fault, or between veining on either side of fault traces. This indicates that intensified veining is controlled by location (i.e. interaction zones) rather than fault kinematics.

Plot d. shows a correlation between observed displacement and damage zone widths. All the largest faults, displaced >15 m show significantly narrow damage zones <10 m wide (marked with yellow box). To the contrary, all faults with damage zones wider than 20 m are represented by faults with generally small displacements of <15 m (marked with green box). No faults with both large displacements and wide damage zones are thus observed, indicating that damage zone widths are closely related to the displacement.

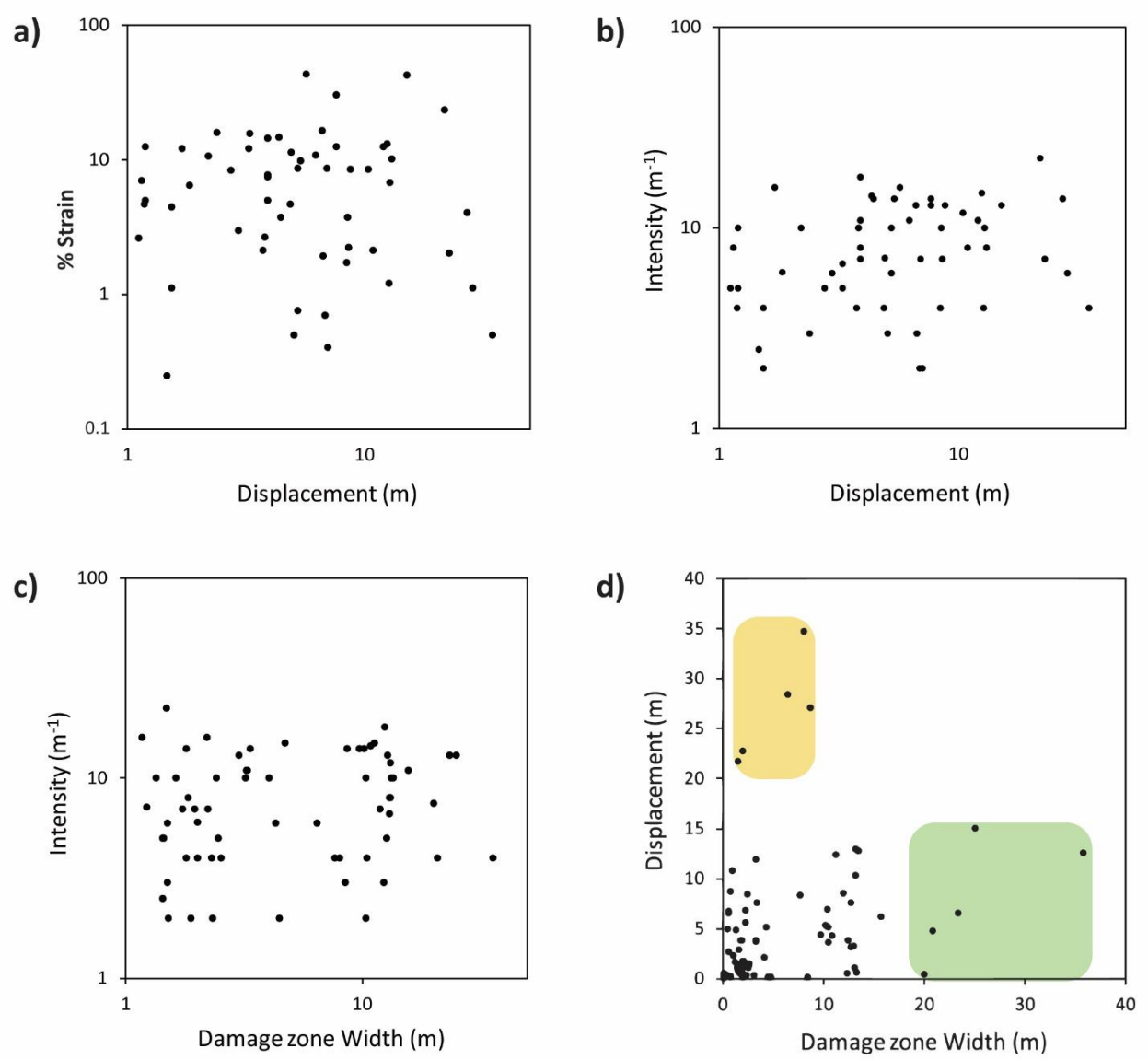

Figure 5.9: Relationship and trends between damage zone width, fault size and veining (i.e. intensity and % strain) presented in scatter plot statistics. a) % strain vs displacement; b) intensity vs displacement; c) intensity vs damage zone width; d) displacement vs damage zone width (yellow box highlight faults of high displacement and narrow damage zones, and green box highlight faults of low displacement and wide damage zones).

Plot a-, b-, c- and d- in Figure 5.10 plots vein intensity in FW vs vein intensity in HW, % strain in FW vs % strain in HW, % strain vs bed thickness and frequency vs bed thickness respectively. Plot a. and b. shows no consistent variation between FW and HW fault blocks.

The influence of lithology and bed thickness on fracture patterns are well known from literature (e.g. Ogata et al. 2014a; Ogata et al. 2014b; Ogata et al. 2014c) and since Skar et al. (2016) found

a strong relationship between fracture frequency and bed thicknesses of shale beds at Kilve, this was tested for the chosen limestone key marker beds. In this study only a slight variation in bed thicknesses (16.5 – 33 cm) are used, to avoid the effect it might have on vein measurements, and plot c. and d. demonstrate that no trend is seen between vein strain/vein frequency and bed thickness of the limestone beds. Thus, bed thickness variations within this study are proven to have no influence on the results.

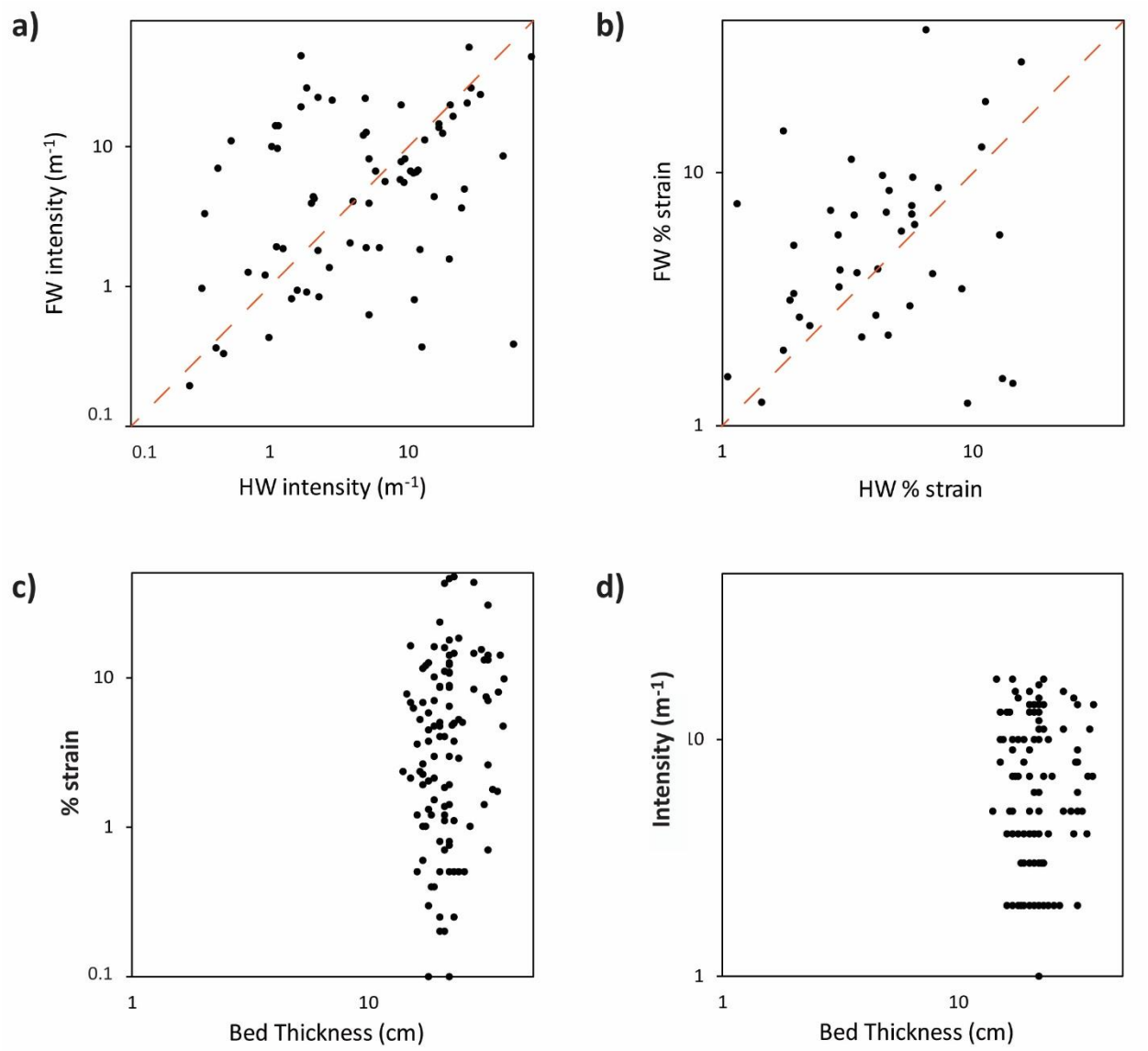

Figure 5.10: Scatter plot statistics comparing veining in HW and FW fault blocks representing FW intensity vs HW intensity (a), and FW strain vs HW strain (b). The effects of bed thickness on veining is illustrated by % strain vs bed thickness (c) and intensity vs bed thickness (d), showing no trends, illustrating that bed variations within this dataset do not have any influence on veining.

The spatial distribution of vein intensity and vein strain (% extension) along-strike fault damage zones were mapped throughout the entire relay fault network, and is presented in contour maps in Figure 5.8b-c. Vein intensities and percentage extension ranges from 0 m^{-1} – 22.5 m^{-1} and 0 – 46 % respectively. Most of the fault damage zones shows low vein intensities (0 - 1 m^{-1}) and only low values of strain (0-5 % extension). However, at areas of fault interaction and fault linkage the intensity and strain is strengthened. Vein intensity shows high values in abutting zones (e.g. area where N-dipping faults abut FS2, Fig. 5.8b – i.) and splay zones (e.g. the eastern splay zone of FS1, Fig. 5.8b – ii.). Furthermore, at these areas of interaction, values of percentage extension over 10 % are located, and in contrast to the intensity map, there is a clear increase in strain observed in some fault tips (marked with black circles in Figure 5.8c). These areas of high intensity and strain are areas of low displacements (i.e. fault tips, abutting zones and splay zones) and high complexity. They thus accommodate areas of rapid spatial variations in displacement, where local stress is high.

5.4 Partitioning of strain

The two former sections focused on spatial distribution of faults and veins through the Kilve Pill Relay zone. In this section the amount of total extensional strain of the relay structure is quantified and the partitioning of strain between different extensional structures at different scales (i.e. relay bounding faults, damage faults, veins) is examined. Domino faults within the relay (D3 and D4) are not included, as they are interpreted to represent a regional development of domino faults, not related to the formation of the relay structure.

Seven key marker beds (69, 83, 103, 121, 126, 138, 161, Fig. 5.2a, Table 5.3) with an average dip and dip direction of 16/154 (Fig. 5.2c) were chosen as N-S trending scan lines evenly distributed moving from west to east through the relay, where heaves of faults and apertures of veins were sampled and added together to represent the total extensional strain of each scan line (see section 4.3.3 and appendix II for more details).

As seen in Figure 5.2a, bed 69 is located farthest out on the wave-cut platform to the west, and ranges over the whole relay. It is situated just outside the overlap zone. Bed 85 to 138 are all inside the overlap zone. Bed 85 shows very good exposure and ranges over the complete relay zone, the same with bed 103. Bed 121 is part of a doublet with bed 117, but the thin shale of approximately

10 cm that separates them never disappears, so that it remains isolated. Bed 126 is just outside of the wanted scale range, but is used because it has good exposure, ranges over large parts of the relay and gives the opportunity to test if a slight variation in bed thickness is an important factor affecting veining (Fig 5.10c-d). Bed 121 and 126 miss some exposed bed length near the cliff where it is covered by large pebbles. Bed 138 covers only the northern half of the relay, and is only included to make the sampling as evenly distributed within the relay as possible for the creation of the contour maps (Fig 5.8b-c). It is not put in focus in this interpretation due to undersampling. Bed 161 cover the relay in the east, partly inside and outside of the overlap zone. It is mostly traced in the cliff, and some bed length is not sampled due to lack of good exposure. The contribution from bed 138 and 161 is thus thought to be higher than seen in Figure 5.11.

Table 5.3: 3-D structural measurements done at key limestone marker beds within the Kilve Pill Relay and calculated extensions of these.

	Average thickness (cm)	Average dip/dip direction	Length in N-S direction (m)	% extension major faults	% extension damage related faults	% extension veins	Total % extension
Bed 69	21.5	162/16	81.4	41 %	14 %	7 %	62 %
Bed 85	20.0	150/19	80.2	26 %	30 %	9 %	65 %
Bed 103	16.5	161/19	80.6	27 %	48 %	4 %	79 %
Bed 121	22.0	152/17	88.4	30 %	35 %	5 %	70 %
Bed 126	33.0	147/17	92.2	29 %	33 %	7 %	69 %
Bed 138	17.5	146/11	52.9	38 %	20 %	1 %	59 %
Bed 161	21.5	160/11	102.2	31 %	21 %	3 %	55 %

The overall trend seen for the applied total extensional strain within the relay (Fig. 5.11a, Table 5.3) shows a maximum of 79 % at bed 103 in the center of the relay zone, but shows an overall average of ~70 % that is seen over the whole zone. Undersampling in bed 138 and 161 create a slight decrease from this average value to the east, so estimating an approximately equal total % extension over the whole zone seems probable.

The contribution of different scale structures (i.e. relay bounding faults, damage faults and veins) is illustrated in Figure 5.11b and Table 5.3. Strain contribution from the relay bounding faults (pale grey) is quite constant from west to east, averaging around 30 % showing a small increase in both

the western and eastern end. Damage faults (dark grey) are also averaging around 30 %, and show a slight increase in applied strain moving into the relay zone. Veining (black) shows a considerably lower overall contribution, averaging around 5 % with no observed trend throughout the whole area. Compared to the faults, veining thus contributes to <5 % of the total strain within the relay (c.f. Putz-Perrier and Sanderson 2008a). The fact that the contribution of both relay bounding faults and damage related faults averages around 30 % indicate that there is a strain compatibility over the whole relay, even though the partitioning of different structures changes through the zone. Relay bounding faults contribute more outside the overlap zone, and damage faults contribute more inside the overlap zone.

This summarizes nicely the former observations done on the spatial distribution of strain of faults and veins throughout the relay zone between FS1 and FS2. Total stratigraphic separation increases in the overlap zone due to a large contribution of damage related faults (Fig. 5.4), and the spatial heterogeneity of stratigraphic separation shows that outside the relay deformation is focused on main faults, but entering the relay the heterogeneity decreases and deformation becomes more distributed across it due to development of smaller faults (Fig. 5.5). This is illustrated as a slight increase of total extensional strain in the middle of the overlap zone (Fig. 5.11a), contributed from the arrival of damage related structures (Fig 5.11b). The spatial distribution of veining shows that vein intensity (Fig. 5.8b) and vein strain (Fig. 5.8c) is localized in areas of fault interaction and at fault tips, which are features commonly found in linkage damage zones. The overlap zone of the Kilve Pill Relay is such a zone, and since areas of interaction and fault tips are distributed homogeneously throughout the relay structure, total extensional strain represented by veining is generally stable and low through the entire overlap zone (Fig. 5.11b).

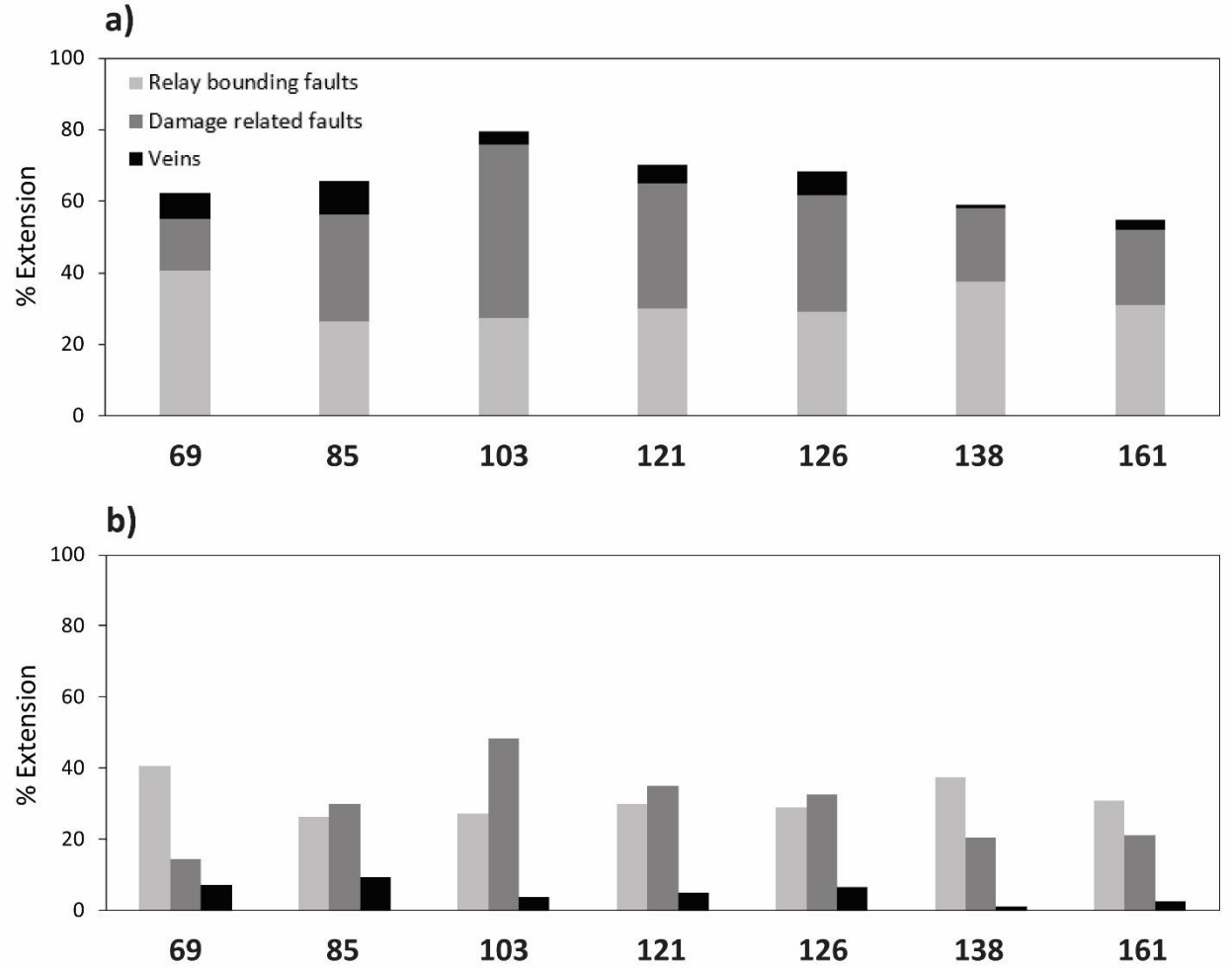

Figure 5.11: Observed brittle structures are divide into three groups; main faults = pale grey; damage related faults = dark grey; veins = black), and their contribution to total extensional strain (a) and their individual partitioning (b) is illustrated in histograms. Note that overall there is a strain compatibility maintained between the different structures through the relay, where a decrease in applied strain from damage related structures within the overlap zone is corrected for by an increase of applied strain from damage related faults. Veining shows a general small contribution of <5 % over the whole area.

6 Results – Tip damage zones

Three fault tip zones of mesoscale faults have been mapped in detail (see Figure 3.1c for locations), and this part of the study focuses on deformation at fault tips, where distribution of deformation along strike the fault zones is documented in times of displacement and veining. The fault tips included in the study are a fault zone at Lilstock (section 6.1.) and two fault zones at East Quantocks Head, named locality A (section 6.2.) and locality B (section 6.3).

6.1 Fault tip zone at Lilstock

Lilstock is located approximately 3.5 km east of Kilve (Fig. 3.1c) and provides a more complex deformation history than at Kilve (see section 3.2), but the fault zone examined does not show any signs of strike-slip or reverse reactivation. The wave-cut platform displays the same interbedded shale and limestone stratigraphy of the Lower Jurassic (Peacock and Sanderson 1999), but located lower in the sequence than at Kilve, somewhere within the Aldersgrove Beds (Fig. 3.2). The fault zone (called locality F in field) is located approximately 120 m out on the wave-cut platform (British National Grid: 31 8022/14 5472) (Fig. 6.1a), and is only reached during hours around low tide. The fault system is observed through eight limestone beds, moving down stratigraphy towards east. The limestone beds show high intensity of veins associated with the faulting, together with Cenozoic to recent jointing.

6.1.1 General structure of the fault array

In map-view, the whole fault array is 72 m long, and consists of four connected, N-dipping normal fault segments (FN1, FN2, FN3 and FN4, Fig. 6.1b). The fault array has an en-échelon geometry, trending approximately E-W. The fault segments have lengths and maximum displacements ranging from 25 to 50 m and 0.1 to 0.83 m respectively (Table 6.1). The eastern extent of FN4 was not examined. The individual (d-x) profiles of the faults are mainly bell-curved (Fig. 6.1c), and increase in both length and maximum displacement from west to east. This indicates that the part of the system examined represents a mesoscale fault tip, tipping out to the west, and the fault system might have grown to the east.

Three relays are observed between the main fault segments (overlap zone i., ii., and iii., Fig. 6.1b) with widths ranging from 1.5 to 2.7 m, producing areas of overlap ranging from 19.5 to 21.6 m^2 (Table 6.1). At the relay structure between FN1 and FN2 (overlap zone i., Fig. 6.1b) the distribution of displacement on the main faults decreases rapidly. Inside the relay eight small-scale faults contribute to maintain coherency of the system by contributing displacement in the overlap zone, indicated by the smooth cumulative profile (i.e. dashed red line, Fig. 6.1c). Even with some damage faults on the ramp, this relay structure seems soft linked in plan-view. For the relay between FN2 and FN3 (overlap zone ii., Fig. 6.1b) and FN3 and FN4 (overlap zone iii., Fig. 6.1b) decrease in displacement is observed where the main faults overlap (Fig. 6.1c). This creates an overall smooth convex-up cumulative profile indicating that this is a coherent fault system (Walsh et al. 2003). The overlap zone between FN2 and FN3 can also be observed in cross-section which exposes hard linkage between them (Fig. 6.1d). FN2 is a synthetic splay of FN3 indicating that faults FN1, FN2 and FN3 form a bifurcating fault tip of the overall fault system. In the overlap zone between FN3 and FN4, fault segment FN3 tips out to the east and displacement transfer to FN4 happens through a breach in the relay ramp.

Table 6.1: Overview table presenting measurements of fault segments (FN1 – FN4), and overlap zones (i. – iii.) of the Lilstock fault zone.

	Segment length (m)	Maximum displacement (m)	Relay width (m)	Overlap area (m^2)	Dip - dip direction relay ramp
FN1	23.4	0.10			
FN2	18.7	0.83			
FN3	44.8	0.69			
FN4	12.1	0.33 (observed)			
Overlap zone i.			2.7	21.6	05/316
Overlap zone ii.			2.0	20.0	06/298
Overlap zone iii.			1.5	19.5	10/222

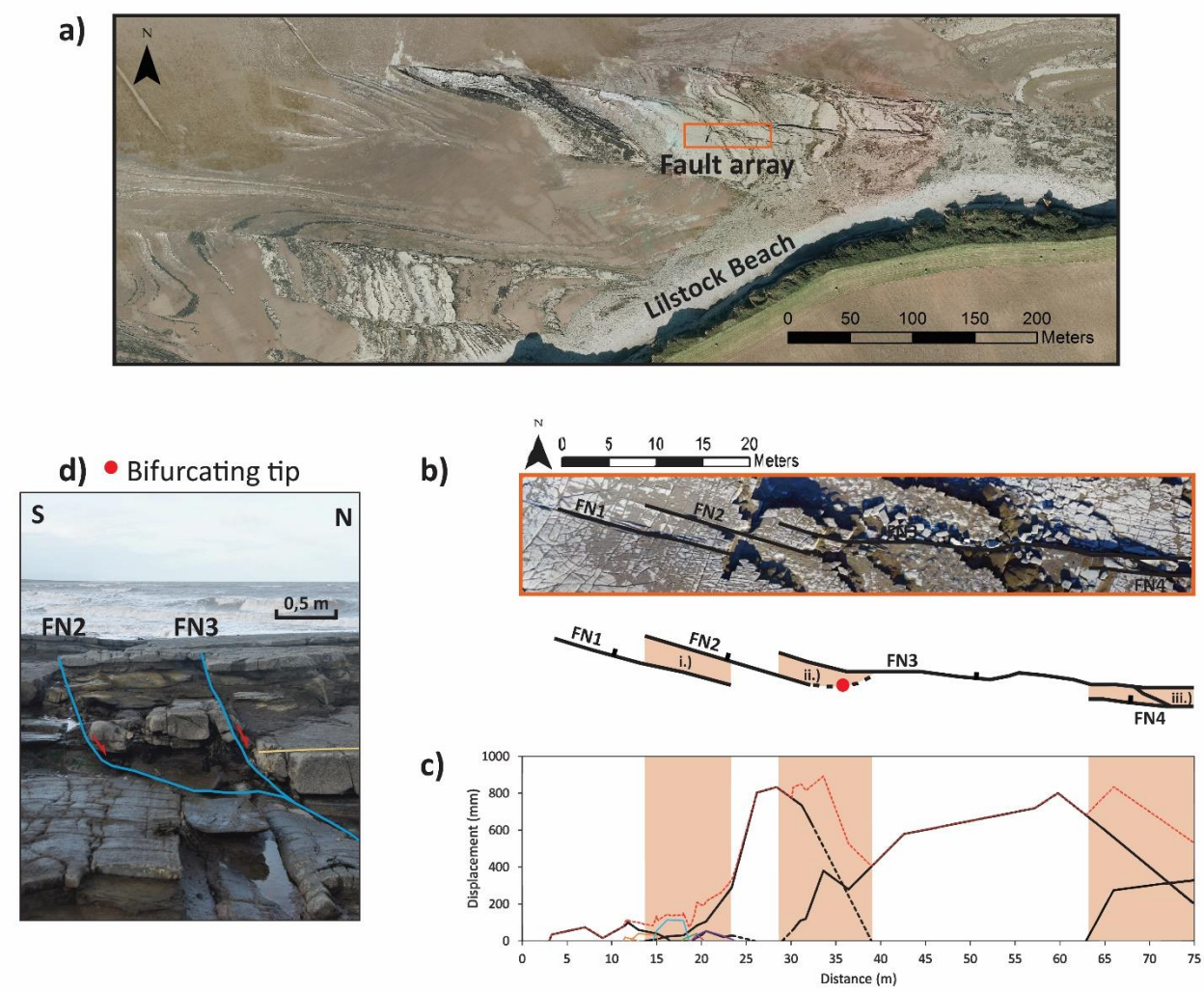

Figure 6.1: a) Overview map of Lilstock Beach highlighting the placement of the studied fault array in the orange box. b) Zoom-in on the en-échelon fault array, consisting of four N-dipping normal fault segments (FN1, FN2, FN3 and FN4), first presented in plan-view on a map, then as a simple line interpretation. Fault movement is illustrated by tick marks on HW side, and overlap areas between faults are colored and numbered (i. – iii.). c) (d-x) profile along strike of the fault array where main fault segments are plotted as black solid lines (i.e. dashed black lines where observations are missing). Damage related faulting in the linkage area between FN1 and FN2 is added as colored profiles (found in separate (d-x) profile in Figure 6.2). The red dashed line shows the cumulative total of displacement. d) Picture of hard linkage observed between fault segment FN2 and FN3 in cross-section, where FN2 is a synthetic splay of FN3. The location of this observation is marked with a red dot in b).

6.1.2 Faulting and displacement between en-échelon segments within fault tip

The relay zone between en-échelon fault segments FN1 and FN2 (Fig. 6.2a) is the only relay that is wholly observed in one bed, and is thus used to map damage without needing to consider other effects such as lithology and bed thickness. Figure 6.2b display the geometries of, and the interactions between the different fault segments of the relay zone, where FN1 and FN2 bounds the relay. FN1 consists of three linked fault segments (including the damage related segment represented in blue), while FN2 consists of four fault segments, three of them visibly linked in plan-view. Eight damage related small faults with planar geometries are found within the relay ramp. Overlap between these segments produces even smaller relay ramps (i.e. marked as grey shades). Displacement is therefore transferred between the relay bounding fault segments through both brittle and non-brittle deformation, at different scales.

Figure 6.1c illustrates the displacement profiles of FN1 and FN2 and the damage related faults. The decrease of displacement on the main faults is accompanied by damage faults transferring displacement. The displacements of the damage related faults are generally low, ranging from 0 - 0.1 m, and they all show approximate bell-shaped profiles, increasing in maximum displacement to the center of the fault. The overall maximum displacement of all eight faults is found in the center of the overlap zone. A profile adding all the damage faults together would thus produce one convex-up bell shaped profile, similar to those seen for single, isolated faults (Walsh and Watterson 1989). This illustrates that strain coherency is maintained through all scales in the overlap zone, displayed by the cumulative profile (dashed red line, Fig. 6.2c). Note that the contribution of damage related veins to the overall strain is not taken into consideration in this plot (see section 6.1.3) which would have increased the profiles some.

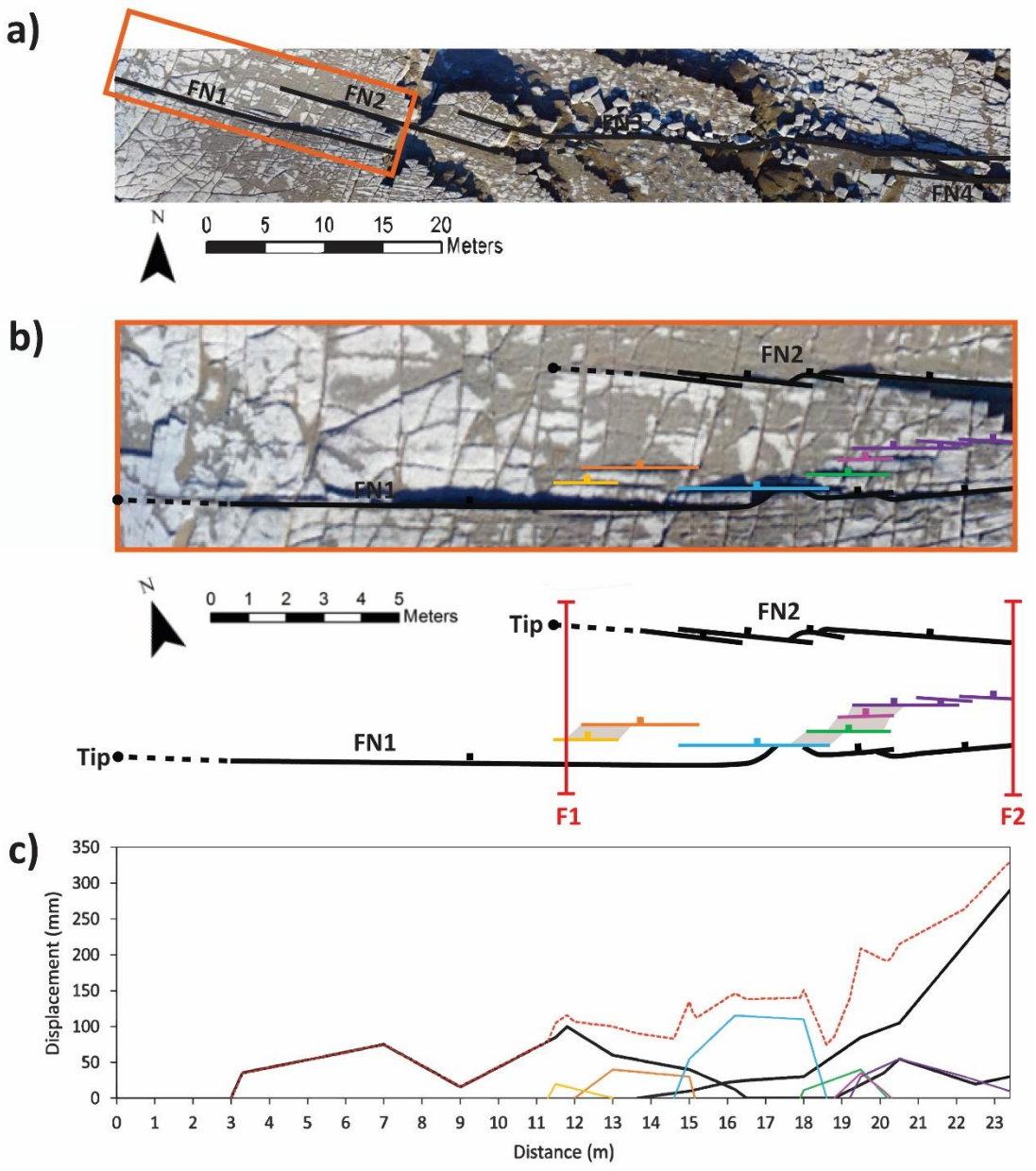

Figure 6.2: Detailed study of relay zone between en-echelon fault segments FN1 and FN2. a) Overview map of fault array, highlighting the studied relay structure in orange box. b) Zoom-in on the relay structure, first presented in plan-view on a map, then as a simple line interpretation. Fault movement is illustrated by tick marks on hanging wall side. Main faults are drawn in thick black lines, and damage related faulting in thin colored lines. Small-scale relay ramps observed in overlap zones between the damage related faults are shaded grey. Fault tips are marked as dots in the end of a dashed line representing veining continuing the fault laterally. Placement of vein transect F1 and F2 covering the width of the relay zone represented by N-S trending red lines. c) (d-x) profile of the relay bounding faults, color coded to match the fault map in (b). Red dashed line represents the cumulative total of displacements. Note the increase in intensity of damage related faulting in the overlap area of the main faults.

6.1.3 Spatial distribution of faults and veins in the damage zone

High intensity calcite veining within this fault array is associated with both relay bounding- and damage related faults, showing a close relationship between faults and veining. The veins constitute the tips of the faults as well as being part of the fault core, and are also extensively distributed across the damage zone of the relay structure.

The extent of veining normal to fault strike was mapped over the entire relay structure (Fig. 6.3a), illustrating the geometry and extent of the damage zone. The FW side of FN1 has a broad damage zone (3.5 – 7.0 m wide) along the entire strike of the fault, and the linkage zone also shows high vein intensity. Moving out from the relay zone (i.e. immediately west of the FN2 tip), the damage zone decreases in width rapidly and veining is mainly located on the HW side of FN1. For FN2 the same relationship is seen with more veining in the FW fault block than the HW fault block, and the damage zone only extends ~0.5 m north into the HW fault block, mainly in the area around the tip of the fault. This indicates that the damage zone geometry is mainly controlled by the overall fault structure of the bifurcating tip zone (i.e. the en-échelon array trending E-W (fig. 6.1b), and not each individual fault segment).

Vein data along two N-S oriented transects (F1 and F2, Fig. 6.3a) illustrate the spatial distribution of damage related structures at different parts of the relay zone, where both vein apertures and fault heaves were quantified to compare the relative contributions to extensional strain (Fig. 6.3b). The transects cover the whole width of the relay ramp, as well as parts of the damage zone outside. F1 is outside the overlap zone, whereas F2 is inside the overlap zone. The total amount of extensional strain produced by faults and veining at F1 and F2 was 11 % and 15 % respectively (Fig. 6.3b). The percentage extension contributed by veining is approximately 8 % for both transects, whereas the contribution from faulting increases significantly from 2 - 7 %. Included in the heaves of the faults are the veining in the fault core. For F1 and F2 the contribution of veining in the fault core to the total heave was ~50 % and ~75 % respectively. Since the number of faults do not increase significantly from one transect to the other, it is thought that the mineralized fault cores are the main contributors to the increase in fault related extension from F1 to F2.

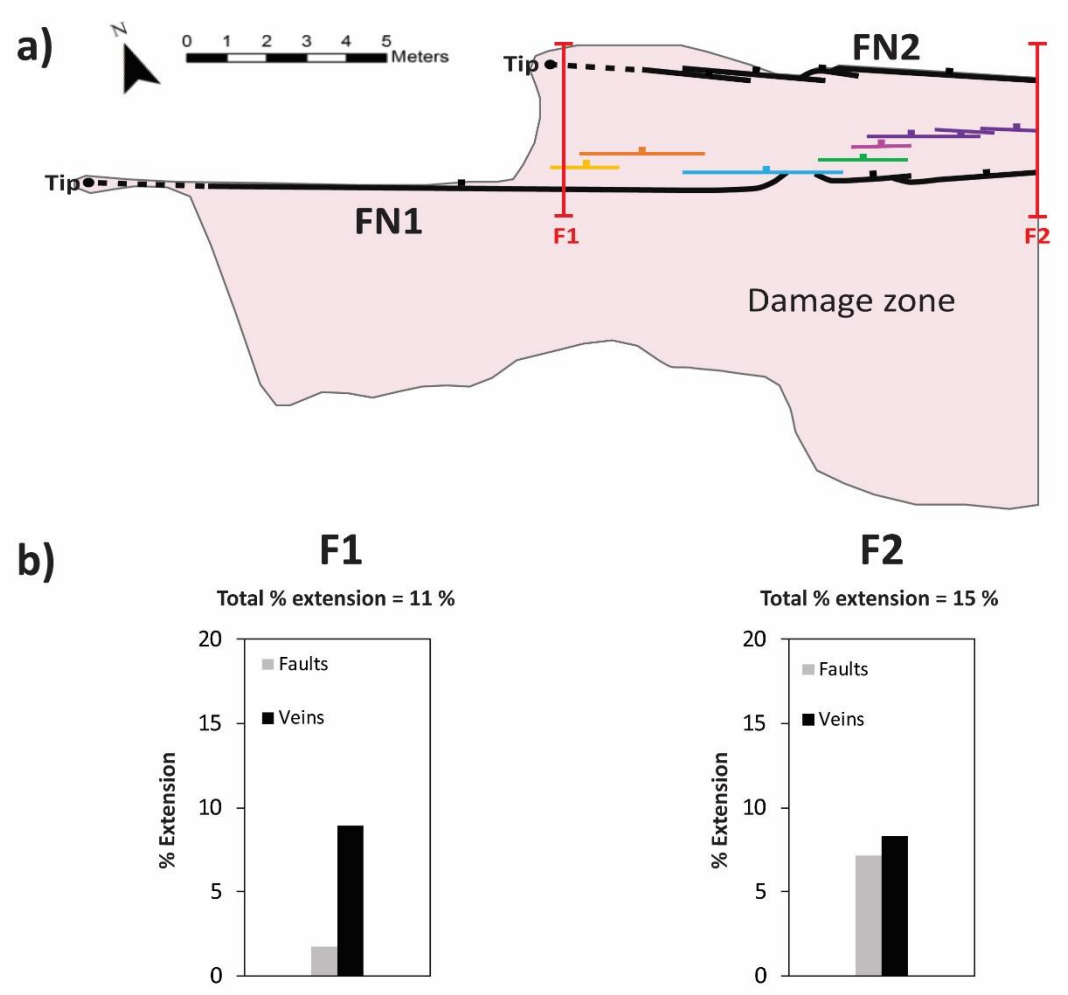

Figure 6.3: a) Map representing the damage zone geometry in plan-view of the relay observed between en-échelon fault segments FN1 and FN2. The transects F1 and F2 are marked by N-S trending red lines. b) Histogram showing the contribution of percentage extension of faults and veins for transect F1 and F2. Mineralized fault cores are included in the fault extensions.

Cumulative plots of frequency and extension along each transect (Fig.6.4a) illustrate the spatial heterogeneity of damage structures and extension over the relay zone, including both faults and veins. The structure frequency is fairly constant, supported by low V_f values ranging from 0.21 to 0.25. Higher values of V_e indicate a localization of extension, with the highest value of 0.48 found at F1 (i.e. nearly outside the damage zone). In Figure 6.4b the fault extensions have been removed, displaying similar low V_f values, and fairly uniform curves of vein extension (especially for F2). This suggests that veining is widely, and fairly homogeneously developed within the damage zone, with extension localized on developing faults. Similar results were found by Roberts et al. (1999)

in a N-dipping fault region located to the east of Kilve Pill. They interpreted this as tip damage zone development with extension fractures (fine veins) superposed by dilation of veins as slightly later faults propagate. This is essentially the model applied to Kilve in general by Putz-Perrier and Sanderson (2008a), and is supported by veins continuing faults laterally in fault tips, and the mineralization of fault cores.

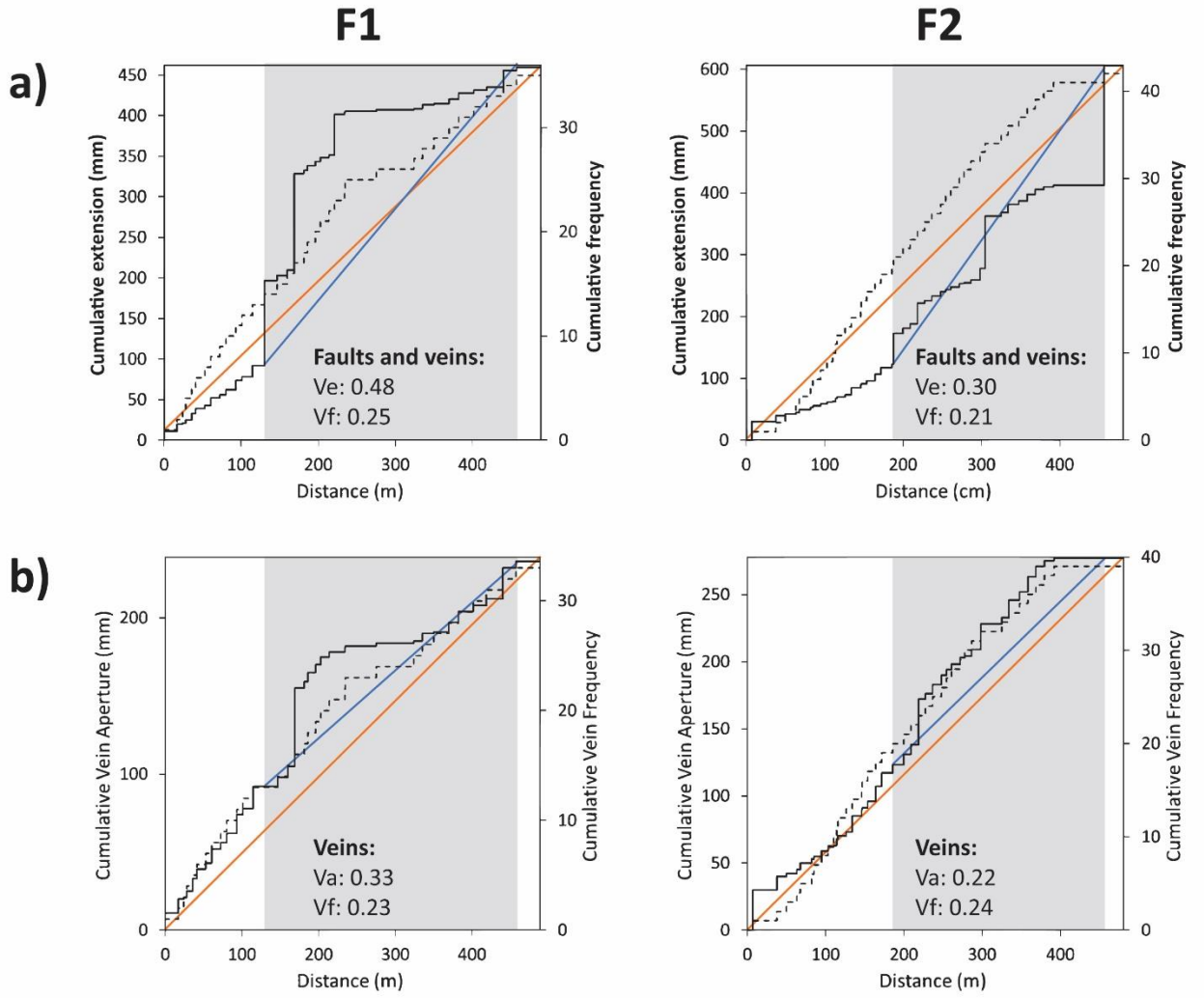

Figure 6.4: Non-normalized cumulative plots that represent spatial heterogeneity of veins and faults (a) and only veins (b) of F1 and F2. V_e = heterogeneity measurements of extension; V_f = heterogeneity measurements of fault- and vein frequency; V_a = heterogeneity measurements of vein aperture. Black solid line = extensions and apertures; black dashed lines = frequencies. The gradients of V_e/V_a and V_f of the curves in both (a) and (b) are marked in blue and orange respectively, where the gradients of V_e and V_a only cover the relay structure (shaded grey).

6.2 Fault tip zone at locality A – East Quantocks Head

The fault studied in locality A (British National Grid: 313226/144127) (Fig. 6.5a) is a N-dipping E-W trending normal fault observed on the wave-cut platform. A 66 m along-strike profile was mapped through eleven limestone marker beds. It is difficult to distinguish exactly where within the stratigraphy this group of beds is located, but it is somewhere within bed 83 – 109 (Fig. 6.5b). Bed names are thus given after locality numbering, giving them names A1 - A11. The fault tip to the west is detected in bed A1 and A2, displaced from the main profile to the south (~15 m) by a left lateral strike-slip fault. Very small displacements (< 0.01 m) are only observed in bed A4 and A5, which are incorporated in the amplitude of observed monoclines, which correspond to displacement in the presented (d-x) profile (Fig. 6.6b). The fault tip is thus revealed through fault related folding and increase in vein intensity along the fault trace rather than observed displacements.

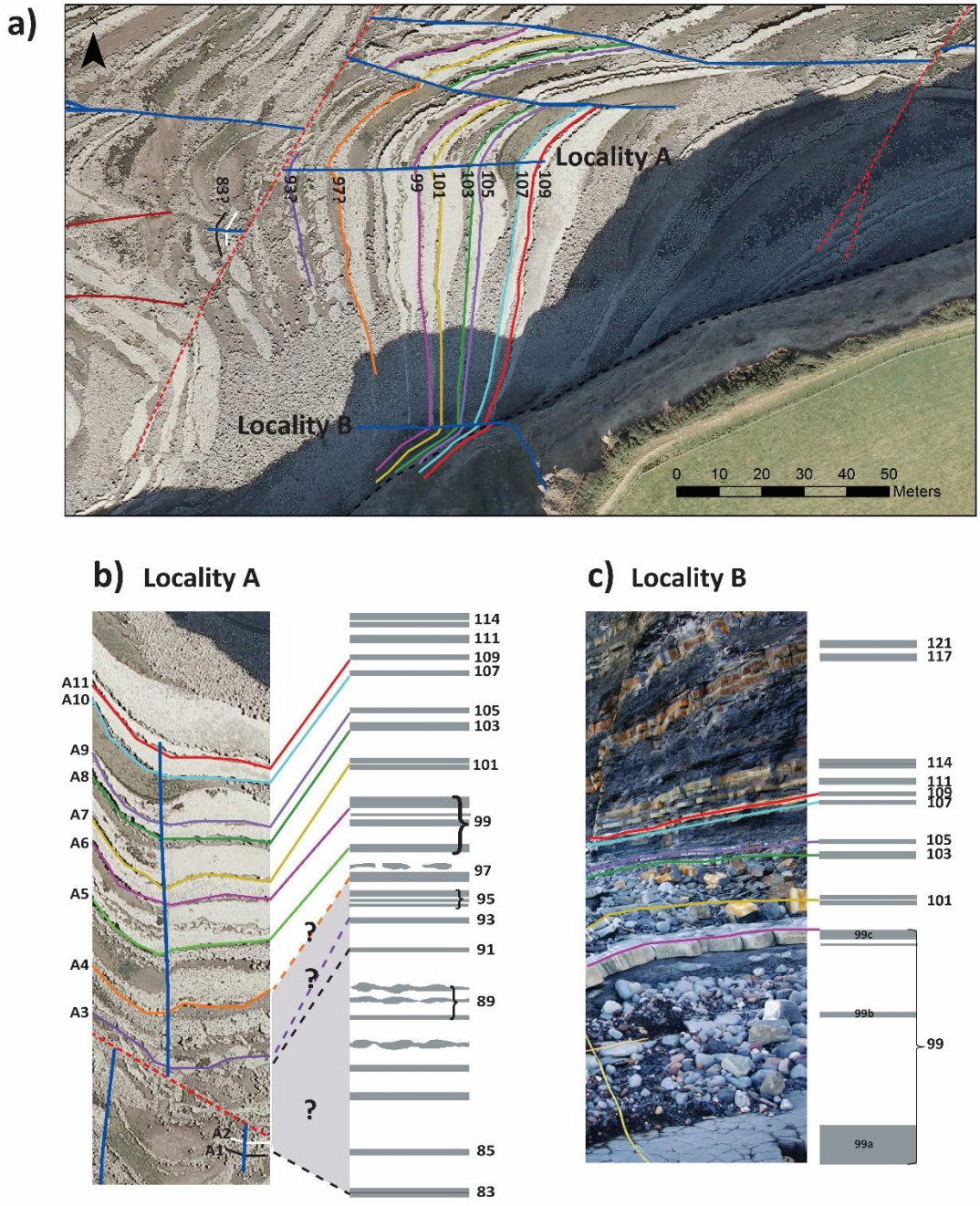

Figure 6.5: a) Overview map showing the location of the tip zones studied at locality A and B, East Quantocks Head. Faults (S-dipping = red, N-dipping = blue, strike-slip = dashed red) and stratigraphy (colored and named with marker bed numbers) is interpreted where possible. b) Part of stratigraphy studied in the tip zones at locality A and B represented by observed sections of the stratigraphic log presented in figure 3.2. At locality A it is difficult to distinguish exactly where within the stratigraphy some beds lie, so the beds examined are given names after locality numbering (A1 – A11).

Photographs of four beds (A3, A5, A7, A11, Fig 6.6a) illustrate the geometries of veins and bedding along strike. Bed A11 (red) is planar and dipping 10/063. Veins perpendicular to bed surface and with constant thicknesses throughout the whole bed section is observed. Bed A7 (green) shows a gentle and wide monocline bed geometry (Table 6.2) with a high on the FW side and a low on the HW side of the fault. Veins rotate with folding to keep normal to the bed surface. A thickness variation of the veins creates wedge-shaped vertical geometries, with thickening in the bed top at the FW side, and thinning in the bed top at the HW side (as described in section 5.3.1). Veins are few and thick, and the fault core is also mineralized. In bed A5 (pink) the monocline is more prominent and narrow, and veining shows the same geometries but apertures are decreasing and number of veins increasing. Bed A3 (orange) is located 11.6 m from the western fault tip, with a widening monocline. Veining is numerous and spread out, but has relatively small apertures. Veins still show bed related rotation and wedge shapes.

Table 6.2: Measurements of monoclines along strike fault tip at locality A, East Quantocks Head.

Bed number	Bed geometry	Monocline amplitude - fault displacement (m)	Monocline width (m)	Dip of monocline limb
A11	Planar	-	-	-
A7	Folded	0.25	1.60	18°
A5	Folded	0.23	0.67	30°
A3	Folded	0.20	0.95	20°

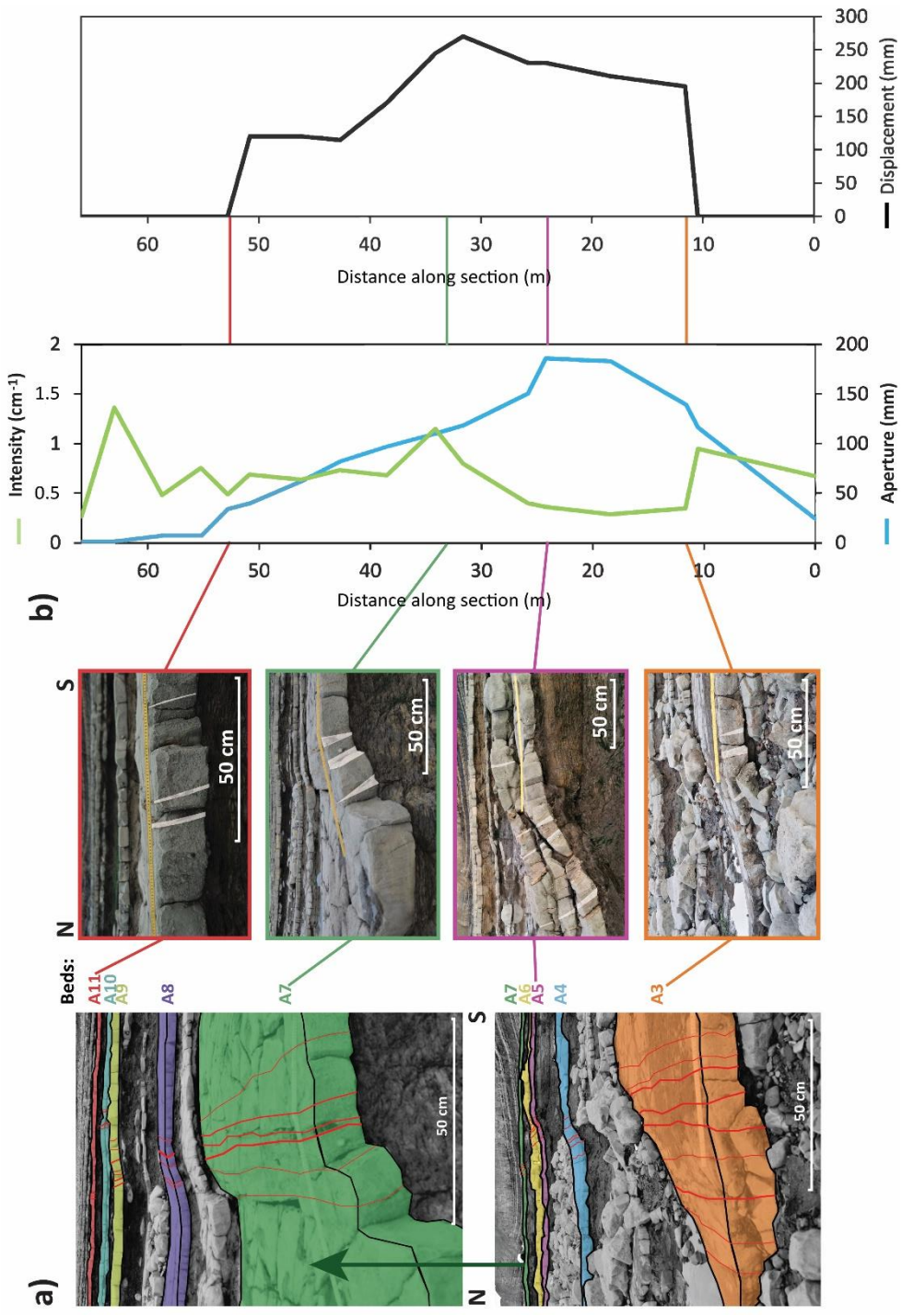

Figure 6.6: Tip damage zone at East Quantocks Head – locality A. a) Plan-view photo with interpretation of marker beds within the stratigraphic section (A1 – A11). Since bed A1 and A2 is displaced 15 m away from the rest of the beds, these are left out of the plan-view photo, but included in the along strike profiles in b). Veining is illustrated in red. Four photographs of bed A3, A5, A7 and A11 illustrate the variations in geometrical relationships between veining and bedding, color coded to match the beds in the plan-view photo. b) Along strike profiles of intensity (green), aperture (blue) and displacement (black). The displacements also include the amplitude of the monocline. The location of the four cross-section photos are marked.

Figure 6.6b illustrates profiles representing displacement, vein intensity and total aperture along strike the fault based on transects oriented normal to the fault trace, taken at each bed trailing the fault from east to west. The displacement profile has a convex-up bell shape with a displacement maximum of 0.27 m, placed in the center of the observed fault length. Displacement decreases toward both east and west, and is only observed in 42.3 m of the total 66.0 m fault trace length. Where the curve starts to reach small displacements, the decrease is rapid, illustrated in steep gradients. This corresponds to the description of (d-x) profiles of isolated faults with restricted fault tips (e.g. Muraoka and Kamata 1983; Peacock and Sanderson 1991), where fault tip restriction is characterized by the high displacement gradient in the tip zone. Total aperture along strike shows a shape similarity to the displacement curve, with a convex-up bell shape, with a peak of total maximum aperture of 186 mm. Vein intensities are alternating along strike, averaging around 0.65 m^{-1}. It is still worth noting the prominent peak in maximum vein intensity of 1.36 m^{-1}, located to the east of the profile, where no displacement and no considerable vein aperture is detected. This might suggest increased vein intensities in areas of low displacement.

6.3 Fault tip zone at locality B – East Quantocks Head

The fault studied in locality B (British National Grid: 31 4241/14 4068) (Fig. 6.5a), is partly observed in the cliff, and partly on the wave-cut platform. The section is thus curved, and oblique to dip, giving an approximate down-dip observation in the cliff, changing to more along strike the fault plane on the foreshore. This makes the tip approximately parallel to the fault slip sense in the cliff, shifting to approximately normal to fault slip sense on the wave-cut platform. The fault is N-dipping and trends E-W, with a distinct fault displacement observed in the cliff that decreases down stratigraphy before reaching the tip zone (i.e. process zone) on the wave-cut platform. The fault can be followed through ten limestone marker beds, where bed 99 consist of a group of three beds (Fig. 6.5c).

Photographs of bed 99a, 99c, 101 and 117 (Fig. 6.7a) illustrate the variations in geometrical relationships between veining and bedding. Bed 117 (orange) is observed in the vertical section of the cliff, where the bed is displaced and shows prominent fault drag as the bed is folded and steeply rotated within the fault core (Table 6.3). Displacement measurements includes the effect of fault drag. A broad mineralized fault core is enclosed by a narrow zone of thick veins. Rotated wedge-

shaped veins are seen cross-cut by vertical and fault plane parallel veins (Fig. 6.8). This can be explained by later vertical veining associated with kinematic slip of the fault (i.e. wall damage related veining) cross-cutting earlier rotated veins produced in the fault tip damage zone. Bed 101 (blue) is displaced and shows a prominent monocline structure with some thick rotated veins within the fold hinges. The wedge shape of the veins is protruding. The folding of the monocline structure decrease in bed 99c (pale pink), and veining is represented by generally smaller veins distributed further away from the fault core. In bed 99a (grey) there is only observed a narrow tip zone of veining in plan-view. The bed, being planar and dipping 08/064, shows no evidence of fault related folding.

Table 6.3: Measurements of monoclines along strike fault tip at locality B, East Quantocks Head.

Bed number	Bed geometry	Monocline amplitude - displacement (m)	Monocline width (m)	Dip of monocline limb
117	Folded	1.49	0.31	70°
101	Folded	0.50	0.43	35°
99c	Folded	0.13	0.50	30°
99a	Planar	-	-	-

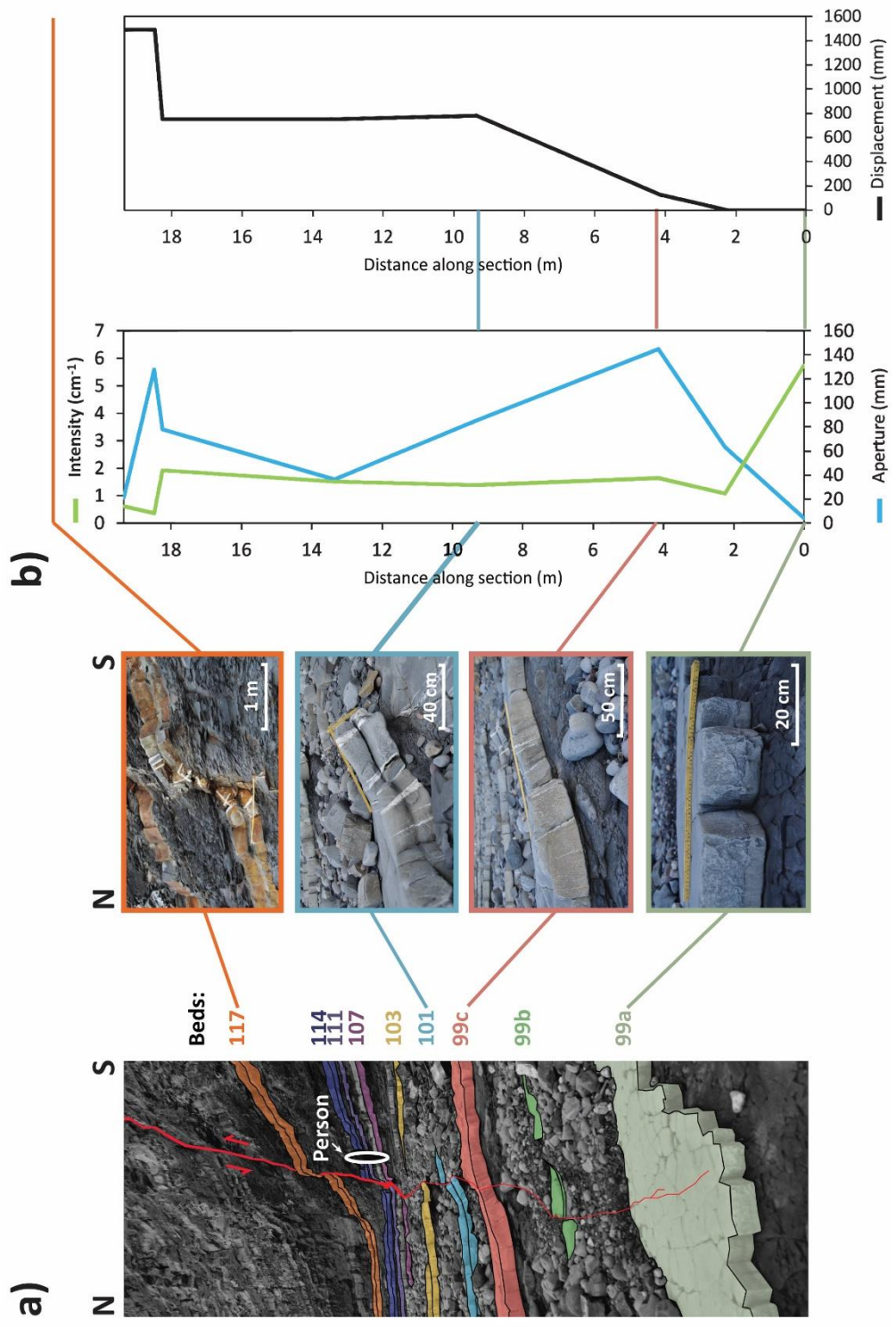

Figure 6.7: Tip damage zone at East Quantocks Head – locality B. a) Plan-view photo with interpretation of marker beds (99 a-c, 101, 103, 107, 111, 114 and 117). The fault trace is illustrated as a red line, showing the tip (veining) in bed 99a evolving into a N-dipping fault seen in the cliff. Four photographs of bed 99a, 99c, 101 and 117 illustrate the variations in geometrical relationships between veining and bedding, color coded to match the beds in the plan-view photo. b) Along strike profiles of intensity (green), aperture (blue) and displacement (black). The displacements also include the amplitude of the monocline. The location of the four cross-section photos are marked.

Vein transects orientated normal to the fault trace were used to create the profiles in Figure 6.7b, which illustrate changes in displacement, vein intensity and total aperture along the fault. Maximum displacement is observed in the cliff, decreasing towards the tip damage zone represented by two major steps at 18.2 - 18.5 m and 4.1 - 9.3 m respectively. The first step has a decrease in displacement of 0.74 m over a short length, while step two shows a decrease of 0.65 m over a longer length. This indicates that the displacement decreases more rapidly where displacements are large, and that it generally decreases toward the fault tip. The curve presenting total vein aperture shows two prominent positive peaks with maximum apertures of 128 and 145 mm, corresponding to the decreases of the displacement profile. The first peak can be caused by prominent veining with large apertures close to the fault, and mineralization of the fault core, while the second peak might be related to increased veining in the process zone. The vein intensity curve shows minimum values in the cliff, and a steady increase to the maximum value of 5.75 m^{-1} at the outer fault tip. This illustrates a general opposing relationship between intensity and displacement, where vein intensity is greatest in the fault tip where displacement is absent, decreasing moving into the slip zone.

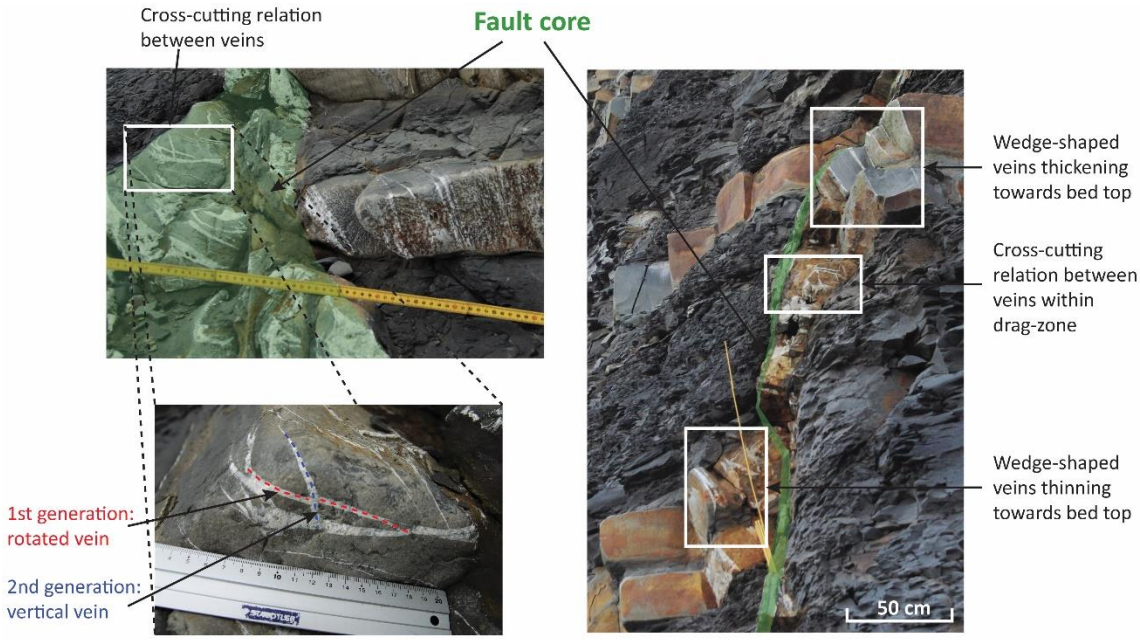

Figure 6.8: Cross-cutting relationship between different generations of veining is seen close to the fault core of the fault examined at locality B where the fault has gained displacement. The 1st generation of veins are represented by wedge-shaped rotated veins produced within the fault tip damage zone of the fault tip. The 2nd generation represent thin vertical, plane parallel veins associated with wall damage, produced by kinematic slip on the fault plane.

6.3.1 Vein distribution within the damage zone

Spatial heterogeneity measurements were done for four vein transects at locality B, to investigate the spatial distribution of veining along strike the fault trace. Figure 6.9 illustrates a schematic plan-view geometry of the damage zone, together with plan-view pictures and drawn transects showing vein distributions. Percentage extension were also calculated. Transect B7 shows a significant displacement on the fault, with a corresponding narrow damage zone of 0.08 m compared with the broad damage zone of 1.43 m in the fault tip damage zone in T3. This supports observations described in the former section, where damage zone widths and vein intensity increases with decreasing displacements. V-values of vein aperture (V_a) decreases significantly from 0.90 to 0.31 moving towards the tip damage zone. This suggests localization of extension on the fault core and few larger veins in the narrow part of the damage zone, whereas widely distributed (and fairly homogenously) small veins develop within the broader process zone, developing into a wide tip damage zone. This is further supported by the general decreasing V-values of vein frequency (0.41 - 0.24) moving towards the fault tip. Putting these observations together implies localization of damage and narrowing of damage zone width with growing displacement. Calculated percentage extension shows a generally equal extension within the damage zone of the three first transects (B3 – B5) ranging from 9 – 19 %, but at T7, where displacement is prominent, percentage extension increases rapidly to 68 %. This illustrates that fault displacement is the most important contributor to extension.

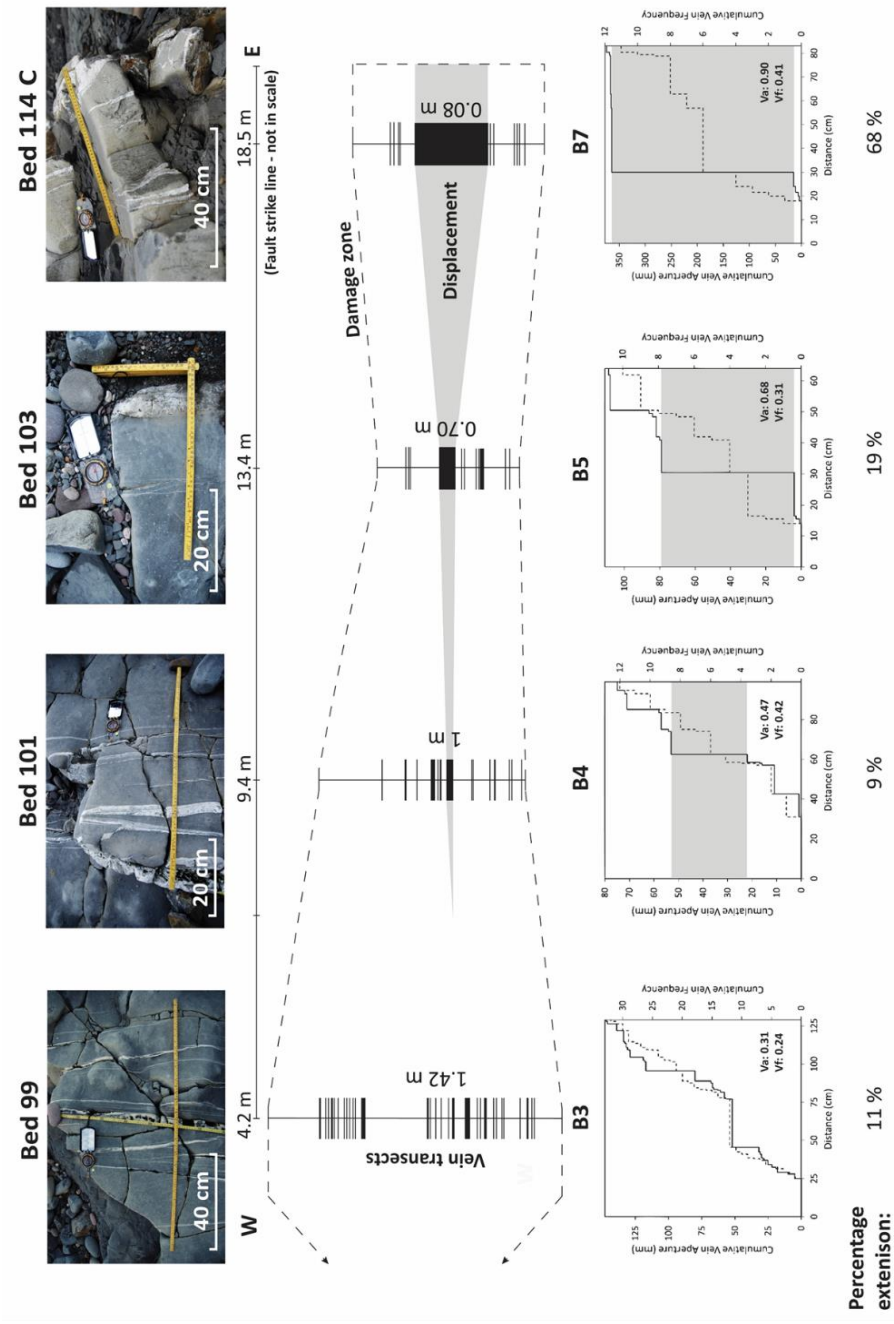

Figure 6.9: Schematic plan-view geometry of damage zone and veining along strike of the fault tip zone at locality B. It presents four chosen vein transects (B3, B4, B5, B7) illustrated by photographs, a drawn vein transect showing vein apertures and frequencies, and a cumulative plot for spatial heterogeneity of vein aperture (V_a) and vein frequency (V_f). From E to W, the figure shows changes from the slip zone to the process zone of the fault. From the drawn vein transects, a damage zone has been outlined by dashed black line, and the grey area represents the fault core where displacement is observed (also marked on the cumulative plots). The cumulative plots are non-normalized, and show the heterogeneity measurements of vein aperture as solid black line (V_a), and heterogeneity measurements of vein frequency in dashed black line (V_f), where the overall trend is a change from localized to distributed deformation moving from E to W (V_a decreases from 0.90 – 0.31).

6.4 Localization of fault tip zones and scale dependent damage

The three investigated tip zones can be placed within the model of fault tip modes of Kim et al 2004 (Fig. 6.10a). The fault zone at Lilstock and the fault tip at locality A are observed in map-view, and the fault tip is oriented normal to the main slip sense of the fault. They are thus representing mode III presentations of their fault tips. Locality B represents a mixed mode presentation, where the part in the cliff is observed in cross-section parallel to the main fault slip sense, representing a mode II dominated fault tip, and the part on the wave-cut platform is observed in map-view normal to the main fault slip sense, representing a mode III dominated fault tip.

Figure 6.10b mark the fault traces on a conceptual elliptic fault plane, giving an overall picture of what parts of the fault plane that are studied. This shows that the fault tip in locality A is tipping out in both directions, and that the rest of the observed fault trace may represent the wall damage of the fault. The same is the case for the fault zone at Lilstock, where a fault tip damage zone (which also is a linkage damage zone) transforms into a wall damage zone as the slip of the faults increases. The wall damage zones consist of large extension fractures (veins) that are sub-parallel to faulting, and Kim et al. (2004) propose that this type of wall damage initiated as veins produced in mode III fault tips, incorporated in the slip zone as the fault grows. Additional slip related damage may also occur, and this explains how an observed damage zone might display damage structures representing more than one of the three location-based groups of damage zones (Kim et al. 2004) (Fig. 2.5). This is illustrated at Lilstock, where both linkage damage and wall damage is represented in the bifurcating tip zone, overall representing a tip damage zone. This suggests that the definition of damage zones based on their location is depending on both chosen scale and the definition selected for different parts of a fault array. As Lilstock is interpreted as a bifurcating tip zone, it is drawn as a slight up-dip tip on the fault plane, while the fault tip at locality B rather represents a down-dip tip (Fig. 6.10b), as it is observed down stratigraphy from the cliff-section to the wave-cut platform.

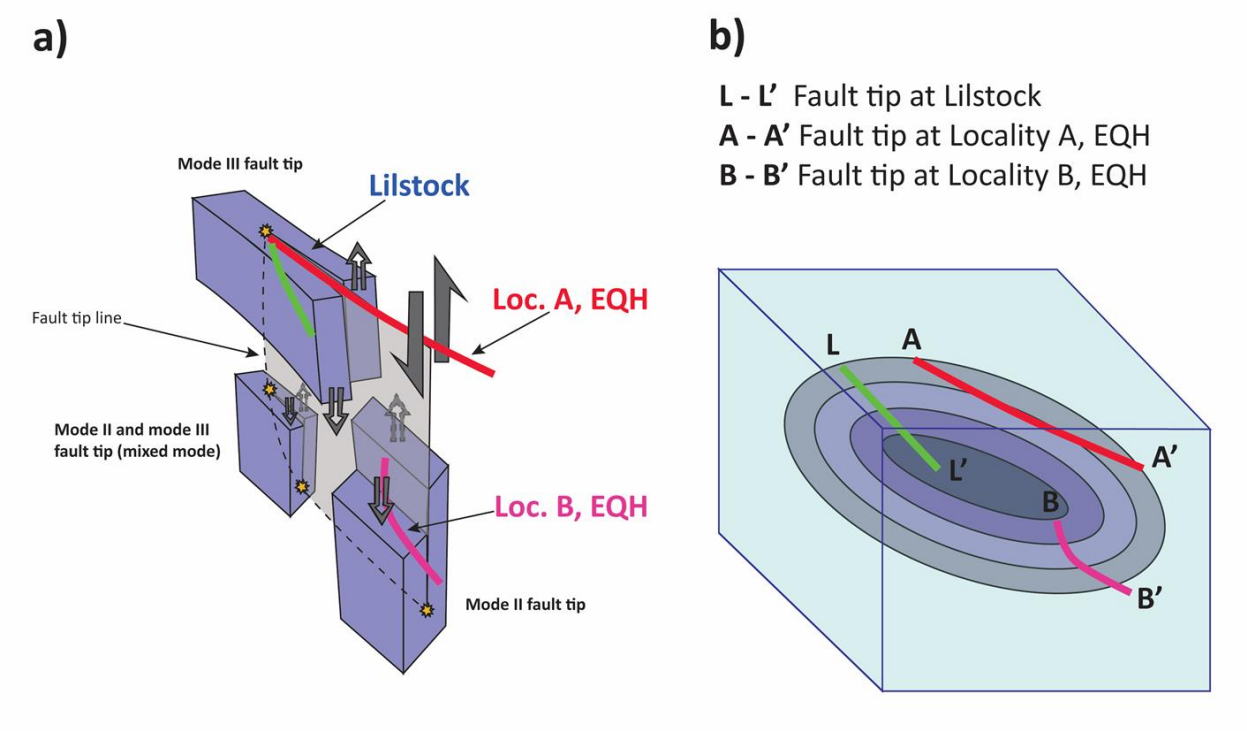

Figure 6.10: a) The schematic model of fault tip modes presented in Figure 2.6 is used to illustrate what fault tip mode each of the three studied fault tip zones (Lilstock = green, locality A = red, locality B = pink) represent. Lilstock and locality A represent mode III fault tips, while locality B represents a mixed mode fault tip, dominated by mode II sliding in the cliff, and mode III tearing on the wave-cut platform. b) A conceptual model of a fault plane is presented to illustrate the interpreted spatial location of the fault tip zones on a complete fault plane, where Lilstock is interpreted to be an example of an up-dip tip, locality A a lateral tip and locality B a down-dip tip.

7 Discussion

In chapter 5 and 6 data are presented to describe and quantify damage zones associated with normal faults, where the focus has been on distribution of deformation within these zones. This chapter starts with a presentation of different damage zones identified during the study (section 7.1), followed by interpretation and discussion of the results in order to shed light on development of veining around faults (section 7.2), partitioning of deformation in fault linkage zones (section 7.3) and spatial heterogeneity of deformation at different scales (section 7.4). Finally, implications of the presented research will be seen in the light of scaling of deformation, and fluid flow within normal fault networks.

7.1 Damage zones within normal fault networks

Different types of damage zones within a normal fault network in Jurassic rocks along the Somerset coast were characterized and quantified in terms of their brittle deformation, both in the fault zone (i.e. measurements of displacements), and within the damage zone (i.e. vein sampling and displacement measurements). Damage zones were grouped using the classification of Kim et al. (2004) (Fig. 2.5) and McGrath and Davison (1995). Their classification is based on the location of the damage zone in relation to the main fault trace, but there is no quantification of damage related structures within these zones.

By characterizing deformation around normal faults at Kilve, Lilstock and East Quantocks Head and quantifying spatial variations in structural intensity, strain and heterogeneity, several types of damage zones have been identified. Using a conceptual model of a normal fault network (Fig. 7.1) the identified damage zones are shown by key locations examined within this study. The model includes linkage damage zones, which are represented by fault splays and abutting relations observed within the fault network at the Kilve Pill Relay (Fig. 5.1a). Relay ramp damage zones are a specific type of linkage damage zone between two subparallel fault segments dipping in the same direction, and several of these have been studied, like the partly breached relay at Kilve (Fig. 5.1a) or the seemingly soft linked relay structures within the fault tip zone at Lilstock (Fig. 6.2). This fault zone has been interpreted to be a bifurcation tip zone, thus also representing an up-dip

tip. Tip damage zones representing both mode II and mode III slip, where seen at East Quantocks Head (Fig. 6.6, 6.7), while wall damage zones related to kinematic slip of growing faults were seen generally along mature faults (Fig. 5.1a). These different types of damage zones will now be discussed in the light of their formation, geometry, damage distribution and importance in normal fault networks.

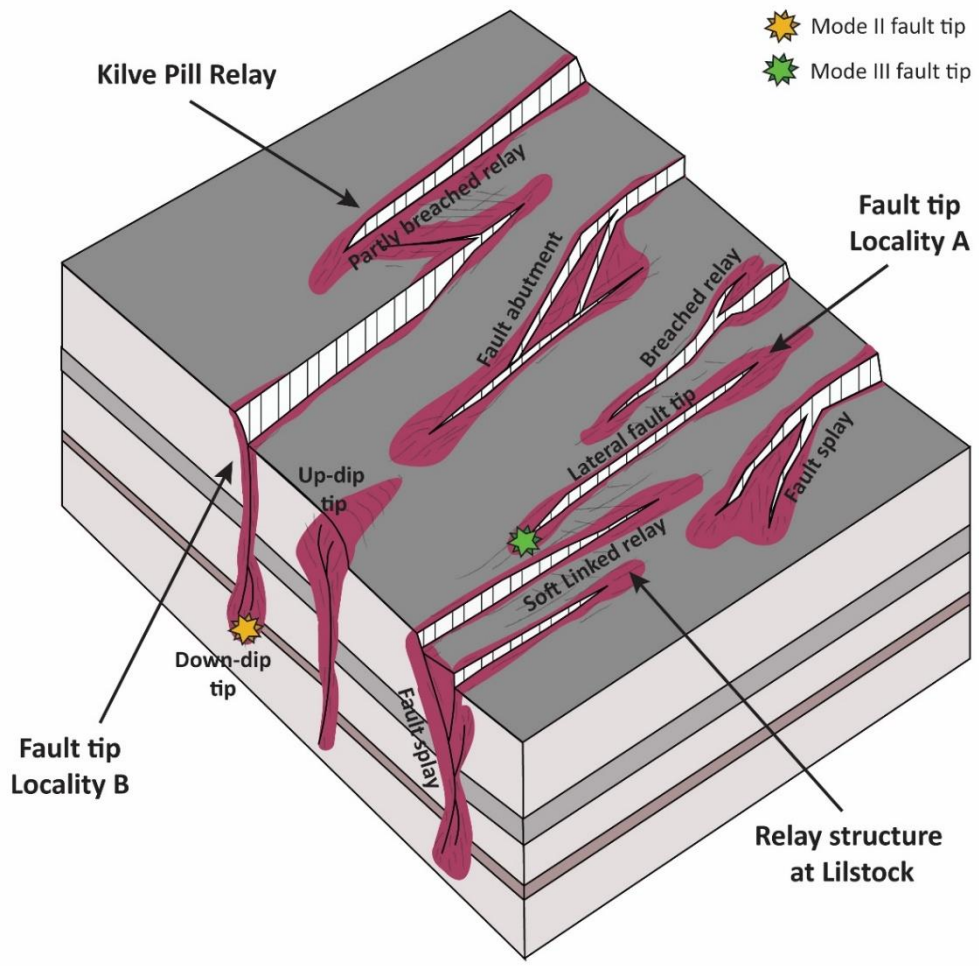

Figure 7.1: Conceptual model of normal fault network showing main structural features examined during this study, labelled with key locations. At Kilve, a structure representing a stage 3 relay ramp (sensu Peacock and Sanderson 1991) was studied. At Lilstock, a normal fault array with en-échelon geometry containing several overlap zones was examined, interpreted as a bifurcating tip zone with hard linkage of fault segments through fault splays in the sub-surface. This represents an up-dip fault tip. The fault tip damage zones (locality A and B) observed at East Quantocks Head may represent a lateral tip and a down-dip tip, respectively. Locality A also represents a mode III tip, and locality B a mixed mode tip. Fault interactions as fault splays and fault abutments are other features of interest, showing increased structural complexity in associated wider damage zones. The extent of the damage zones is marked in red in the model.

7.2 Development of veining around faults

In the limestone beds of the Somerset coast, the brittle wall rock damage is mainly represented by calcite veins, and secondary faults. The veins are oriented normal to N-S extension (even when faults are not) and only located close to, or in association with faults, indicating that they are part of the fault damage zones. As faults die out laterally, veins form tip damage zones continuing the fault trace laterally. The association of faults and veins has been widely recognised, for example Peacock and Sanderson (1992) suggested that the faults initiated as veins (or later mineralized open fractures), and Roberts et al. (1999) suggested that dilation of veins are expected as growing faults propagate. Putz-Perrier and Sanderson (2008a) quantified both veins and faults at the Somerset coast, to investigate the spatial distribution of these structures on a regional scale. They found that vein strain is highly localized, which supports the interpretation made during this study, that veining in the Kilve area is related to fault damage zones, and therefore localized around, and close to faults. This association between faults and veins is seen in the damage maps produced of the relay zone at Kilve (Fig. 5.8), the damage zone map of the relay ramp at Lilstock (6.3a), and in the fault tip studies at East Quantocks Head (Fig. 6.6, 6.7).

As the study of Putz-Perrier and Sanderson (2008a) was regional, veining around single faults was not their main focus. Valuable information can be added to this by implementing vein data from this study, where damage has been quantified (Fig. 6.9) and documented spatially around single fault traces (Fig. 6.6, 6.7). To illustrate main changes of distribution of deformation and vein characteristics along a single fault trace, a model in three stages is produced (Fig. 7.2). Stage 1 corresponds to the typical high strain area of fault tips described in other literature (e.g. McGrath and Davison 1995; Kim et al. 2004), referred to as the process zone (sensu Scholz et al. 1993) where fault propagation leads to the formation of a tip damage zone. Veins show planar geometries, not affected by the slight folding of the bed. Vein apertures are small, and the intensity high, producing a wide zone of deformation. In stage 2 fewer and larger veins are distributed close to the growing fault plane, moving into the slip zone of the fault. Veins produced in the tip damage zone now show wedge shaped geometries, and a clear rotation to keep normal to the bedding plane as this folds in a prominent fault propagation fold (Gawthorpe et al. 1997). At stage 3 the fault core has grown large, and the fault is significantly displaced, where slip of the fault produces fault drag (Reches and Eidelman 1995). The damage zone is narrow, and only consists of few extremely

rotated wedge-shaped veins, cross-cut by thinner vertical, fault parallel veins. These vertical veins are interpreted to be related to the kinematic slip of the fault, and thus part of the wall damage zone. The wedge-shaped veins produced in the process zone of the fault tip (i.e. tip damage) have now been merged into the wall damage of the fault, as the process zone is incorporated into the fault slip zone.

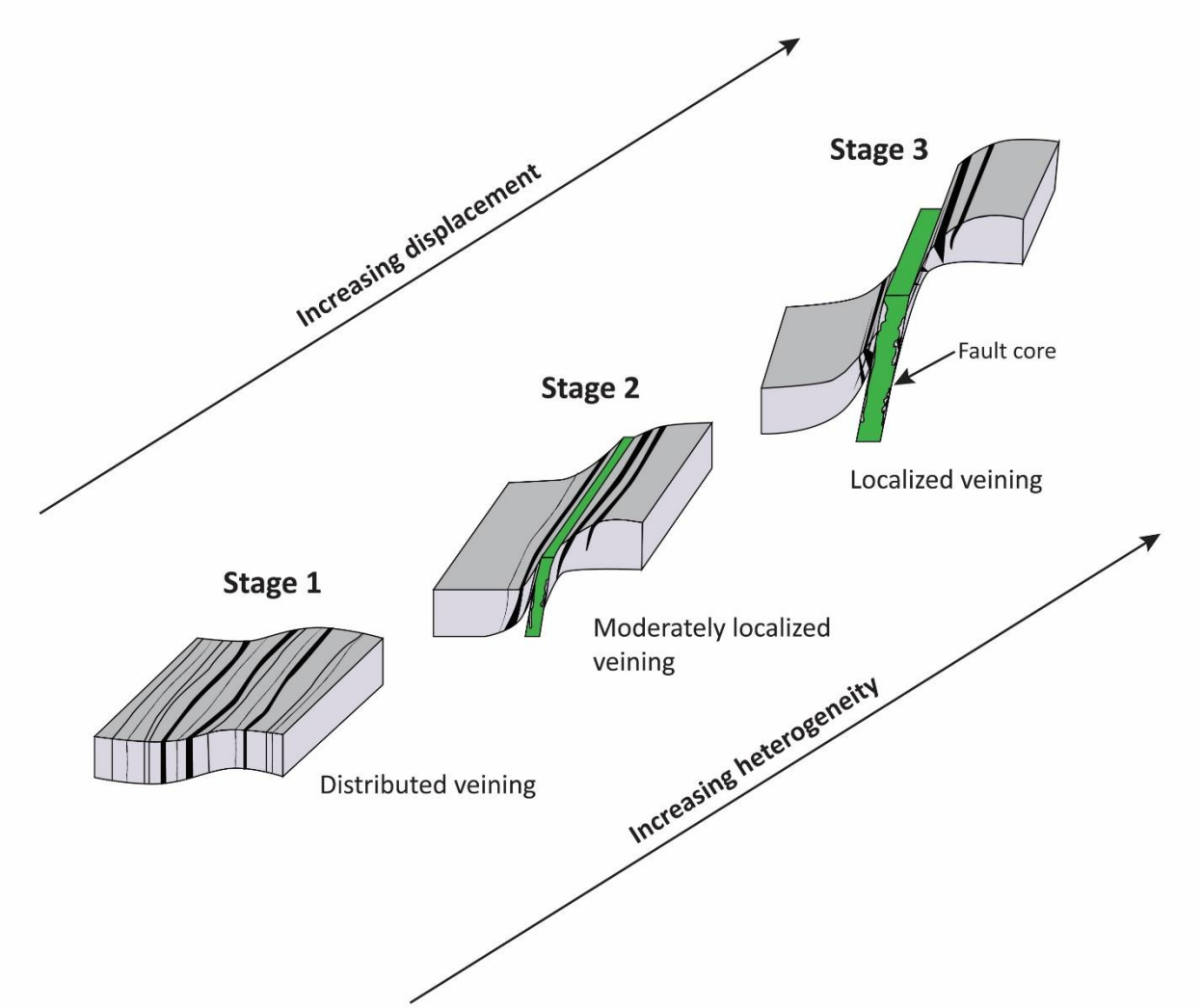

Figure 7.2: Conceptual model that illustrates distribution of veining along strike a normal fault tip observed in limestone bedding. The model shows three stages of deformation associated with fault tip damage zones, increasing both displacement and vein heterogeneity from stage 1 - 3. The stages include: (1) numerous veins widely distributed within a broad damage zone; (2) small displacement creating a fault, while remining veins are more localized around the fault core (green); (3) slip increases, creating drag along the fault plane, while even thicker wedge-shaped and rotated veins are localized around the fault core. These are cross-cut by vertical, plane parallel veins. Bedding has a slight monocline geometry in the process zone (stage 1) growing into stage 2, replaced by fault drag in stage 3.

These stages illustrate a change from distributed to localized deformation moving from the process zone to the slip zone of the fault. This is supported by transect B3 (stage 1) and B7 (stage 3) in Figure 6.9, where the spatial heterogeneity of aperture (V_a) changes from 0.31 – 0.90 respectively. This is related to the narrowing of the damage zone, and the concentration of deformation on few structures moving from stage 1 to 3, which suggest that the localization of deformation might be related to maturity of the fault, connecting change in distribution of deformation to fault growth.
The model also suggests that deformation produced in the process zone has a stronger control on the geometry of the damage zone than kinematic slip of the fault, as damage zone width is found to decrease with increasing displacement. This observation contradicts what would be expected in generic wall damage models, where a power-law relationship between damage zone width and displacement is found (e.g. Knott 1994; Knott et al. 1996; Beach et al. 1999; Shipton and Cowie 2001; Childs et al. 2009). These studies predict that as a fault grows, the stress building up on the fault plane will increase proportionally with fault size, creating a wider damage zone (Cowie and Scholz 1992b; Shipton and Cowie 2001). By implying that damage zone development in the study area is mainly controlled by deformation in fault tip process zones and areas of fault interaction rather than in slip zones, this contradicting relation can be explained as the studies mentioned only focuses on wall damage zones. There might be a scaling relationship between wall damage zones and displacement, but this study shows that there are not a relationship between tip/linkage damage zones and displacement. Scatter plots of displacement against vein strain (Fig. 5.9a) and vein intensity (Fig. 5.9b) from the relay study at Kilve back this up, showing no trend between veining and displacement. This indicates that veining is not specifically related to kinematic slip of faults, suggesting that slip is of minor importance regarding damage zone development in the fault network, which rather is controlled by the location of fault tip zones and fault interactions.

Still, this does not explain why damage associated with the tip damage zone seems to disappear along the fault trace as the fault gains displacement (stage 3, Fig.7.2). This might be explained by the process of fault drag, where parts of wall rock (containing damage related structures) are dragged into the fault core (Rykkelid and Fossen 2002). The interbedded succession with alternating limestone and shale layers where these faults are studied consist of two very different layer properties, the shales being much less competent than the limestones. This alternation in rock strength over generally thin layers, can make it easier for the rock in close relation to the fault plane breaking, and becoming a part of it (Schöpfer et al. 2007). Interlayer slip or flow may cause

the less competent shales to rearrange and be pushed away from the high stress zone during flexural folding associated with friction on the fault plane. This may leave the limestone beds as thin slices of easily trapped rock (e.g. Donath and Parker 1964; Behzadi and Dubey 1980). The observed damage zone geometry also implies that the plane of the fault must be smooth, so that new damage (i.e. wall damage) will not develop extensively due to kinematic stress concentrations. Smooth fault planes are mostly associated with evolved faults (Wibberley et al. 2008), indicating that the fault has matured at this stage. This suggests that damage zone formation is not only controlled by the stress system (e.g. Kim et al. 2000; Nicol et al. 2002; Berg and Skar 2005), rheological properties of the rock (e.g. McGrath and Davison 1995; Skar et al. 2016) and fault interactions and segmentation (e.g. Walsh et al. 2003; Fossen et al. 2005; Childs et al. 2009), but also by irregularities of the fault plane (e.g. Childs et al. 2009) and maturity of the fault (e.g. Shipton and Cowie 2001). No defining trends between fault displacement and veining (Fig. 5.9a-b) indicate that veining is not proportional to kinematic slip of the fault, a scenario that is most likely on a smooth planar fault plane.

7.3 Partitioning of deformation in fault linkage zones

S_S-profiles made over the fault zones at Kilve (Fig. 5.4b) and the (d-x) profiles of the fault zone at Lilstock (Fig. 6.1b) highlight the distribution and partitioning of deformation along strike of faults that are interacting or linking. Earlier, this approach has been applied to investigate trends between the stage of evolution of a relay structure and the geometry of its (d-x) profile, and four stages of relay growth are proposed (Peacock and Sanderson 1991) (Fig. 2.4). A novel approach in this study was not only mapping displacement of the relay bounding faults, as seen in most earlier studies (e.g. Peacock and Sanderson 1991; Huggins et al. 1995; Childs et al. 1995; Willemse 1997; Walsh et al. 2003; Long and Imber 2011; Nixon et al. 2014a) but also quantifying and mapping displacement of damage related faults. Both examples from Kilve (Fig. 5.4b) and Lilstock (Fig 6.1b) indicate a high in displacement contribution of damage related structures in linkage areas of relay bounding faults, demonstrating that damage structures account for the displacement deficit on the relay bounding faults within the zone of overlap.

The two relay bounding faults FS1 and FS2 of the Kilve Pill Relay (Fig. 5.4a) are interpreted as a linkage zone because they show interaction by a decrease in displacement as they approach each

other (e.g. Willemse 1997; Walsh et al. 2003), corresponding with a rapid decrease in gradient of their stratigraphic separation-profile (Fig. 5.4b) as they enter the fault overlap zone (e.g. Peacock and Sanderson 1991). The contribution of damage related faults is notable ~45 % to the overall deformation within the relay zone. This corresponds well with former studies implying that linkage damage zones between fault segments are areas of intensified deformation (c.f. Kim et al. 2004; Fossen et al. 2005; Kim and Sanderson 2010). This illustrates that rapid decrease in displacement seen in overlap zones of faults is corrected for by the presence of damage related structures. It is thus reasonable to suggest that when such a profile is produced (e.g. from data gathered from a seismic survey, where only major faults are within the scale range), small-scale damage related structures would be expected in the area where the displacement minima is seen. The expected correction would produce a smoother cumulative profile with an overall convex-up bell shape. This is supported by Peacock and Sanderson (1991), that suggest that anomalies in (d-x) profiles that do not match the bell-shaped profile of a traditional isolated fault (Walsh and Watterson 1989), may be corrected for by smaller brittle structures or ductile deformation such as bed rotation and folding.

The displacement-distance profile of the western part of the fault zone at Lilstock shows a displacement asymmetry (Fig. 6.1c), where maximum displacement, as well as the fault segment lengths, decrease to the west. This is because the profile represents the tip of a fault, and the rest of the profile is not seen. Hard linkage is also observed in cross-section through a synthetic splay between FN2 and FN3 (Fig. 6.1d), even though no clear linkage is observed on the bedding plane (Fig.6.1b). The fault array is interpreted to be a bifurcating tip zone illustrating that faults are discontinuous and segmented in three-dimensions. High resolution 3-D seismic surveys have shown that normal fault segments that appear soft linked in plan-view, may be linked in the sub-surface along branch lines (Childs et al. 1995; Walsh et al. 1999) or branch points (Childs et al. 1995), supporting this interpretation. It has also been argued that linkage in the sub-surface can be detected using the observation of displacement distributions. Soliva et al. (2008) tested this by using both field data and 3-D numerical modeling and found striking similarities between the two, and thus proposed that displacement gradient asymmetry between relay bounding faults may indicate fault breaching at depth. They present a profile of fault segments from Nigüelas, Spain (Fig. 7.3a), which shows a similar displacement asymmetry to the en-échelon segments observed at Lilstock (Fig. 7.3b). Since hard linkage is physically observed between fault segments within

this array, it represents a positive test of the assumptions of Soliva et al. (2008), strengthening their hypothesis.

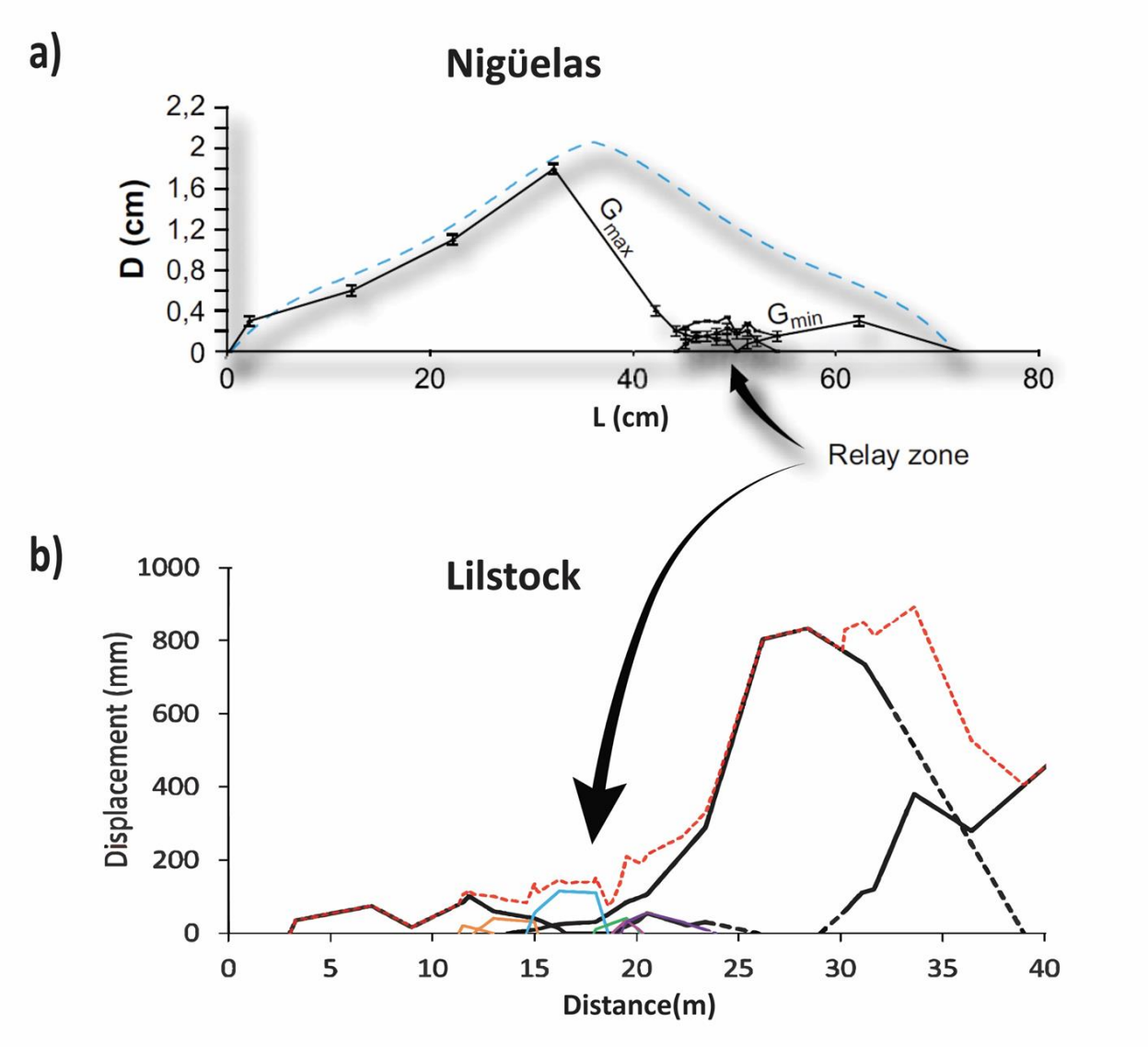

Figure 7.3: Comparing (d-x) profile of Nigüelas fault zone, Spain (a) from Soliva et al. (2008), with profile made from the Lilstock fault zone during this study (b). Both profiles show asymmetry in displacement of the two relay bounding fault segments, which can indicate hard linkage in the sub-surface.

7.4 Spatial heterogeneity of deformation at different scales

Examining heterogeneity of deformation at different scales shows similar results through the whole study; that heterogeneity generally increases moving away from damage zones. The large-scale example is represented by heterogeneity plots produced over faults within the linkage zone at Kilve (Fig 5.5), while a small-scale example is given from the fault tip zone at locality B at East Quantocks Head (Fig. 6.9), where deformation on the main fault plane and damage related veining is included.

The spatial heterogeneity decreases moving from outside, to inside the overlap zone of the relay at Kilve (e.g. V_{Ss} decreases from 0.80 to 0.33, Fig. 5.5b). This indicates that deformation is localized primarily on the main fault structures (i.e. relay bounding faults and domino faults) outside the overlap zone. Moving into the overlap zone, deformation becomes distributed between numerous structures, mostly represented by damage related faulting. This agrees with observations by Nixon et al. (2014b), where the distribution of strain contributed by minor faulting around the major Rangitaki Fault, NZ, was studied. They found that the fault network changes character along strike, where deformation is localized on the Rangitaki Fault where it shows large displacements, exchanged by distributed faulting where minor faults dominate. Nixon et al. (2014b) link this change with the establishment of more segment linkage, maturing the fault zone with breaching of segment overlap zones. This explanation can be transferred to Kilve, where deformation is localized in areas where only main faults contribute to the total strain, which may represent a mature stage of fault evolution (e.g. Childs et al. 1995; Nicol et al. 2016). Whereas the fault arrays within the overlap zone show homogeneously distributed deformation over numerous smaller structures, and thus may represent a less mature stage of fault system evolution (e.g. Meyer et al. 2002; Walsh et al. 2002; Childs et al. 2003).

Both fault tip studies at East Quantocks Head (section 6.2 and 6.3) and the fault tip model presented in section 7.2 (Fig. 7.2) shows that damage becomes more localized moving away from the tip damage zone of a fault. Figure 7.2 illustrates distributed deformation in the tip damage zone (stage 1) by numerous small veins in a wide zone, changing gradually to localized deformation represented by a distinct fault plane with displacement (stage 3). This indicates that the distribution of deformation changes from distributed to localized with increased slip of the fault, which can be

related to fault growth. This is in agreement with Nixon et al. (2014b) where they argue that localization of strain to main fault segments of a fault zone is a progressive process (Walsh et al. 2003; Cowie et al. 2005), that happens gradually by the transfer of fault activity from surrounding structures onto main fault segments (Walsh et al. 2003). This is seen in the tip zone study as deformation transferred from veining and folding in the process zone, to the dominant fault plane in the slip zone.

These results suggest that spatial distribution of deformation is variable within large-scale fault networks and along single fault traces, but that they show a similarity of increased heterogeneity moving away from damage zones that do not seem to be scale dependent. The quantitative measure of heterogeneity along a single fault trace is a novel observation of this study, adding valuable knowledge on deformation distribution on a small-scale, to former studies of fault and damage zone development (e.g. Knott 1994; Beach et al. 1999; Shipton and Cowie 2001; Choi et al. 2016). The findings further suggest that distribution variation is mainly controlled by localization at fault interaction zones (e.g. Cartwright et al. 1995; Fossen et al. 2005) and possibly maturation of the fault (e.g. Du Bernard et al. 2002; Childs et al. 2009).

7.5 Implications

7.5.1 The importance of scaling

Different interaction zones of faults have been identified and studied in this thesis, and the general relationship that is seen for all of them, is that they show a significant contribution of smaller damage related structures. The fault network studied within the mesoscale (hundreds of meters) relay structure at Kilve (Fig. 5.1a) consist of a network of normal faults with lengths and vertical sizes generally < 10 m, representing linkage damage of the relay structure. The en-échelon fault array at Lilstock (tens of meters) (Fig. 6.1b) produces linkage damage between overlapping segments, where smaller faults are created. Both locations also show veining associated with damage zones of single faults, picturing a complex network of different scale structures within fault interaction zones. Most of the observed damage is faults and veins under seismic resolution, that consequently would be missed in a seismic survey (Rotevatn and Fossen 2011).

Damage zones of single faults within the studied limestone bedding are mainly represented by calcite veining, which represent small-scale deformation (section 5.3). Veins were quantified and represented in contour maps (Fig. 5.8b-c) from the Kilve Pill Relay displaying high vein intensities and strain located within areas of fault interaction and in fault tips. These areas constitute the widest damage zones (Fig. 5.8a), as isolated faults show generally low vein intensities and strain in narrow damage zones. Spatial heterogeneity measures (Fig. 5.5) also show that the distribution of deformation increases moving into the relay zone, where fault frequencies and fault interactions increases. This indicates that there is a relationship between intensified deformation, which implies an increase in small-scale structures, and increased zones of fault interaction.

These observations are in agreement with Fossen et al. (2005), which examined outcrop examples of fault interactions, to document and predict a quantitative relationship between sub-seismic deformation and patterns of fault interaction. They found that the complexity of areas of fault interaction is generally higher than for a single isolated fault. Wider damage zones are produced in these areas, and fracture intensity and pattern complexity increase as well, as observed and presented in this study (Fig. 5.8). Additionally, the results are supported by former documentation of deformation heterogeneity (e.g. Putz-Perrier and Sanderson 2008a, 2008b; Nixon et al. 2011; Nixon et al. 2014b) which provide implications that damage zones show more complexity than single isolated faults, which correspond to areas of increased sub-seismic fracturing (Fossen et al. 2005).

Due to the restricted resolution of seismic surveys (vertical and horizontal resolution > 10 m (e.g. Enge et al. 2007)), outcrop analogues are used so that geologists can observe and better understand structures that are under seismic resolution. Nixon et al. (2012) actually tested how different parameters in fracture networks are effected when studied at different resolution, and found that spatial arrangement, topology and distribution of strain all vary with resolution. This emphasizes that structures of different scales need to be investigated, to capture their influence and contribution to the overall system.

The study area of this thesis provides an analogue of a normal fault network in an interbedded limestone-shale succession, where structures of three orders of magnitude can be studied in relation to each other, and where the aspect of their relative spatial distribution in the network is easily determined. It includes structures like the relay bounding faults FS1 and FS2 of the Kilve

Pill Relay (Fig. 5.1a), which are over seismic resolution, small-scale faults under seismic resolution represented by damage related faults inside the relay (Fig. 5.1a), and veining associated with fault damage zones (Fig. 5.7, 5.8b-c). This provides an opportunity to investigate the relationship between different scale structures both over and under seismic resolution in detail, and the study also offers a quantitative description of the partitioning of strain between them (Fig. 5.10.b). The contribution to strain from each structure shows that main structural features (large faults) contribute to most of the strain, but that contribution from smaller damage related faults actually is significant, especially within areas of fault interaction. This suggests that contribution of strain by damage related structures are important to consider in strain analysis.

7.5.2 Structural controls of fluid flow in normal fault networks

The fact that most of the documented damage related structures in this study are under seismic resolution, and consequently would be missed in a seismic survey, is an important observation as structures like these might have implications on rock permeability and trap integrity (Gartrell et al. 2004). Damage zones may provide implications for fluid flow, as fracture systems related to damage zones can represent potential barriers or conduits to fluid flow (e.g. Bense and Person 2006; Rotevatn et al. 2007). The flow possibilities within the fracture networks at Somerset at present are low or absent, due to mineralization of the fractures system. This might have been another case at the time of faulting, when fractures may have been open. The fracture system is thus only an analog of fracture evolution within damage zones, but given that the fracture system works as an open conduit, knowledge on its evolution and extent is valuable.

The vein strain contour map of the Kilve Pill Relay (Fig. 5.8c) is based on fracture apertures, that show an increase of dilation in areas of fault interaction and fault tip zones. This indicates that these areas are high strain zones of increased extension, which could have had an increased control on potential fluid flow before mineralization. Studies that are field based, or uses flow models show evidence that fluid flow is strongly controlled by fracture apertures, intersection between fractures, and the development of damage zones (Leckenby et al. 2005; Kim and Sanderson 2010).

Damage zones have been studied widely regarding their controlling powers on fluid flow (e.g. Huyakorn et al. 1983; Curewitz and Karson 1997; Jiang et al. 1997; Gartrell et al. 2004; Fossen et al. 2005; Bense and Person 2006; Rotevatn et al. 2007), and especially in the petroleum industry

knowledge on fracturing in damage zones is important, regarding the huge influence choices made on often restricted data can have economically. Provided that damage related small-scale structures impede fluid flow, Fossen et al. (2005) discuss that areas of fault interaction should be of concern in a hydrocarbon production situation. With findings of this study a supplement to important knowledge regarding this topic is applied, by adding a quantitative measure on the spatial distribution of damage related structures within complex interaction zones (Fig. 5.8b-c). From a reservoir perspective, this knowledge can be used to develop a more robust model of fluid flow within normal fault networks where linkage damage zones are present, that can decrease uncertainties around the flow possibilities in these zones.

8 Conclusions and further work

8.1 Conclusions

Using traditional field data combined with interpretation of aerial photographs and analysis in ArcGIS the damage zones and distribution of deformation associated with relays and tip zones of normal faults were assessed at a range of scales. The field work was performed in the alternating limestone-shale successions at the Somerset coast, UK, more specifically at Kilve, Lilstock and East Quantocks Head. The study includes detailed fault mapping based on stratigraphic separations and displacements, and documentation of associated damage zones by mapping damage related structures (i.e. small faults and veins). Deformation was thus quantified at different scales to investigate partitioning of strain and variation of deformation within damage zones of normal faults. Data were further analysed using ArcGIS, together with spatial heterogeneity analysis and displacement profiles. Conclusions drawn from the produced data assembly can be divided into three sections, starting with general damage zone characteristics, leading to a closer description of damage zones of relay structures and fault tips.

8.1.1 General damage zone characteristics within a normal fault network

- Calcite veins sub parallel to fault orientations only located close to, and in association with faults within the limestone beds of the Somerset coast, indicating that veining is mainly related to fault damage zones. The extent of veining moving normal from the fault trace thus defines damage zone widths of this study.
- Damage zones are widest in areas of fault interaction (i.e. relay zones, fault splays, cross-cutting or abutting fault terminations) and in fault tips, and generally narrow along mature, planar faults.
- Damage zone contour maps show high values of vein intensity (~11.5 m^{-1} – 22.5 m^{-1}) at fault interactions, while vein strain (% extension) shows high values (~23 % - 46.1 %) at fault interactions and fault tips. Strain is thus localized within linkage damage zones and tip damage zones, representing areas of high local stress.

- Analysis of spatial heterogeneity of deformation over both relay structures and fault tips show that deformation changes from distributed to localized moving out from the damage zone. This is explained by a decrease in structure intensity, localizing deformation on a few main structures. Localization of deformation may thus be related to maturity of the studied system.
- How to define damage zones depends on what classification you use, the chosen scale range at which observations are done, and how the studied fault system is defined. This is because different groups of damage zones can overlap and co-exist.

8.1.2 Damage zones of relay structures

- Ss-distance profiles show overlap between normal faults (i.e. relay structures) as a displacement minima, while damage related structures contribute to a vast amount of the overall displacement (~45 %), localized in the overlap zone. Damage related structures thus correct for the separation minima in the profile representing relay bounding faults, maintaining strain coherency. This is illustrated by a cumulative profile moving closer to a traditional convex-up profile of an isolated fault.
- Brittle structures are grouped into three types after their scale range; relay bounding faults, damage related faults and veins. Calculated applied total extensional strain shows an overall increase within the relay zone, caused by the appearance of damage related structures. An overall strain compatibility is maintained over the relay, even though the partitioning of different structures changes through the zone. Relay bounding faults contribute more outside the overlap zone, and damage faults contribute more inside the overlap zone.
- Asymmetry in the partitioning of deformation (i.e. displacement) between fault segments that are observed in plane-view as soft linked, may indicated hard linkage in the sub-surface. This might occur in bifurcating tip zones, and breaching at depth might be detected in an asymmetric displacement-distance profile of the overlapping faults in plan-view.

8.1.3 Damage zones of fault tips

- Process zones of fault tips are characterized by wide tip damage zones where vein intensities are high and apertures low. Fault propagation folding also accommodate to the total

deformation, and create wedge-shaped geometries of veins that rotate with the fold. Moving along strike, slip increases on the fault and drag of bedding is prominent.

- The damage zone widths decrease progressively with increased displacement. This is possibly caused by the destruction of the damage zone as a fault matures, where the tip damage zone is implemented in the slip zone, and possibly dragged into the active fault plane. New slip related damage (i.e. wall damage) is not prominent due to the observed narrow damage zone width, that might be caused of smoothening of the fault plane as the fault grows.

By constructing a detailed fault map displaying spatial variations of large-scale fault geometry, fault interactions and fault displacement, variations in both fault network geometries and deformation has been captured. By supplementing this with field observations documenting small-scale veining associated with fault damage zones, a quantification of distribution of brittle deformation at different scales has been performed in these zones. From this a more robust structural model regarding distribution of deformation within fault damage zones can be constructed, where the contribution of damage structures is proven to be of importance to the overall deformation of the fault system. They contribute to total extensional strain, and are seen as the reason for maintained strain coherency in zones of fault interaction. Similarities seen regarding distribution of deformation within fault networks and for individual small faults suggest that localization of deformation moving away from damage zones also happens at the scale of small faults. This knowledge can be applied with interpretation of fault structures in seismic data, as the same characteristics of deformation distribution is observed at different scales.

8.2 Further work

This study provides a quantified documentation on spatial distributions of brittle structures both in a fault network setting, and in a single fault setting. These are combined into a model of fault and damage zone growth that actually describes the contribution of deformation of different brittle structures during this evolution. Building out from this, there are several questions and avenues for further work, and some suggestions are listed below:

- A study of multiple relays that represents different stages of evolution can give a more robust implication on what impact damage related structures actually have on the total extensional

strain within overlap zones, and if there is a trend following the evolution of a relay. This type of study could also look for trends between different fault interactions based on their partitioning to overall brittle strain distribution.

- During the spring 2016 some seismic lines were taken across the relay structure west of the Kilve Pill Box, and an interpretation of these would shed a light on how the faults, that in this study only are observed in plan-view, actually occur in the vertical section. Vertical fault interactions can be studied, and a three-dimensional model of the relay ramp can be produced. A growth model of the relay is also something that would be interesting to create, where data from this study on damage zone evolution can be implemented.
- Findings of spatial distribution of damage from this study can be implemented in fluid flow simulation, where fault tips and areas of fault interaction can be tested in terms of their presence as conduits or barriers to fluid flow.
- This study provides the first attempt on using displacement-distance profiles to illustrate distribution of damage related deformation along strike faults, in comparison to only focusing on the relay bounding faults as done in earlier literature. This is a method that should be further tested.
- The use of aerial photographs to interpret stratigraphic separations of an area has also created an opportunity to do a lot of work on mapping displacement without the necessity of travelling out in field and do the measurements by hand, which can be both time consuming and expensive. This method can thus be applied to other fields and areas of interest.

9 References

Aydin, A., 2000. Fractures, faults, and hydrocarbon entrapment, migration and flow. *Marine and petroleum geology* **17**, 797-814.

Aydin, A., & Schultz, R. A., 1990. Effect of mechanical interaction on the development of strike-slip faults with echelon patterns. *Journal of Structural Geology* **12**, 123-129.

Bastesen, E., & Braathen, A., 2010. Extensional faults in fine grained carbonates–analysis of fault core lithology and thickness–displacement relationships. *Journal of Structural Geology* **32**, 1609-1628.

Bastesen, E., & Rotevatn, A., 2012. Evolution and structural style of relay zones in layered limestone–shale sequences: insights from the Hammam Faraun Fault Block, Suez rift, Egypt. *Journal of the Geological Society* **169**, 477-488.

Beach, A., Welbon, A. I., Brockbank, P. J., & McCallum, J. E., 1999. Reservoir damage around faults: outcrop examples from the Suez rift. *Petroleum Geoscience* **5**, 109-116.

Behzadi, H., & Dubey, A., 1980. Variation of interlayer slip in space and time during flexural folding. *Journal of Structural Geology* **2**, 453-457.

Bense, V., & Person, M., 2006. Faults as conduit-barrier systems to fluid flow in siliciclastic sedimentary aquifers. *Water Resources Research* **42**.

Berg, S. S., & Skar, T., 2005. Controls on damage zone asymmetry of a normal fault zone: outcrop analyses of a segment of the Moab fault, SE Utah. *Journal of Structural Geology* **27**, 1803-1822.

Bonnet, E., Bour, O., Odling, N. E., Davy, P., Main, I., Cowie, P., & Berkowitz, B., 2001. Scaling of fracture systems in geological media. *Reviews of geophysics* **39**, 347-383.

Brooks, M., Trayner, P. M., & Trimble, T. J., 1988. Mesozoic reactivation of Variscan thrusting in the Bristol Channel area, UK. *Journal of the Geological Society* **145**, 439-444.

Caine, J. S., Evans, J. P., & Forster, C. B., 1996. Fault zone architecture and permeability structure. *Geology* **24**, 1025-1028.

Cartwright, J. A., Trudgill, B. D., & Mansfield, C. S., 1995. Fault growth by segment linkage: an explanation for scatter in maximum displacement and trace length data from the Canyonlands Grabens of SE Utah. *Journal of Structural Geology* **17**, 1319-1326.

Chadwick, R., 1986. Extension tectonics in the Wessex Basin, southern England. *Journal of the Geological Society* **143**, 465-488.

Chester, F., & Logan, J., 1986. Implications for mechanical properties of brittle faults from observations of the Punchbowl fault zone, California. *Pure and Applied Geophysics* **124**, 79-106.

Chester, F. M., Evans, J. P., & Biegel, R. L., 1993. Internal structure and weakening mechanisms of the San Andreas fault. *Journal of Geophysical Research: Solid Earth* **98**, 771-786.

Childs, C., Manzocchi, T., Walsh, J. J., Bonson, C. G., Nicol, A., & Schöpfer, M. P., 2009. A geometric model of fault zone and fault rock thickness variations. *Journal of Structural Geology* **31**, 117-127.

Childs, C., Nicol, A., Walsh, J. J., & Watterson, J., 1996a. Growth of vertically segmented normal faults. *Journal of Structural Geology* **18**, 1389-1397.

Childs, C., Nicol, A., Walsh, J. J., & Watterson, J., 2003. The growth and propagation of synsedimentary faults. *Journal of Structural Geology* **25**, 633-648.

Childs, C., Watterson, J., & Walsh, J., 1995. Fault overlap zones within developing normal fault systems. *Journal of the Geological Society* **152**, 535-549.

Childs, C., Watterson, J., & Walsh, J., 1996b. A model for the structure and development of fault zones. *Journal of the Geological Society* **153**, 337-340.

Choi, J.-H., Edwards, P., Ko, K., & Kim, Y.-S., 2016. Definition and classification of fault damage zones: a review and a new methodological approach. *Earth-Science Reviews* **152**, 70-87.

Cowie, P. A., & Scholz, C. H., 1992a. Physical explanation for the displacement-length relationship of faults using a post-yield fracture mechanics model. *Journal of Structural Geology* **14**, 1133-1148.

Cowie, P. A., & Scholz, C. H., 1992b. Growth of faults by accumulation of seismic slip. *Journal of Geophysical Research: Solid Earth* **97**, 11085-11095.

Cowie, P. A., & Scholz, C. H., 1992c. Displacement-length scaling relationship for faults: data synthesis and discussion. *Journal of Structural Geology* **14**, 1149-1156.

Cowie, P. A., & Shipton, Z. K., 1998. Fault tip displacement gradients and process zone dimensions. *Journal of Structural Geology* **20**, 983-997.

Cowie, P. A., Underhill, J. R., Behn, M. D., Lin, J., & Gill, C. E., 2005. Spatio-temporal evolution of strain accumulation derived from multi-scale observations of Late Jurassic rifting in the northern North Sea: A critical test of models for lithospheric extension. *Earth and Planetary Science Letters* **234**, 401-419.

Curewitz, D., & Karson, J. A., 1997. Structural settings of hydrothermal outflow: Fracture permeability maintained by fault propagation and interaction. *Journal of Volcanology and Geothermal Research* **79**, 149-168.

Dart, C. J., McClay, K., & Hollings, P. N., 1995. 3D analysis of inverted extensional fault systems, southern Bristol Channel basin, UK. *Geological Society, London, Special Publications* **88**, 393-413.

Donath, F. A., & Parker, R. B., 1964. Folds and folding. *Geological Society of America Bulletin* **75**, 45-62.

Du Bernard, X., Labaume, P., Darcel, C., Davy, P., & Bour, O., 2002. Cataclastic slip band distribution in normal fault damage zones, Nubian sandstones, Suez rift. *Journal of Geophysical Research: Solid Earth* **107**, ETG 6-1 - ETG 6-12.

Enge, H. D., Buckley, S. J., Rotevatn, A., & Howell, J. A., 2007. From outcrop to reservoir simulation model: Workflow and procedures. *Geosphere* **3**, 469-490.

Engelder, T., 1987. Joints and shear fractures in rock. *In: B.K. Atkinson (eds) Fracture mechanics of rock, Academic Press*, 27-69.

Engelder, T., & Peacock, D. C., 2001. Joint development normal to regional compression during flexural-flow folding: the Lilstock buttress anticline, Somerset, England. *Journal of Structural Geology* **23**, 259-277.

Faulkner, D., Mitchell, T., Jensen, E., & Cembrano, J., 2011. Scaling of fault damage zones with displacement and the implications for fault growth processes. *Journal of Geophysical Research: Solid Earth* **116**.

Fossen, H., Johansen, T. E. S., Hesthammer, J., & Rotevatn, A., 2005. Fault interaction in porous sandstone and implications for reservoir management; examples from southern Utah. *AAPG Bulletin* **89**, 1593-1606.

Fossen, H., & Rotevatn, A., 2016. Fault linkage and relay structures in extensional settings—A review. *Earth-Science Reviews* **154**, 14-28.

Gamond, J., 1987. Bridge structures as sense of displacement criteria in brittle fault zones. *Journal of Structural Geology* **9**, 609-620.

Gartrell, A., Zhang, Y., Lisk, M., & Dewhurst, D., 2004. Fault intersections as critical hydrocarbon leakage zones: integrated field study and numerical modelling of an example from the Timor Sea, Australia. *Marine and petroleum geology* **21**, 1165-1179.

Gawthorpe, R. L., Sharp, I., Underhill, J. R., & Gupta, S., 1997. Linked sequence stratigraphic and structural evolution of propagating normal faults. *Geology* **25**, 795-798.

Glen, R. A., Hancock, P. L., & Whittaker, A., 2005. Basin inversion by distributed deformation: the southern margin of the Bristol Channel Basin, England. *Journal of Structural Geology* **27**, 2113-2135.

Griffiths, P., 1980. Box-fault systems and ramps: atypical associations of structures from the eastern shoulder of the Kenya Rift. *Geological Magazine* **117**, 579-586.

Gudmundsson, A., Simmenes, T. H., Larsen, B., & Philipp, S. L., 2010. Effects of internal structure and local stresses on fracture propagation, deflection, and arrest in fault zones. *Journal of Structural Geology* **32**, 1643-1655.

Hemelsdaël, R., & Ford, M., 2016. Relay zone evolution: a history of repeated fault propagation and linkage, central Corinth rift, Greece. *Basin Research* **28**, 34-56.

Hesthammer, J., & Fossen, H., 1998. The use of dipmeter data to constrain the structural geology of the Gullfaks Field, northern North Sea. *Marine and petroleum geology* **15**, 549-573.

Huggins, P., Watterson, J., Walsh, J., & Childs, C., 1995. Relay zone geometry and displacement transfer between normal faults recorded in coal-mine plans. *Journal of Structural Geology* **17**, 1741-1755.

Huyakorn, P. S., Lester, B. H., & Faust, C. R., 1983. Finite element techniques for modeling groundwater flow in fractured aquifers. *Water Resources Research* **19**, 1019-1035.

Imber, J., Tuckwell, G., Childs, C., Walsh, J., Manzocchi, T., Heath, A., Bonson, C., & Strand, J., 2004. Three-dimensional distinct element modelling of relay growth and breaching along normal faults. *Journal of Structural Geology* **26**, 1897-1911.

Jiang, Z., Oliver, N. H., Barr, T. D., Power, W. L., & Ord, A., 1997. Numerical modeling of fault-controlled fluid flow in the genesis of tin deposits of the Malage ore field, Gejiu mining district, China. *Economic Geology* **92**, 228-247.

Kamerling, P., 1979. The geology and hydrocarbon habitat of the Bristol Channel Basin. *Journal of Petroleum Geology* **2**, 75-93.

Kelly, P., Peacock, D., Sanderson, D., & McGurk, A., 1999. Selective reverse-reactivation of normal faults, and deformation around reverse-reactivated faults in the Mesozoic of the Somerset coast. *Journal of Structural Geology* **21**, 493-509.

Kim, Y.-S., Andrews, J. R., & Sanderson, D. J., 2000. Damage zones around strike-slip fault systems and strike-slip fault evolution, Crackington Haven, southwest England. *Geosciences Journal* **4**, 53-72.

Kim, Y.-S., Peacock, D., & Sanderson, D. J., 2003. Mesoscale strike-slip faults and damage zones at Marsalforn, Gozo Island, Malta. *Journal of Structural Geology* **25**, 793-812.

Kim, Y.-S., Peacock, D. C., & Sanderson, D. J., 2004. Fault damage zones. *Journal of Structural Geology* **26**, 503-517.

Kim, Y.-S., & Sanderson, D. J., 2005. The relationship between displacement and length of faults: a review. *Earth-Science Reviews* **68**, 317-334.

Kim, Y.-S., & Sanderson, D. J., 2010. Inferred fluid flow through fault damage zones based on the observation of stalactites in carbonate caves. *Journal of Structural Geology* **32**, 1305-1316.

Knott, S., 1994. Fault zone thickness versus displacement in the Permo-Triassic sandstones of NW England. *Journal of the Geological Society* **151**, 17-25.

Knott, S. D., Beach, A., Brockbank, P. J., Brown, J. L., McCallum, J. E., & Welbon, A. I., 1996. Spatial and mechanical controls on normal fault populations. *Journal of Structural Geology* **18**, 359-372.

Krantz, R. W., 1988. Multiple fault sets and three-dimensional strain: theory and application. *Journal of Structural Geology* **10**, 225-237.

Larsen, P.-H., 1988. Relay structures in a Lower Permian basement-involved extension system, East Greenland. *Journal of Structural Geology* **10**, 3-8.

Leckenby, R. J., Sanderson, D. J., & Lonergan, L., 2005. Estimating flow heterogeneity in natural fracture systems. *Journal of Volcanology and Geothermal Research* **148**, 116-129.

Lloyd, A. J., Savage, R. J. G., Stride, A. H., & Donovan, D. T., 1973. The geology of the Bristol Channel floor. *Philosphical Transactions of the Royal Society of London* **274A**, 595-626.

Long, J. J., & Imber, J., 2011. Geological controls on fault relay zone scaling. *Journal of Structural Geology* **33**, 1790-1800.

Long, J. J., & Imber, J., 2012. Strain compatibility and fault linkage in relay zones on normal faults. *Journal of Structural Geology* **36**, 16-26.

Loveless, S., Bense, V., & Turner, J., 2011. Fault architecture and deformation processes within poorly lithified rift sediments, Central Greece. *Journal of Structural Geology* **33**, 1554-1568.

Maerten, L., 2000. Variation in slip on intersecting normal faults- Implications for paleostress inversion. *Journal of Geophysical Research* **105**, 553-565.

Martel, S. J., & Boger, W. A., 1998. Geometry and mechanics of secondary fracturing around small three-dimensional faults in granitic rock. *Journal of Geophysical Research: Solid Earth* **103**, 21299-21314.

McGrath, A. G., & Davison, I., 1995. Damage zone geometry around fault tips. *Journal of Structural Geology* **17**, 1011-1024.

Meyer, V., Nicol, A., Childs, C., Walsh, J., & Watterson, J., 2002. Progressive localisation of strain during the evolution of a normal fault population. *Journal of Structural Geology* **24**, 1215-1231.

Morley, C., & Nixon, C., 2016. Topological characteristics of simple and complex normal fault networks. *Journal of Structural Geology* **84**, 68-84.

Muraoka, H., & Kamata, H., 1983. Displacement distribution along minor fault traces. *Journal of Structural Geology* **5**, 483-495.

Myers, R., & Aydin, A., 2004. The evolution of faults formed by shearing across joint zones in sandstone. *Journal of Structural Geology* **26**, 947-966.

Nemcok, M., Gayer, R., & Miliorizos, M., 1995. Structural analysis of the inverted Bristol Channel Basin: implications for the geometry and timing of fracture porosity. *In: Buchanan, J. G. and Buchanan, P. G. (Eds) Basin Inversion. Geological Society Spesial Publication* **88**, 355-392.

Nicol, A., Childs, C., Walsh, J., Manzocchi, T., & Schöpfer, M., 2016. Interactions and growth of faults in an outcrop-scale system. *Geological Society, London, Special Publications* **439.** , SP439. 439.

Nicol, A., Gillespie, P. A., Childs, C., & Walsh, J. J., 2002. Relay zones between mesoscopic thrust faults in layered sedimentary sequences. *Journal of Structural Geology* **24**, 709-727.

Nixon, C., Bull, J. M., & Sanderson, D. J., 2014b. Localized vs distributed deformation associated with the linkage history of an active normal fault, Whakatane Graben, New Zealand. *Journal of Structural Geology* **69**, 266-280.

Nixon, C. W., Sanderson, D. J., & Bull, J. M., 2011. Deformation within a strike-slip fault network at Westward Ho!, Devon UK: Domino vs conjugate faulting. *Journal of Structural Geology* **33**, 833-843.

Nixon, C. W., Sanderson, D. J., & Bull, J. M., 2012. Analysis of a strike-slip fault network using high resolution multibeam bathymetry, offshore NW Devon UK. *Tectonophysics* **541**, 69-80.

Nixon, C. W., Sanderson, D. J., Dee, S. J., Bull, J. M., Humphreys, R. J., & Swanson, M. H., 2014a. Fault interactions and reactivation within a normal-fault network at Milne Point, Alaska. *AAPG Bulletin* **98**, 2081-2107.

Ogata, K., Senger, K., Braathen, A., & Tveranger, J., 2014a. Fracture corridors as seal-bypass systems in siliciclastic reservoir-cap rock successions: Field-based insights from the Jurassic Entrada Formation (SE Utah, USA). *Journal of Structural Geology* **66**, 162-187.

Ogata, K., Senger, K., Braathen, A., Tveranger, J., & Olaussen, S., 2014b. Fracture systems and meso-scale structural patterns in the siliciclastic Mesozoic reservoir-caprock succession of the Longyearbyen CO2 Lab project: implications for geologic CO2 sequestration on Central Spitsbergen, Svalbard. *Norwegian Journal of Geology* **94**, 121-154.

Ogata, K., Senger, K., Braathen, A., Tveranger, J., & Olaussen, S., 2014c. The importance of natural fractures in a tight reservoir for potential CO2 storage: a case study of the upper Triassic–middle Jurassic Kapp Toscana Group (Spitsbergen, Arctic Norway). *Geological Society, London, Special Publications* **374**, 395-415.

Palmer, C. P., 1972. The Lower Lias (Lower Jurassic) between Watchet and Lilstock in North Somerset (United Kingdom). *Newsletters on Stratigraphy* **2**, 1-30.

Peacock, D., 1991. Displacements and segment linkage in strike-slip fault zones. *Journal of Structural Geology* **13**, 1025-1035.

Peacock, D., 2002. Propagation, interaction and linkage in normal fault systems. *Earth-Science Reviews* **58**, 121-142.

Peacock, D., Knipe, R., & Sanderson, D., 2000. Glossary of normal faults. *Journal of Structural Geology* **22**, 291-305.

Peacock, D., Nixon, C., Rotevatn, A., Sanderson, D., & Zuluaga, L., 2016. Glossary of fault and other fracture networks. *Journal of Structural Geology* **92**, 12-29.

Peacock, D., & Sanderson, D., 1991. Displacements, segment linkage and relay ramps in normal fault zones. *Journal of Structural Geology* **13**, 721-733.

Peacock, D., & Sanderson, D., 1992. Effects of layering and anisotropy on fault geometry. *Journal of the Geological Society* **149**, 793-802.

Peacock, D., & Sanderson, D., 1994a. Geometry and development of relay ramps in normal fault systems. *AAPG Bulletin* **78**, 147-165.

Peacock, D., & Sanderson, D., 1994b. Strain and scaling of faults in the chalk at Flamborough Head, UK. *Journal of Structural Geology* **16**, 97-107.

Peacock, D., & Sanderson, D., 1995. Strike-slip relay ramps. *Journal of Structural Geology* **17**, 1351-1360.

Peacock, D., & Sanderson, D., 1996. Effects of propagation rate on displacement variations along faults. *Journal of Structural Geology* **18**, 311-320.

Peacock, D. C. P., 2004. Differences between veins and joints using the example of the Jurassic limestones of Somerset. *Geological Society, London, Special Publications* **231**, 209-221.

Peacock, D. C. P., Nixon, C. W., Rotevatn, A., Sanderson, D. J., & Zuluaga, L. F., 2017. Interacting faults. *Journal of Structural Geology* **97**, 1-22.

Peacock, D. C. P., & Sanderson, D. J., 1999. Deformation history and basin-controlling faults in the Mesozoic sedimentary rocks of the Somerset coast. *Proceedings of the Geologists Association* **110**, 41-52.

Perrin, C., Manighetti, I., & Gaudemer, Y., 2016. Off-fault tip splay networks: A genetic and generic property of faults indicative of their long-term propagation. *Comptes Rendus Geoscience* **348**, 52-60.

Pollard, D., & Segall, P., 1987. Theoretical displacements and stresses near fractures in rock: with applications to faults, joints, veins, dikes, and solution surfaces. *In: B.K. Atkinson (eds) Fracture mechanics of rock, Academic Press* **277**, 277-349.

Pollard, D. D., & Aydin, A., 1988. Progress in understanding jointing over the past century. *Geological Society of America Bulletin* **100**, 1181-1204.

Putz-Perrier, M. W., & Sanderson, D. J., 2008a. Spatial distribution of brittle strain in layered sequences. *Journal of Structural Geology* **30**, 50-64.

Putz-Perrier, M. W., & Sanderson, D. J., 2008b. The distribution of faults and fractures and their importance in accommodating extensional strain at Kimmeridge Bay, Dorset, UK. *Geological Society, London, Special Publications* **299**, 97-111.

Rawnsley, K. D., Peacock, D. C. P., Rives, T., & Petit, J. P., 1998. Joints in the Mesozoic sediments around the Bristol Channel Basin. *Journal of Structural Geology* **20**, 1641-1661.

Reches, Z. e., 1978. Analysis of faulting in three-dimensional strain field. *Tectonophysics* **47**, 109-129.

Reches, Z. e., & Eidelman, A., 1995. Drag along faults. *Tectonophysics* **247**, 145-156.

Roberts, S., Sanderson, D., & Gumiel, P., 1999. Fractal analysis and percolation properties of veins. *Geological Society, London, Special Publications* **155**, 7-16.

Rotevatn, A., & Fossen, H., 2011. Simulating the effect of subseismic fault tails and process zones in a siliciclastic reservoir analogue: Implications for aquifer support and trap definition. *Marine and petroleum geology* **28**, 1648-1662.

Rotevatn, A., Fossen, H., Hesthammer, J., Aas, T. E., & Howell, J. A., 2007. Are relay ramps conduits for fluid flow? Structural analysis of a relay ramp in Arches National Park, Utah. *Geological Society, London, Special Publications* **270**, 55-71.

Rotevatn, A., Tveranger, J., Howell, J., & Fossen, H., 2009. Dynamic investigation of the effect of a relay ramp on simulated fluid flow: geocellular modelling of the Delicate Arch Ramp, Utah. *Petroleum Geoscience* **15**, 45-58.

Rykkelid, E., & Fossen, H., 2002. Layer rotation around vertical fault overlap zones: observations from seismic data, field examples, and physical experiments. *Marine and petroleum geology* **19**, 181-192.

Sanderson, D. J., 2016. Field-based structural studies as analogues to sub-surface reservoirs. *Geological Society, London, Special Publications* **436**, 207-217.

Sanderson, D. J., & Nixon, C. W., 2015. The use of topology in fracture network characterization. *Journal of Structural Geology* **72**, 55-66.

Sanderson, D. J., & Zhang, X., 1999. Critical stress localization of flow associated with deformation of well-fractured rock masses, with implications for mineral deposits. *Geological Society, London, Special Publications* **155**, 69-81.

Scholz, C., Dawers, N., Yu, J. Z., Anders, M., & Cowie, P., 1993. Fault growth and fault scaling laws: preliminary results. *Journal of Geophysical Research: Solid Earth* **98**, 21951-21961.

Schöpfer, M. P., Childs, C., & Walsh, J. J., 2007. Two-dimensional distinct element modeling of the structure and growth of normal faults in multilayer sequences: 2. Impact of confining pressure and strength contrast on fault zone geometry and growth. *Journal of Geophysical Research: Solid Earth* **112**.

Segall, P., & Pollard, D., 1980. Mechanics of discontinuous faults. *Journal of Geophysical Research: Solid Earth* **85**, 4337-4350.

Segall, P., & Pollard, D. D., 1983. Nucleation and growth of strike slip faults in granite. *Journal of Geophysical Research: Solid Earth* **88**, 555-568.

Shipton, Z., & Cowie, P., 2001. Damage zone and slip-surface evolution over μm to km scales in high-porosity Navajo sandstone, Utah. *Journal of Structural Geology* **23**, 1825-1844.

Shipton, Z. K., Evans, J. P., Robeson, K. R., Forster, C. B., & Snelgrove, S., 2002. Structural heterogeneity and permeability in faulted eolian sandstone: Implications for subsurface modeling of faults. *AAPG Bulletin* **86**, 863-883.

Shipton, Z. K., Soden, A. M., Kirkpatrick, J. D., Bright, A. M., & Lunn, R. J., 2006. How thick is a fault? Fault displacement-thickness scaling revisited. *Earthquakes: Radiated energy and the physics of faulting*, 193-198.

Sibson, R., 1977. Fault rocks and fault mechanisms. *Journal of the Geological Society* **133**, 191-213.

Skar, T., Berg, S. S., Gabrielsen, R. H., & Braathen, A., 2016. Fracture networks of normal faults in fine-grained sedimentary rocks: examples from Kilve Beach, SW England. *Geological Society, London, Special Publications* **439**, SP439. 410.

Soliva, R., Benedicto, A., Schultz, R., Maerten, L., & Micarelli, L., 2008. Displacement and interaction of normal fault segments branched at depth: Implications for fault growth and potential earthquake rupture size. *Journal of Structural Geology* **30**, 1288-1299.

Soliva, R., & Schultz, R. A., 2008. Distributed and localized faulting in extensional settings: insight from the North Ethiopian Rift–Afar transition area. *Tectonics* **27**, TC2003.

Torabi, A., & Berg, S. S., 2011. Scaling of fault attributes: A review. *Marine and petroleum geology* **28**, 1444-1460.

Trudgill, B., & Cartwright, J., 1994. Relay-ramp forms and normal-fault linkages, Canyonlands National Park, Utah. *Geological Society of America Bulletin* **106**, 1143-1157.

Van Hoorn, B., 1987. The South Celtic Sea / Bristol channel Basin: origin, deformation and inversion history. *Tectonophysics* **137**, 309-334.

Vermilye, J. M., & Scholz, C. H., 1998. The process zone: A microstructural view of fault growth. *Journal of Geophysical Research* **103**, 12223-12237.

Walsh, J., Bailey, W., Childs, C., Nicol, A., & Bonson, C., 2003. Formation of segmented normal faults: a 3-D perspective. *Journal of Structural Geology* **25**, 1251-1262.

Walsh, J., Nicol, A., & Childs, C., 2002. An alternative model for the growth of faults. *Journal of Structural Geology* **24**, 1669-1675.

Walsh, J., & Watterson, J., 1987. Distributions of cumulative displacement and seismic slip on a single normal fault surface. *Journal of Structural Geology* **9**, 1039-1046.

Walsh, J., Watterson, J., Bailey, W., & Childs, C., 1999. Fault relays, bends and branch-lines. *Journal of Structural Geology* **21**, 1019-1026.

Walsh, J. J., & Watterson, J., 1988. Analysis of the relationship between displacements and dimensions of faults. *Journal of Structural Geology* **10**, 239-247.

Walsh, J. J., & Watterson, J., 1989. Displacement gradients on fault surfaces. *Journal of Structural Geology* **11**, 307-316.

Walsh, J. J., & Watterson, J., 1991. Geometric and kinematic coherence and scale effects in normal fault systems. *In: Roberts A. M., Yielding G., Freeman B. (eds) The geometry of Normal Faults. Geological Society Spesial Publication* **56**, 193-203.

Watson, D., 1999. The natural neighbor series manuals and source codes. *Computers & Geosciences* **25**, 463-466.

Watterson, J., 1986. Fault dimensions, displacements and growth. *Pure and Applied Geophysics* **124**, 365-373.

Watterson, J., Nicol, A., Walsh, J., & Meier, D., 1998. Strains at the intersections of synchronous conjugate normal faults. *Journal of Structural Geology* **20**, 363-370.

Wheeler, R. L., & Dixon, J. M., 1980. Intensity of systematic joints: methods and application. *Geology* **8**, 230-233.

Whittaker, A. G., G.W., 1983. Geology of the Country Around Weston-super-Mare, memoir for 1:50,000 geological sheet 279 new series, with parts of sheet 263 and 295. *Geological Survey of Great Britain*.

Wibberley, C. A., Yielding, G., & Di Toro, G., 2008. Recent advances in the understanding of fault zone internal structure: a review. *Geological Society, London, Special Publications* **299**, 5-33.

Willemse, E. J., 1997. Segmented normal faults: Correspondence between three-dimensional mechanical models and field data. *Journal of Geophysical Research: Solid Earth* **102**, 675-692.

Williams, G., & Chapman, T., 1983. Strains developed in the hangingwalls of thrusts due to their slip/propagation rate: a dislocation model. *Journal of Structural Geology* **5**, 563-571.

Wilshire, H., & Kirby, S., 1989. Dikes, joints, and faults in the upper mantle. *Tectonophysics* **161**, 23-31.

Wu, H., & Pollard, D. D., 1995. An experimental study of the relationship between joint spacing and layer thickness. *Journal of Structural Geology* **17**, 887-905.

Zhang, X., & Sanderson, D. J., 1995. Anisotropic features of geometry and permeability in fractured rock masses. *Engineering Geology* **40**, 65-75.

Zhang, X., & Sanderson, D. J., 1996. Effects of stress on the two-dimensional permeability tensor of natural fracture networks. *Geophysical Journal International* **125**, 912-924.

Appendix I – Workflows in ArcGIS 10.4.1

This appendix contains additional information providing a summary of workflows used in ArcGIS. This includes interpretation and analysis of data from aerial photographs, together with data analysis of imported field measurements.

Workflow 1 – Setting up the ArcGIS project

1. Digital aerial photographs of the wave-cut platform at Kilve and Lilstock were downloaded from the Channel Coast Observatory at www.channelcoast.org/. Images can be downloaded as georectified image files (.ecw) and imported directly into ArcMap.
2. The aerial photographs were used for digital mapping of marker beds and faults in the relay ramp damage zone of Kilve and as base maps during field work.
3. A new geodatabase (.gdb) was created in ArcCatalog, where feature classes (points, polylines and polygons) could be created and saved.
4. Feature classes were used to digitize groups of geographic features: Polylines were used for faults, marker beds and cliff contours; Points for stratigraphic separations and vein transect mapping; Polygons for mapping damage zone areas. All feature classes can be created using ArcToolbox. NB. It is important to tick the 'Measure' box when creating features as this automatically calculates geometrical information such as fault length etc.

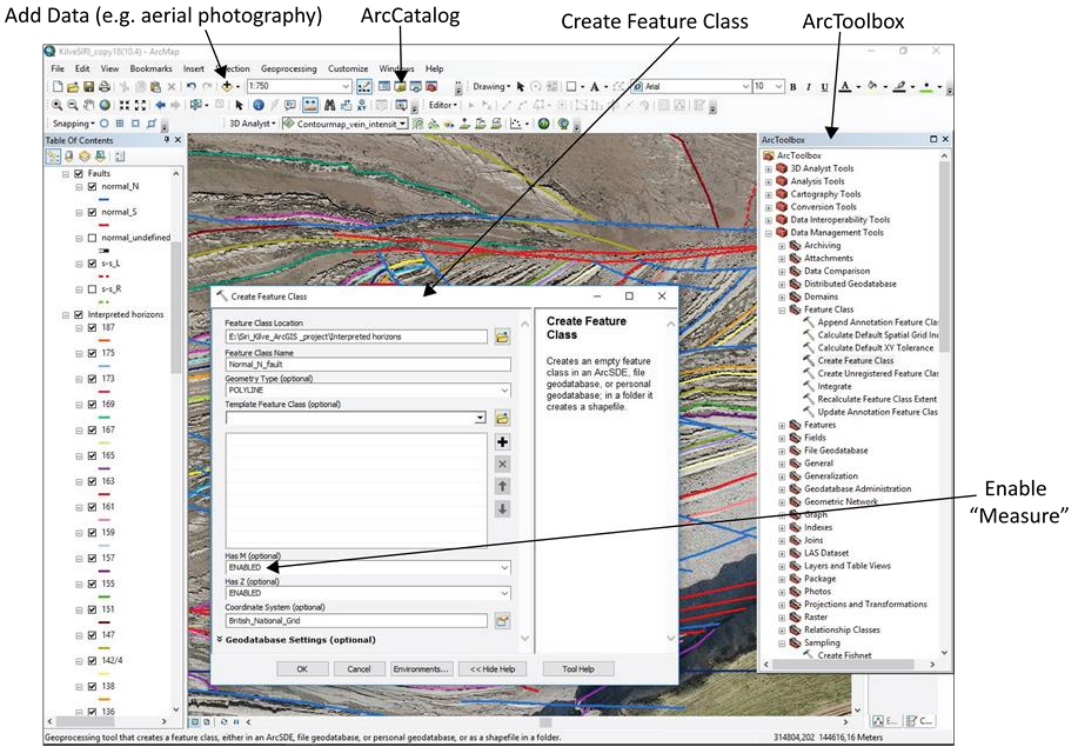

Workflow 2 – Making stratigraphic separation and displacement maps

1. Faults and marker beds were interpreted and digitized from digital aerial photographs and from field observations. In the feature class attribute table different fields for additional information were created, such as fault ID, fault length and dip direction for the fault feature class. Collecting additional information in the attribute table is essential as this can be used for later visual analysis as faults can be displayed by different attributes.

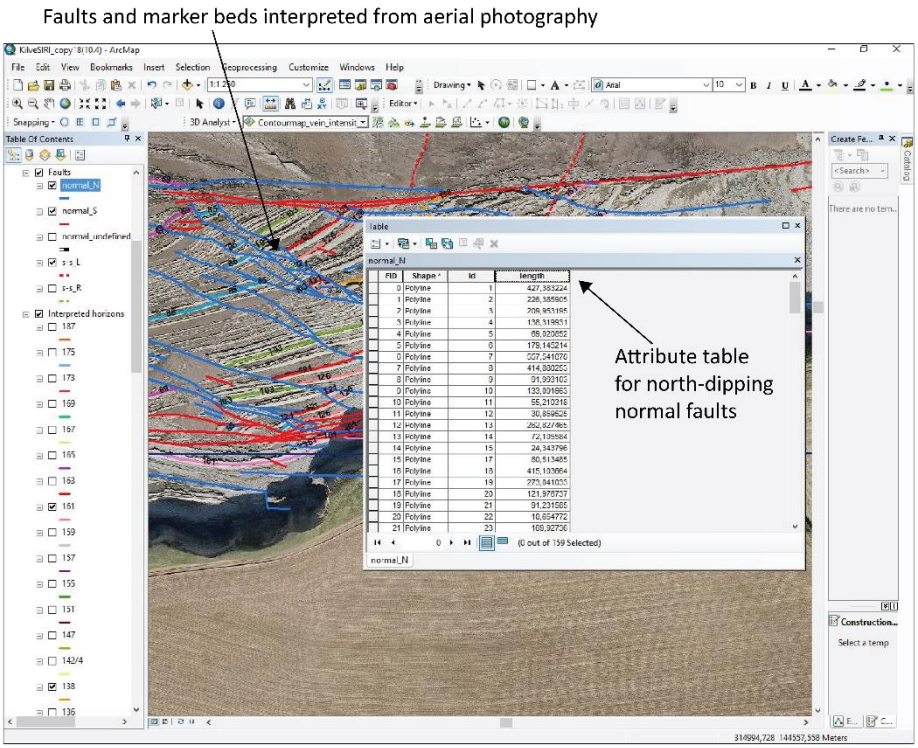

2. Created a new point feature class named ‘Stratigraphic Separations’. Added points where marker beds are cut by faults. It is important that points are ‘snapped’ to the faults.

3. Using the ‘Measuring tool’ on the tool bar the stratigraphic juxtaposition of marker beds across a fault was measured. The stratigraphic separation was then calculated using one of the methods shown below:

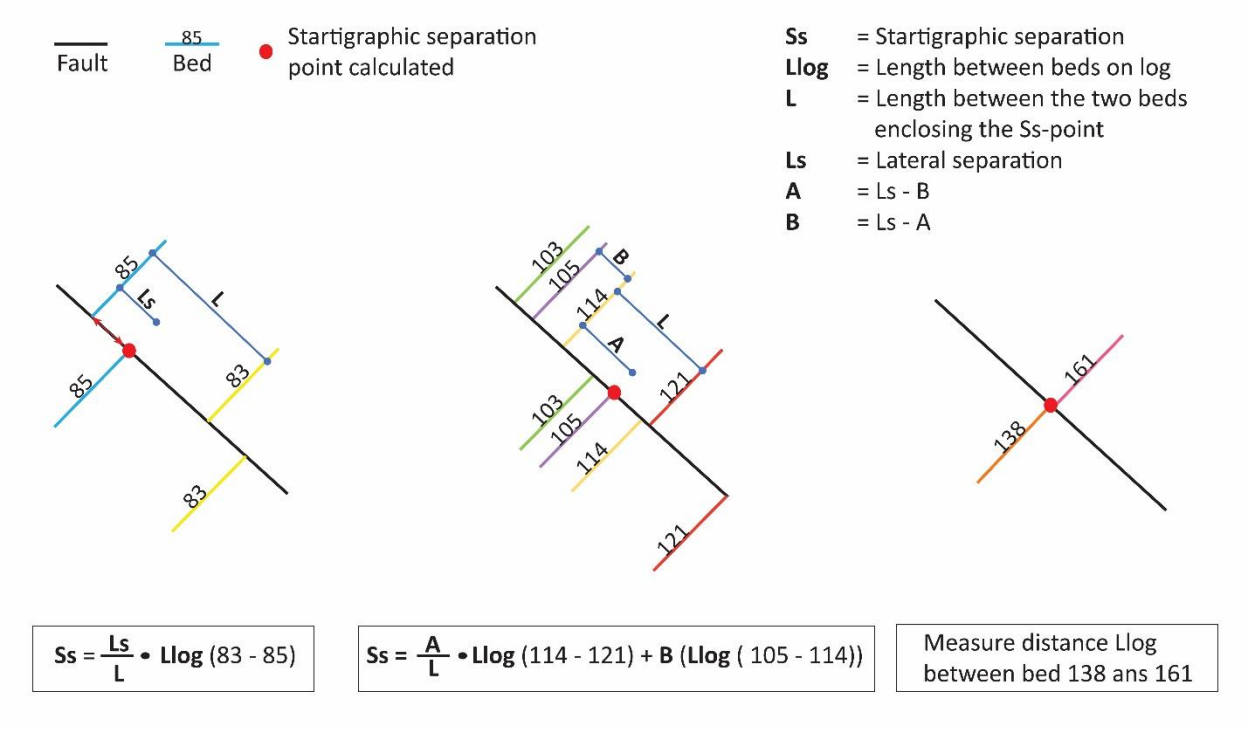

4. Calculated as many stratigraphic separation points as possible along fault traces, and put a zero point at each fault tip.

5. In the attribute table of measured stratigraphic separations new fields were created for *x* and *y* co-ordinates (must be made as *long integer* field) and calculated using the 'Calculate Geometry' option. A new field for *xy* (must be made as *double integer* field) was created, where the product of x and y was calculated using the 'Field Calculator'. This created a unique number for each point that was used later in the process.

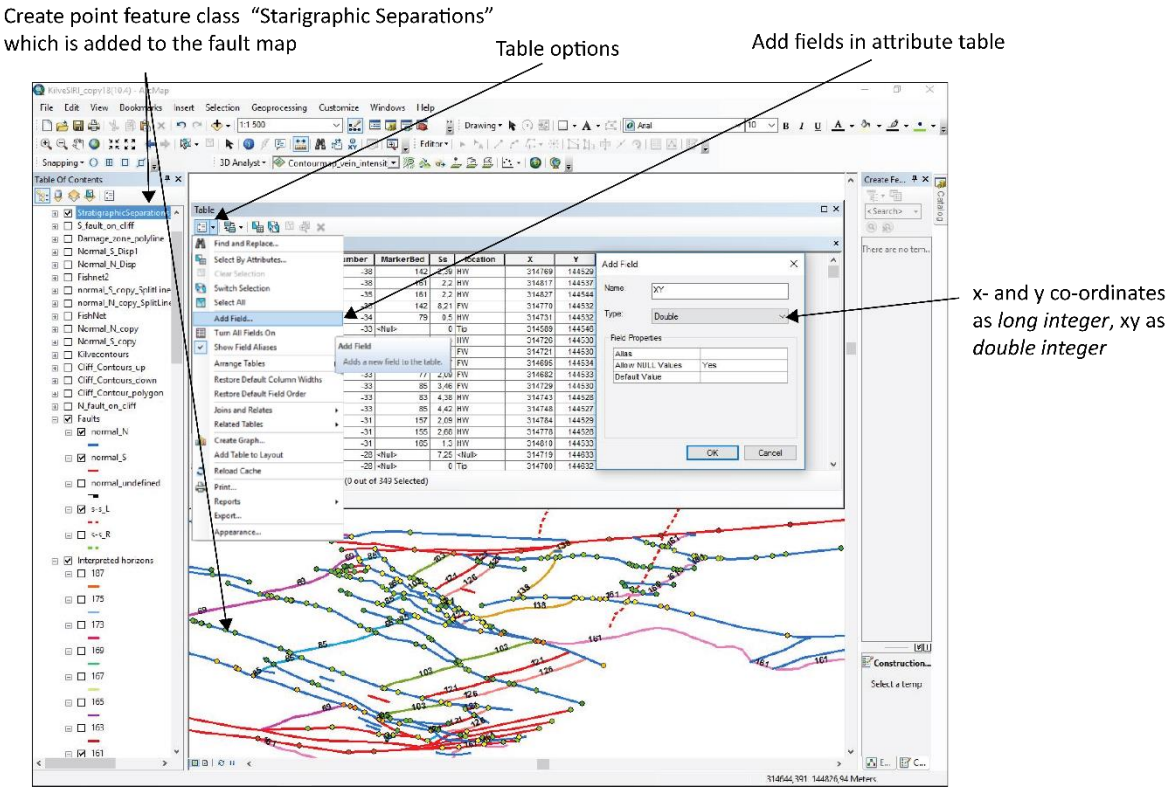

6. The fault polylines were split into segments by the points of stratigraphic separation using ArcToolbox > Data Management Tools > Features > Split Line At Point. This was done for both the N-dipping faults and S-dipping faults which were used as the 'Input Feature', and stratigraphic separations were used as the 'Point Feature Class'. A 'Search Radius' of 0.5 m was used to account for any small errors in point location.

7. A new feature class was created where the faults are segmented. Each segment is divided by a point that corresponds to the location of a stratigraphic separation point.

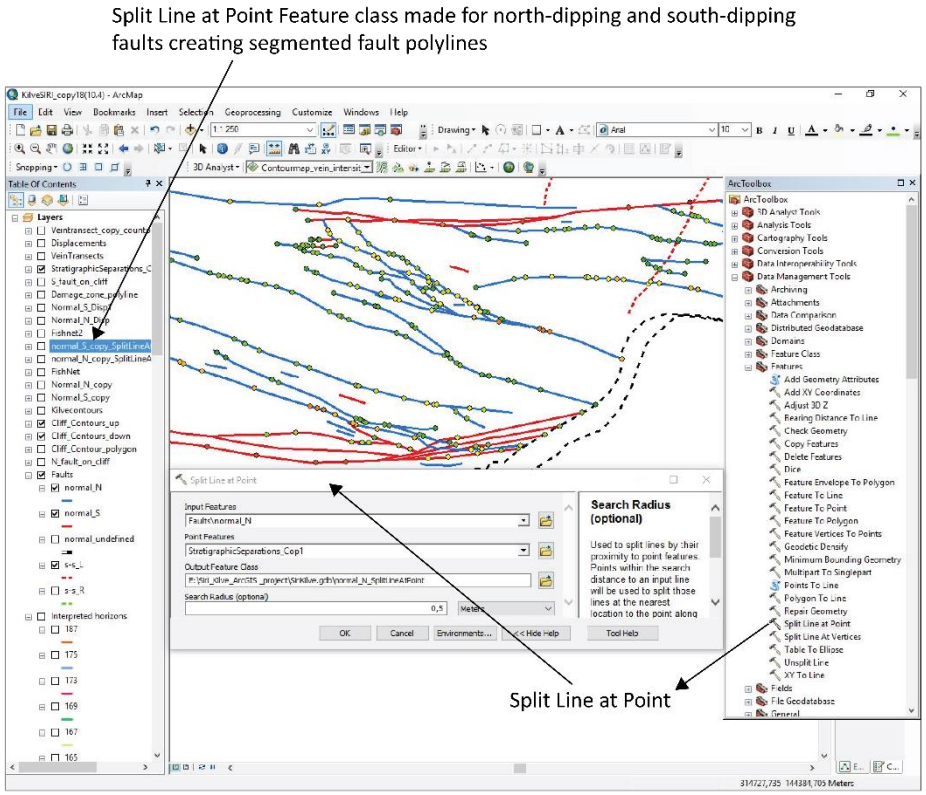

8. Within the attribute table for the segmented fault polylines new fields were added for the *x* and *y* co-ordinates for the start and end point for each fault polyline segment (must be made as *long integer* fields). Used 'Calculate Geometry' to calculate the x and y co-ordinates. Further fields for *xy* start and *xy* end (must be made as *double integer* fields), were created and calculated using the 'Field Calculator'. These were used to join the segmented fault polyline attribute table with the stratigraphic separation attribute table (using *xy* and *xy* start/*xy* end). This makes it possible to transfer attributes from the stratigraphic separation attribute table over to the segmented fault polyline attribute table. The 'Field Calculator' was used to transfer the S_S-values for the start and end points of each segment.

9. After joining and transferring attributes, each line segment will have one S_S-value for each start and end point. These were used to calculate an average S_S-value for each segment in a new field in the attribute table using the 'Field Calculator'.

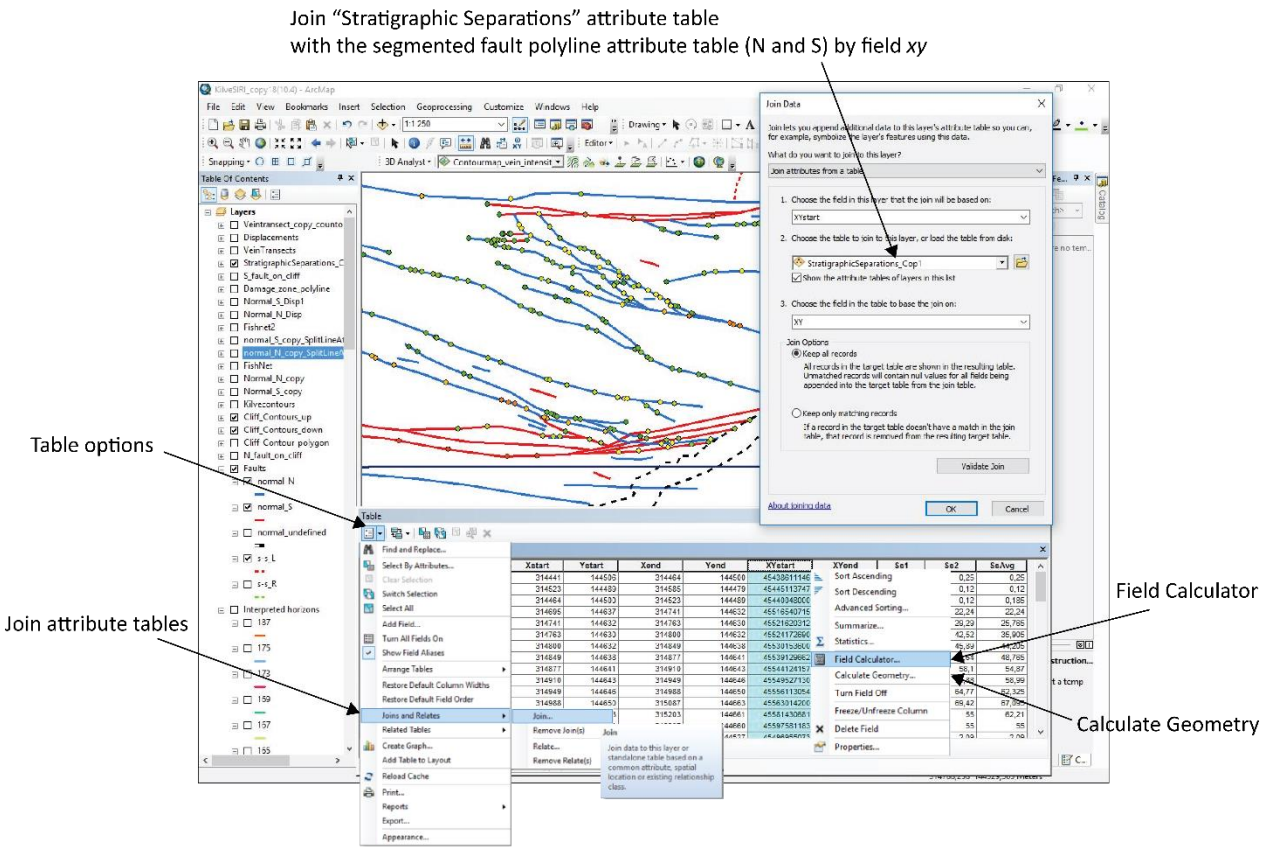

10. Each fault segment could then be visualized based on their average stratigraphic separation values using the 'Symbology' tab in the properties table of the feature class. This was used to create the stratigraphic separation and displacement maps.

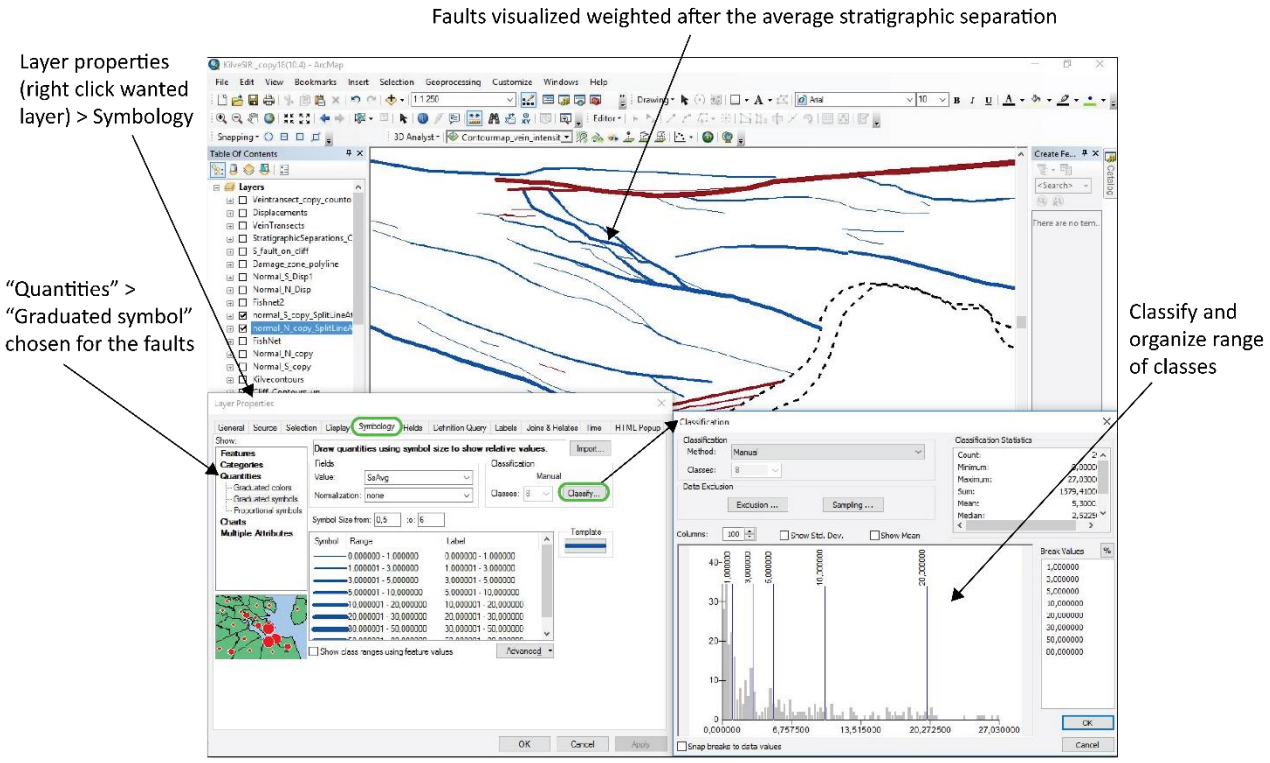

Workflow 3 – Making stratigraphic separation-distance profile

1. The stratigraphic separation map was used to extract data for a stratigraphic separation-distance profile over the whole relay area.

2. This involves multiple vertical line transects from W to E over the relay, created using a Fishnet that was made from ArcToolbox > Sampling > Create Fishnet. In the tool window, the stratigraphic separation point feature class was used as a 'Template Extent', and the following parameters were set: Cell Size Width = 2.5 m; Cell Size Height = 100 m; Geometry type = Polyline. Remember to untick 'Create Label Points'. This created a grid with vertical line transects spaced at 2.5 m.

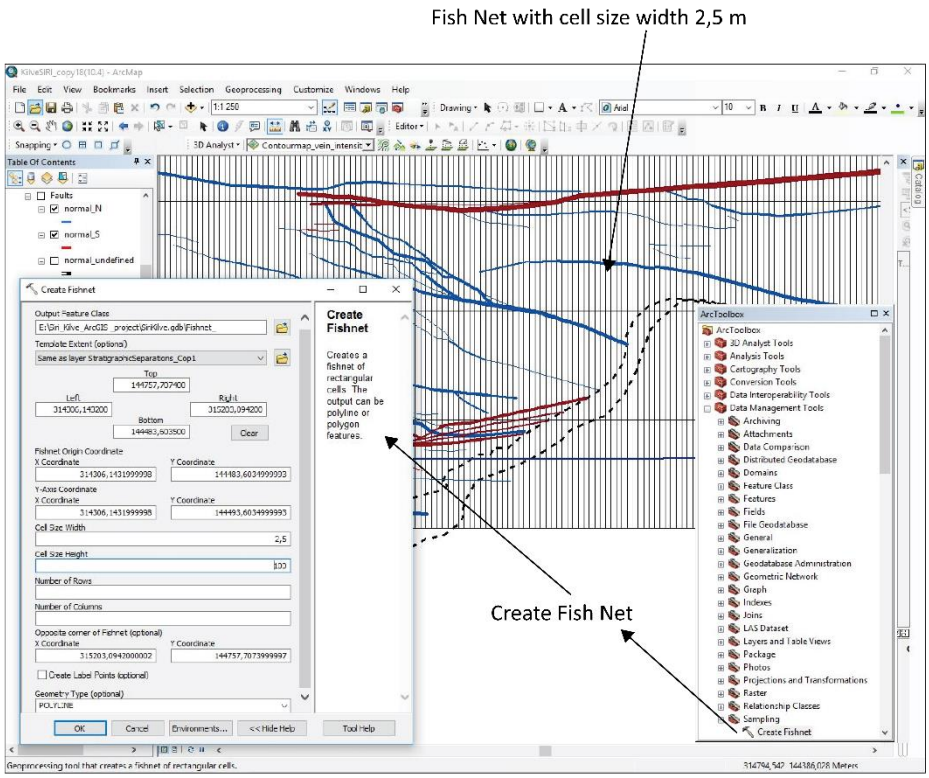

3. Stratigraphic separation values for each fault segment polyline that intersected each transect line were extracted manually into a spreadsheet. The values for each transect were divided into 3 separate groups representing the main S-bounding fault (FS1), main N-bounding fault (FS2) and the damage faults. This data was used to plot the stratigraphic separation-distance profile showing changes in S_S-values along strike of the relay structure, including a cumulative curve.

4. Steps 1 to 3 were used for extracting data for the spatial heterogeneity analysis, where stratigraphic separation values and the placement of faults along 150 m long N-S transects were gathered. Here a Fishnet with the following set parameters were used: Cell Size Width = 25m; Cell Size Height = 50m; Geometry type = Polyline.

Workflow 4 – Creating vein intensity and strain (% extension) contour maps

1. The location of vein transects and measured field data (i.e. aperture, frequency, bed thickness, bed dip and dip direction) were digitized as a point feature class called 'Vein Transects', where all measurements were extracted from spreadsheets into the attribute table. These included points that were marked as zero points, these indicated the width of the damage zones around each fault (attributed as zero aperture and zero frequency).

2. A 'Damage zone' polygon feature class was made using the ArcToolbox, and a polygon was drawn that was snapped to each zero point.

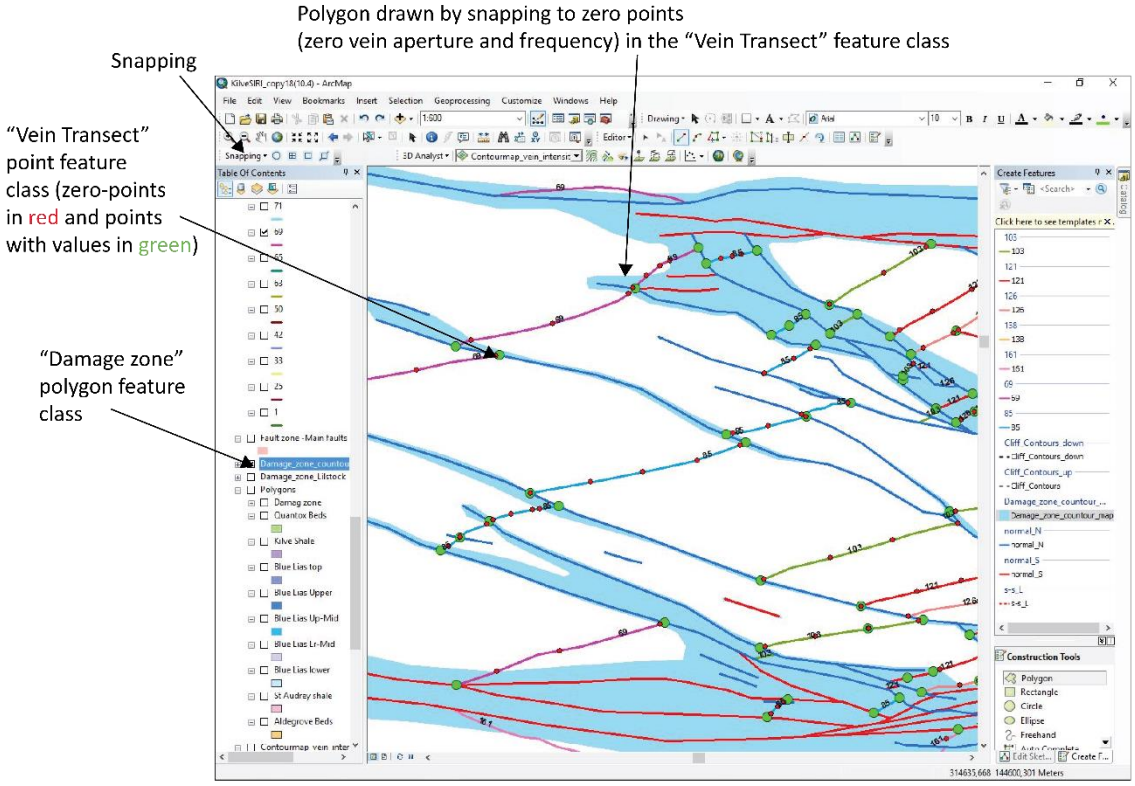

3. To create a contour map of intensity and % extension, these values needed to be calculated. New fields were added in the attribute table and intensity and % extension was calculated using the 'Field Calculator':

   i.) Intensity = frequency of measured veins / transect length

   ii.) % extension = (total aperture / (transect length –total aperture)) ×100

4. To make the contour maps, further points were linearly extrapolated along strike of each fault to create points that were more closely spaced.

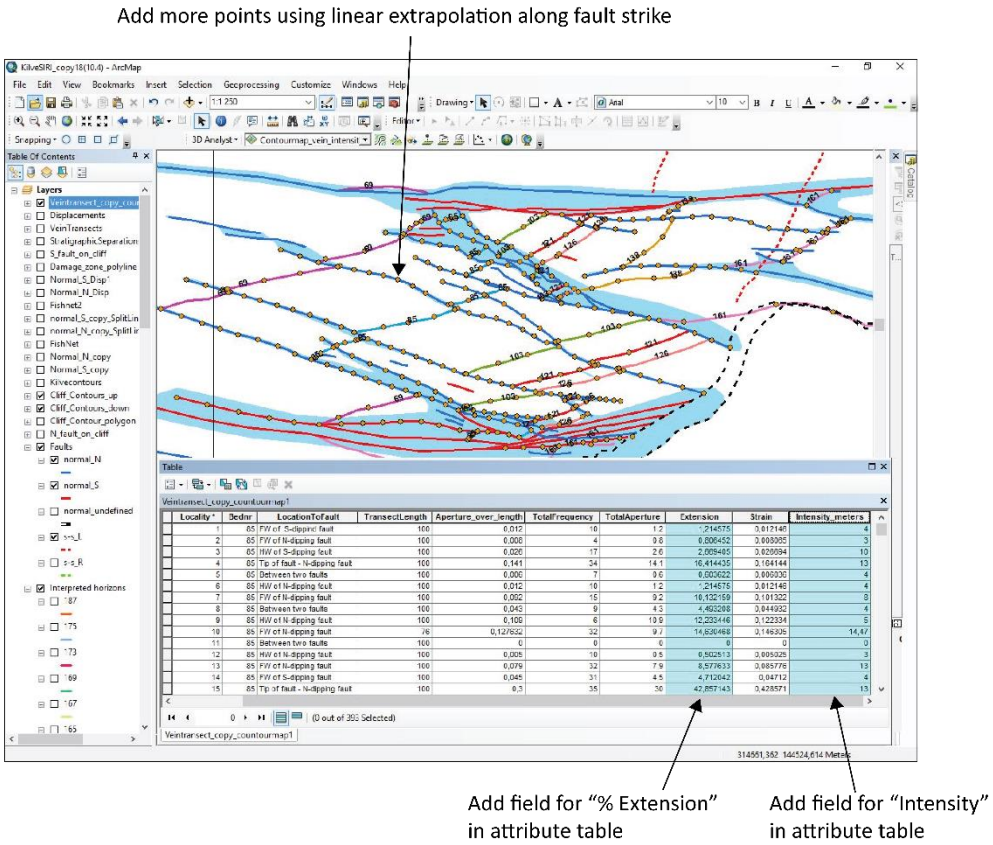

5. An interpolated raster map was created through ArcToolbox > Spatial Analyst Tools > Interpolation > Natural Neighbor. The vein transect feature class was used as the 'Input Point Feature' and Z-value was specified as either the intensity or % extension attribute. An output cell size of 0.1 m was specified. This created a contour map of the selected attributes, interpolated from all the points available within the input feature class.

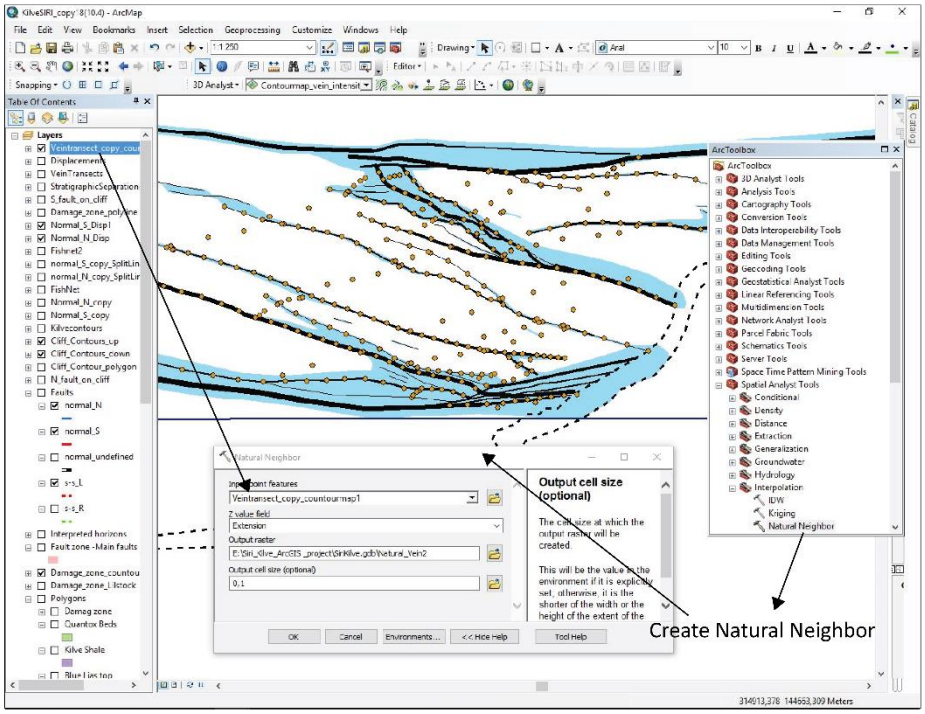

6. The area of the damage zone polygon was extracted from the interpolated raster using ArcToolbox > Spatial Analyst Tools > Extraction > Extract by Mask. Maps were used as 'Input Raster', and the damage zone polygon as 'Feature Mask Data'. Important to go to Environments > Raster Analysis > and set the cell size as 0.1 m.

7. The raster maps can be visualized in a variety of ways using the 'Symbology' tab in the properties table of the raster.

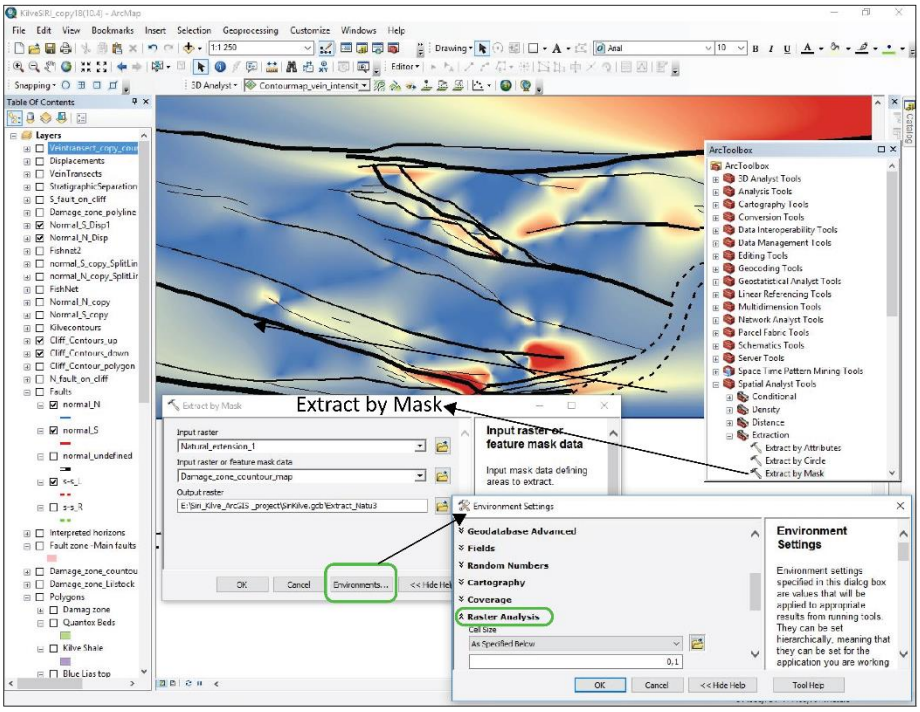

8. Using ArcToolbox > Conversion Tools > Excel > Table To Excel, the attribute table records of the feature class are exported from ArcGIS into data base format (.dbf) which can be viewed and edited in Microsoft Excel. This step is done for all the above-mentioned feature classes, giving useful information that can be manipulated in many ways using spreadsheets.

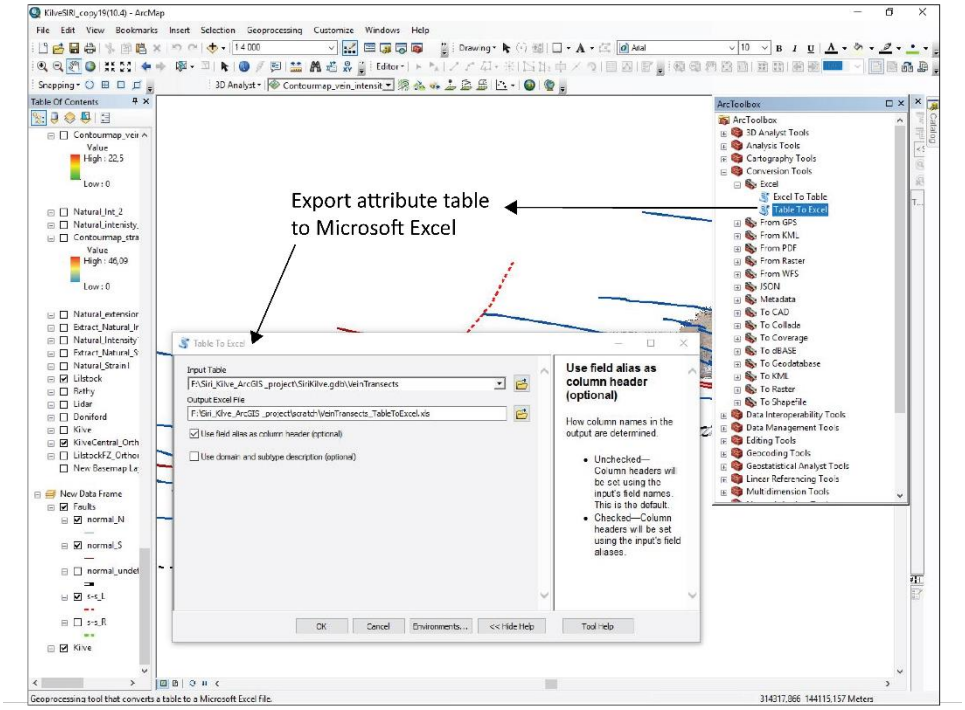

Appendix II – Corrections for fault- and bed orientations

This appendix includes methods used for making corrections for fault and bed orientations. Beds on the wave-cut platform have experienced a slight bed rotation, that needs correcting for. Since the slip vector of the study is approximately N-S, measured dips of both faults and beds were also corrected and re-calculated in the N-S direction. This was done to be able to use the measurements in further extension analysis.

Correction of bed rotation

To calculate correct values of heave for horizontal bedding parallel extension, corrections for bed rotation must be made to the fault and bed dips. In the figure below the average bed and fault orientations used in this study have been plotted in a 3-D stereographic projection and oriented so that the geometric relationship between them is seen in the north-south direction. To correct the fault dips, the dip value for bedding in the N-S orientation (14°) should be added to the N-dipping faults and subtracted from the S-dipping faults. This relationship is because the N-dipping faults have the opposite dip direction to the beds, while the S-dipping faults dip in the same direction (see figure). This correction for bed rotation can be done using the average bed dip (16°) as all the beds mainly dip in the same direction, where the spread in dip measurements is low (i.e. 11° - 19°).

For the corrected values, see table in next section.

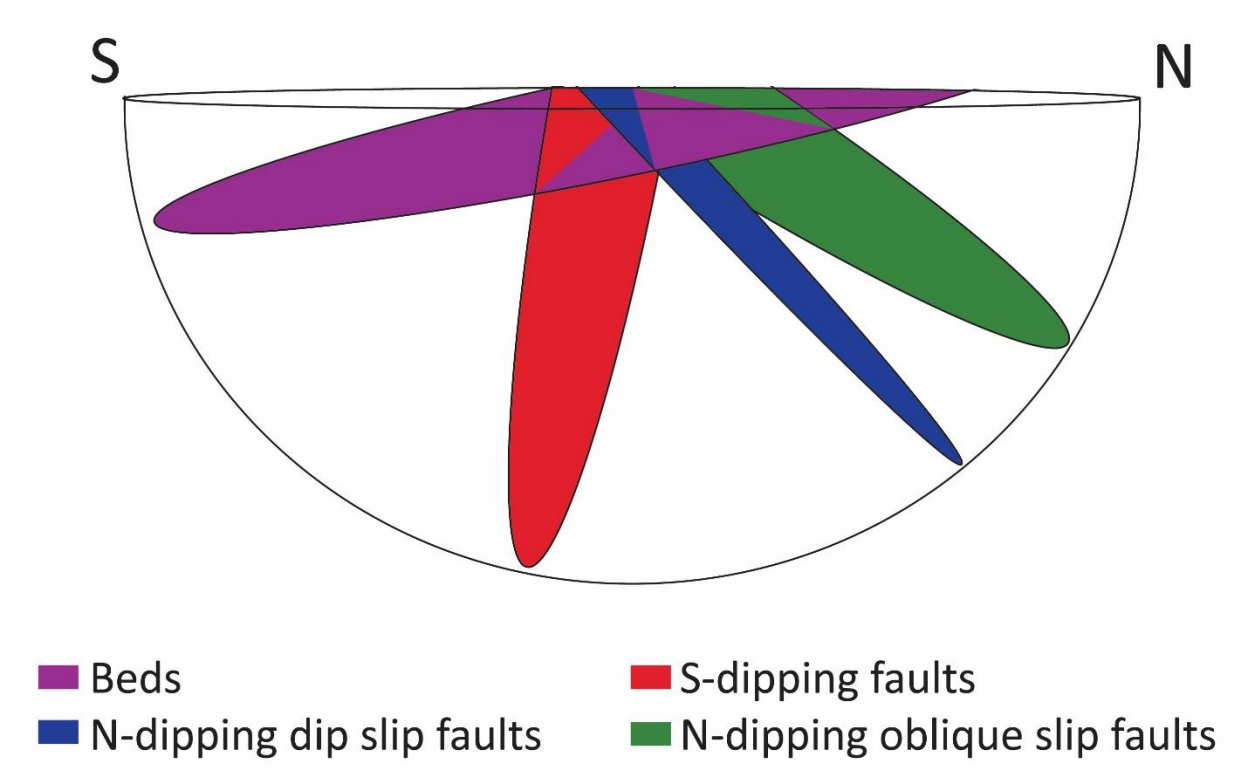

Correction for extension in N-S direction

All measured fault and bedding orientations (dip/dip direction) were plotted on an equal-area stereographic plot and best fit great circles were found for the three different fault groups (i.e. S-dipping faults, oblique-slip N-dipping faults, and dip-slip N-dipping faults), and for the key marker beds. The dips and dip directions of these great circles were used as averages.

Due to the orientation of the faults and the fact that the slip vector of the faults was approximately N-S, the dips of both faults and beds were corrected and calculated in the N-S orientation using the great circles. The table shows the original measured values, the dip corrections for the N-S extension and bed rotation.

	Original dip/dip direction	Corrected dip in N-S direction	Corrected fault dip due to bed rotation
Dip-slip N-dipping faults	50/006	48°	62°
Oblique slip N-dipping faults	41/015	33°	47°
S-dipping faults	82/185	80°	66°
Beds	16/154	14°	